Titre: Title:	A CAD/CAM wideband microwave six-port junction
Auteur: Author:	Sining Wang
Date:	1990
Type:	Mémoire ou thèse / Dissertation or Thesis
Référence: Citation:	Wang, S. (1990). A CAD/CAM wideband microwave six-port junction [Mémoire de maîtrise, École Polytechnique de Montréal]. PolyPublie. https://publications.polymtl.ca/56727/

ISBN 0-315-58128-X

UNIVERSITE DE MONTREAL

ECOLE POLYTECHNIQUE

Ce mémoire intitulé:

A CAD/CAM WIDEBAND MICROWAVE SIX-PORT JUNCTION

présenté par: Sining Wang

en vue de l'obtention du grade de: maître es sciences appliquées (M.Sc.A.) a été dûment accepté par le jury d'examen constitué de:

Cevdet Akyel	D. Sc. A., Président-rapporteur
Renato G. Bosisio	M. Sc. A., Directeur
Fadhel M. Ghannouchi	Ph. D., Codirecteur
Yan Xu	Ph. D.

Sommaire

Depuis l'introduction de la technologie à six-port au début des années soixante-dix, plusieurs méthodes et formalismes ont été utilisés avec succès pour l'étalonnage du reflectometre six-port aussi bien que pour la procedure de mesure entre $1 \sim 100GHz$. Néanmoins, le recours à la technique six-port s'avère toujours nécessaire pour des mesures en balayage de fréquence sur une bande de $100MHz$ et pour des mesures pulsés avec une resolution d'environ $1\mu s$. Afin d' atteindre cet objectif, l'auteur de ce mémoire a recouru à la CAO/FAO pour concevoir et construire une jonction six-port ayant des points q_i quasi-invariables avec la fréquence. Les contributions principales de l'auteur sont les suivantes:

- Des coupleurs large bande, couvrant la bande de fréquence $2 \sim 18\,Ghz$ et ayant des niveaux de couplage très élevès de $1.76\,dB$ et $3\,dB$, ont été conçus, construits et mesurés avec succès.

- Trois différents diviseurs de puissance de type Wilkinson, opérant à la

bande de fréquence $2 \sim 15\,Ghz$, ont été conçus, construits et mesurés. Les résultats ont été satisfaisants. L'utilisation de diviseurs de puissance de type Wilkinson à lignes courbées a permis de maintenir une très bonne isolation (meilleur qu' à $-25\,dB$), entre les deux ports de sortie du diviseur de puissance tout au long de la bande de fréquence $2 \sim 15\,Ghz$.

- L'étalonnage du reflectometre six-port qui repose sur l'utilisation d'une charge coulissante pour obtenir differentes terminaisons étalons. La non disponibilité de telle charge coulissante pour des fréquences superieures à $10GHz$ limite le choix et le nombre des terminaisons étalons. Ce problème a été résolu en utilisant la théorie de la ligne longue (long line theory). Des améliorations appropriées ont été apportées à la théorie afin qu'elle réponde à nos besoins. La validité de ces améliorations a été confirmée par l'étalonnage de la jonction six-port entre $2 \sim 12\,Ghz$ et son utilisation pour mesurer des charges étalons.

- Les formules pour calculer les points q_i de la jonction six-port ont été developpées en se basant sur la méthode de transformation bilinéaire qui permet de calculer les points q_i à partir des paramètres d'ètalonnage de la jonction six-port.

Abstract

Six-port technology was introduced in the early 1970's. Different methods and formalisms to design and build a six-port junction were successfully used for various applications over $1 \sim 100GHz$. However, there still exists the need to apply six-port techniques in wideband applications, such as swept frequency measurements over 100MHz bandwith and microwave pulse measurements with time resolutions better than $1\mu s$. A CAD/CAM wideband six-port junction design with frequency invariant q_i points is carried out in this thesis in order to advance toward the above goals. The main contributions of the author in this thesis are the following: 1) Wideband couplers which cover the frequency range from $2 \sim 18\,GHz$ with very tight coupling levels ($1.76\,dB$ and $3\,dB$ respectively) have been designed and measured successfully. 2) Three different Wilkinson power dividers over the frequency range of $2 \sim 15\,GHz$ have been designed and measured with satisfactory results. A very good isolation (better than $-25\,dB$) between the two output ports of a power divider over the frequency range of $2 \sim 15\,GHz$ has been achieved by using a curved line Wilkinson power divider. 3) Most calibrations at microwave frequencies (up

to 10 GHz) depend on the use of a sliding short circuit to obtain different impedance terminations. However, a commercial sliding short circuit operating above $10\,GHz$ is not yet available. This problem has been solved by using the long line theory with appropriate improvements. The improvements have been confirmed by measuring a known standard using the designed six-port junction over the frequency range of $2 \sim 12\,GHz$. 4) Expressions to calculate q_i points of the designed six-port reflectometer were developed according to a published calibration method. The calculation is based on a bilinear transformation concept, which derives q_i point calculation procedures from the calibration parameters.

Acknowledgement

I would like to acknowledge my supervisor, Professor Renato G. Bosisio. I wish to thank him for receiving me as a visiting scholar , directing me on my research work and supporting me financially through my graduate studies at the Ecole Polytechnique de Montréal.

I would like to acknowledge Dr. Fadhel M. Ghannouchi, my co-director, for his advice, suggestions and encouragements during my research work.

I would like to thank René Archambault and Yvon Lemyre for their assistance in computer programming, constructing and testing the six-port junction and its components.

Acknowledgement should be given to the other students who work in this laboratory for their kindness, help and friendship.

Finally, I wish to thank the *Service des etudes superieures* de l'Ecole Polytechnique and Marcel Arsenault for their successful efforts to obtain my *exemption des droits de scolarité.*

Contents

List of Figures

Chapter 1

Introduction

The behaviour of microwave devices and circuits is currently evaluated by their scattering matrices $[S]$ at each operating frequency. The S parameters of a microwave device can be measured quantitatively, either in the frequency domain or in the time domain. The technique which corresponds to microwave measurements in the time domain is known as Time-Domain Reflectometry (TDR) [1,2,3]. The current techniques which represent the development tendency of microwave measurements in the frequency domain are based on the use of Automatic Network Analysers (ANA) [4,5] and Six-Port Automatic Network Analysers (SPANA) [6,7,8]. The research work in this thesis will concentrate on the design of a wide band six-port junction, a fundamental component of a Six-Port Automatic Network Analyser.

1.1 Automatic Network Analysers

Automatic network analysers (ANA) are available in two types: scalar automatic network analysers (SANA) and vector automatic network analysers (VANA). A schematic diagram of a more versatile VANA is shown in figure (1.1). It can be noted from figure (1.1) that the system is established on the basis of a four port network. With additional switching, multiport networks can be analyzed for both reflection and transmission characteristics [1].

The measurement procedure for ANA is as follows: samples of the input signal (reference) and the reflected (or transmitted) signal are frequency converted to an intermediate frequency (IF), either by coherent sampling or phase locked superheterodyne mixing. The two IF signals are measured by using a vectorial ratio meter. Frequency conversion is unavoidable with a VANA since no phase meter can operate over all the microwave frequency range [4,5].

1.2 Six-Port Reflectometry

The need to measure the phase of the reflection coefficient of a Device Under Test (DUT) by means of ANA can be eliminated by the addition of two detectors to the four-port measurement network mentioned in section (1.1). The intervening network becomes a six-port junction, four ports of which are

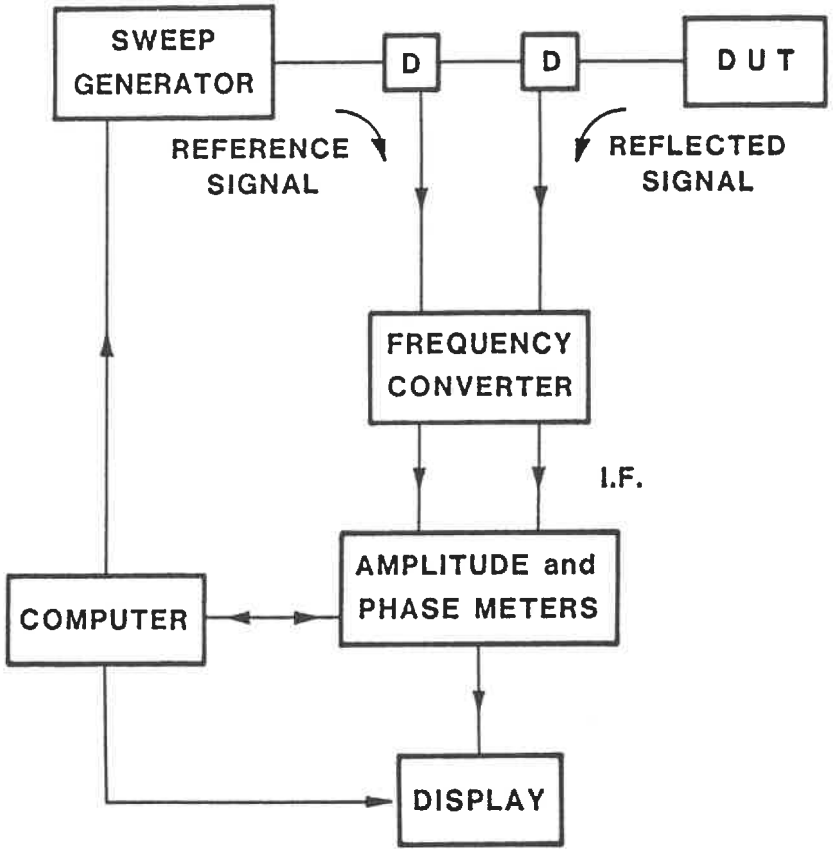

Figure 1.1: A Vector Automatic Network Analyser System

terminated by power detectors, with readings denoted as P_3, P_4, P_5 and P_6. The four power readings are related to the reflection coefficient of a DUT by the following equation (it will be explained in the next chapter) :

$$P_i = |K_i|^2 |b_2|^2 |\Gamma - q_i|^2 \ , \ i = 3, 4, 5 \text{ and } 6 . \tag{1.1}$$

Rewriting Γ and q_i in terms of their real and imaginary components:

$$\Gamma = x + jy ,$$

$$q_i = \alpha_i + j\beta_i \ , \ i = 3, 4, 5 \text{ and } 6 ,$$

then, substituting Γ and q_i into equation (1.1) and simplifying the equation, we can express the reflection coefficient of a DUT by using the following equations [3,10]:

$$x = \frac{U_0 P_3 + U_1 P_4 + U_2 P_5 + U_3 P_6}{P_3 + C_1 P_4 + C_2 P_5 + C_3 P_6} , \tag{1.2}$$

$$y = \frac{V_0 P_3 + V_1 P_4 + V_2 P_5 + V_3 P_6}{P_3 + C_1 P_4 + C_2 P_5 + C_3 P_6} , \tag{1.3}$$

where U_i, V_i and C_i are complex parameters which characterize a six-port junction and can be determined by calibration [10].

The six-port technique has been developed into a valuable precision microwave measurement tool since it was introduced by Engen and Hoer in early 1970's [6,7,8]. The advantages of this type of reflectometer include:

- the absence of any need for frequency conversion and phase meters;

- the absence of any need to match power detectors to the four output ports of a six-port junction and to calibrate them to measure power in an absolute sense;
- it's capability to measure multi-port network (n port) characteristics by using n six-port junctions;
- it's suitability for high power microwave measurements;
- it's suitability for high frequency applications such as millimeter wave and submillimeter wave bands.

Due to these advantages, the six-port measurement technique has been applied to various kinds of microwave measurements. Many efforts to develop optimal six-port junctions have been done in the past [8,11,12,13,14,15,16,17]. However, there still exists an important need to develop six-port design techniques to improve their performance for swept frequency measurements (100MHz bandwith) and pulse microwave measurements (resolution $1\mu s$) over a large bandwidth [18].

This thesis will discuss in detail a computer aided design and computer aided manufacture (CAD/CAM) of a wideband six-port junction with quasi-fixed frequency q_i positions in the Γ plane. Simulated and tested results are also presented in this thesis.

Chapter 2

Six-Port Measurement Technique

2.1 Introduction

Six-port reflectometry is strongly supported by a rigorous theory. The measurement accuracy is an important factor to evaluate the viability of such technique. According to different application needs, specific configurations of six-port junctions are required. Many experts have contributed to the development of the technique. G. F. Engen and C. A. Hoer formulated the initial theory and developed the design considerations in early 1970's [7,8,9,19,20]. These fundamental problems of a six-port design will be discussed in this chapter.

2.2 Analysis of a Six-Port Reflectometer

The operation theory of a six-port reflectometer shown in figure (2.1) is based on the four following equations [21],

$$b_i = M_i a_2 + N_i b_2 \ , \ \ i = 3, 4, 5 \text{ and } 6 \tag{2.1}$$

where a_2 and b_2 are the incident and the emergent signals respectively at port 2 which is connected to a DUT, b_i is the emergent signal at the detector D_i of port i and M_i, N_i are complex system parameters.

Equations (2.1) can be derived by describing the reflectometer in terms of its 36 S parameters and the Voltage Reflection Coefficients (VRC) which are denoted by $\Gamma_i = a_i/b_i$ and associated to detector D_i. If there is only one mode of microwave present at each port, it is convenient to use the complex incident and emergent wave amplitudes a_i and b_i, $(i = 1, \ldots, 6)$ as twelve terminal variables. Suppose that all the detectors and the junction itself are linear, then each b_i is simply composed of the linear combinations of a_i which can be represented by the following matrix,

$$[b] = [S]\,[a] \tag{2.2}$$

where elements of $[S]$ are scattering coefficients normalized to the characteristic impedance of the junction. For each detector connected to port i, the

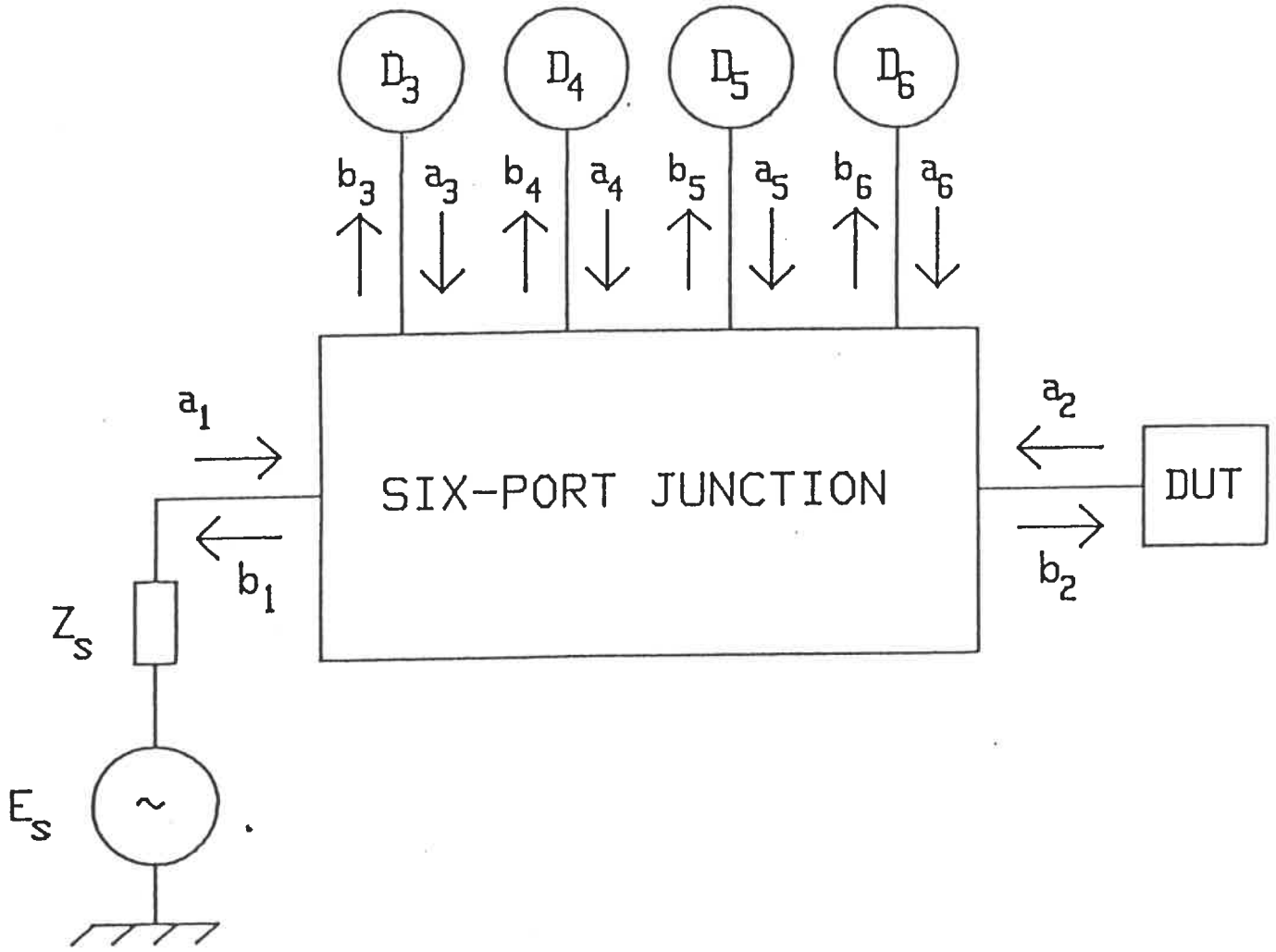

Figure 2.1: Six-port Reflectometer Diagram

substitution of Γ_i into equation (2.2) gives

$$\begin{bmatrix} b_1 \\ b_2 \\ b_3 \\ \vdots \\ b_6 \end{bmatrix} = [S] \begin{bmatrix} a_1 \\ a_2 \\ \Gamma_3 b_3 \\ \vdots \\ \Gamma_6 b_6 \end{bmatrix} \tag{2.3}$$

After simplification, equation (2.3) becomes

$$\begin{bmatrix} b_1 \\ b_2 \\ 0 \\ 0 \\ 0 \\ 0 \end{bmatrix} = \begin{bmatrix} s_{11} & s_{12} & s_{13}\Gamma_3 & s_{14}\Gamma_4 & s_{15}\Gamma_5 & s_{16}\Gamma_6 \\ s_{21} & s_{22} & s_{23}\Gamma_3 & s_{24}\Gamma_4 & s_{25}\Gamma_5 & s_{26}\Gamma_6 \\ s_{31} & s_{32} & (s_{33}\Gamma_3 - 1) & s_{34}\Gamma_4 & s_{35}\Gamma_5 & s_{36}\Gamma_6 \\ s_{41} & s_{42} & s_{43}\Gamma_3 & (s_{44}\Gamma_4 - 1) & s_{45}\Gamma_5 & s_{46}\Gamma_6 \\ s_{51} & s_{52} & s_{53}\Gamma_3 & s_{54}\Gamma_4 & (s_{55}\Gamma_5 - 1) & s_{56}\Gamma_6 \\ s_{61} & s_{62} & s_{63}\Gamma_3 & s_{64}\Gamma_4 & s_{65}\Gamma_5 & (s_{66}\Gamma_6 - 1) \end{bmatrix} \begin{bmatrix} a_1 \\ a_2 \\ b_3 \\ b_4 \\ b_5 \\ b_6 \end{bmatrix} \tag{2.4}$$

Denoting the coefficient matrix in equation (2.4) by $[Sc]$, it can be proved that $\det[Sc] \neq 0$ [21]. By denoting $[Sc]^{-1} = [M]$

$$\begin{bmatrix} a_1 \\ a_2 \\ b_3 \\ b_4 \\ b_5 \\ b_6 \end{bmatrix} = [M] \begin{bmatrix} b_1 \\ b_2 \\ 0 \\ 0 \\ 0 \\ 0 \end{bmatrix} \tag{2.5}$$

the emergent wave at each detector port can be expressed as follows:

$$b_i = m_{i1} b_1 + m_{i2} b_2 \tag{2.6}$$

where

$$b_1 = \frac{1}{m_{21}}(a_2 - m_{22} b_2) \tag{2.7}$$

$$a_2 = m_{21} b_1 + m_{22} b_2$$

Equation (2.1) can be obtained by solving (2.6) and (2.7), where $M_i = m_{i1}/m_{21}$ and $N_i = m_{i2} - m_{22} m_{i1}/m_{21}$. This equation can also be written in terms of b_2 and the reflection coefficient of the DUT $-\Gamma$

$$b_i = (\Gamma M_i + N_i)\, b_2 \tag{2.8}$$

The power reading at each detector D_i can be expressed as follows:

$$P_i = G_i\,(\,|b_i|^2 - |a_i|^2\,) = G_i\,(1 - |\Gamma_i|^2)\,|b_i|^2 \quad , \quad i = 3,\ 4,\ 5 \text{ and } 6 \tag{2.9}$$

Substituting (2.8) into (2.9), we obtain

$$P_i = |K_i|^2\,|b_2|^2\,|\,\Gamma - q_i\,|^2 \quad , \quad i = 3,\ 4,\ 5 \text{ and } 6 \tag{2.10}$$

where $|K_i|^2 = G_i\,|M_i|^2(1 - |\,\Gamma_i\,|^2)$ and $q_i = -N_i/M_i$.

This is the fundamental equation to analyse any six-port junction. All design discussions carried out later are based on it.

2.3 Design Criterion of a Six-Port Junction

The first step to design a six-port juncton is to choose scalar values $|K_i|^2$ and complex coefficients q_i in equation (2.10) according to a given configuration. Moreover, a reference port is usually needed to monitor the input incident power level. For this purpose, a directional coupler is used to sample the incident wave amplitude $|b_2|$. In our six-port configuration, port 3 performs this function, consequently equation (2.10) become:

$$P_3 = |K_3|^2 |b_2|^2 . \tag{2.11}$$

Eliminating $|b_2|^2$ from (2.10) by dividing (2.11), we have

$$\frac{P_i}{P_3} = \frac{|K_i|^2}{|K_3|^2} |\Gamma - q_i|^2 \quad , \quad i = 4, 5 \text{ and } 6 \ . \tag{2.12}$$

Assuming q_i and $|K_i|^2$ are known from calibration and the measurement results P_i ($i = 4$, 5 and 6) are given, it is clear that equation (2.12) represents three circles which are centered at q_i and have radii $\sqrt{P_i}|K_3|/\sqrt{P_3}|K_i|$ respectively in the Γ plane as shown in figure (2.2). Suppose that three q_i points are neither on the same line nor located at the same point, the intersection of the three circles will determine the complex reflection coefficient Γ of the DUT port (both magnitude and phase angle). The design problem then becomes how to select all of the coefficeints q_i and $|K_i|^2$ in equation (2.12).

It should be noted that all of the above discussions and mathematical deduc-

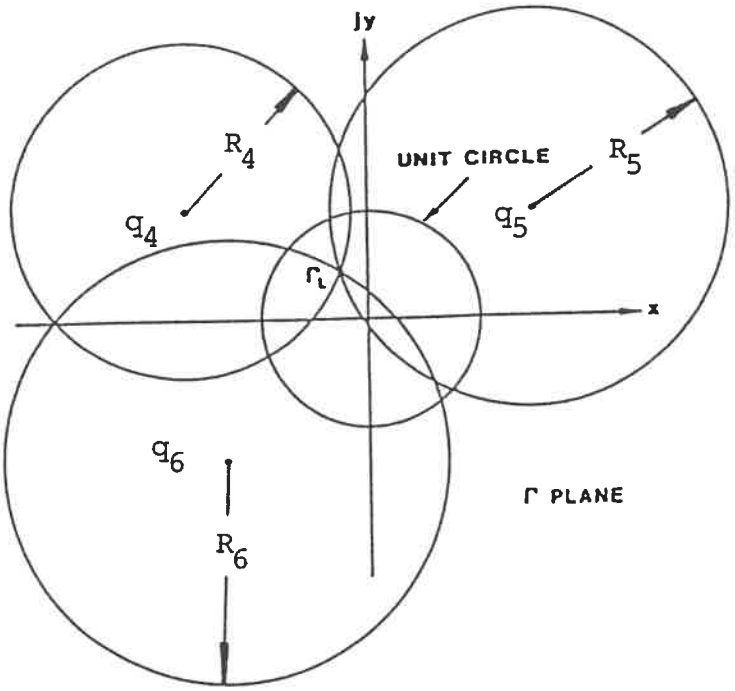

q_i ($i = 4$, 5 and 6) describe the centers of the three circles.
R_i ($i = 4$, 5 and 6) stand for the radii of the three circles, where

$$R_i = \sqrt{P_i}\,|K_3|/\sqrt{P_3}\,|K_i|\,.$$

Figure 2.2: Geometrical Explanation of a Six-port Reflectometer Principle

tions are based on the situation of measurement at a single frequency. This kind of six-port reflectometer can also be used for multifrequency measurements to characterize nonlinear device such as a transistor operated in a nonlinear mode [55]. In these cases, some filters and matching networks should be added between the power detectors and the output ports of the six-port junction in order to separate the signal of each required frequency.

It is evident from inspection of (2.12) that $|K_i|^2$ are scale factors which determine the power levels at the relevant power detectors. Usually these parameters are chosen such that the measured levels are compatible with the dynamic range of power detectors. The major design task, therefore, centers around the choice of q_4, q_5 and q_6. The prospect of achieving a direct measurement of the reflection coefficient magnitude is quite attractive. By choosing q_4, for example, at the center of the unit circle, we can measure directly the reflected wave $|a_2|$ by P_4. There are several considerations, however, which argue against this choice for q_4. The expected deviations of q_4 from zero will eliminate the potential advantages of the six-port junction. A more serious objection arises from the limitation of the power detector dynamic range [9].

From symmetry considerations, the points q_4, q_5 and q_6 of a prefered six-port junction should be located at the vertices of an equilateral triangle, having its center at the origin in the Γ plane. In such case $|q_4| = |q_5| = |q_6|$ while the

relative phase differences between them are 120°. Therefore, the only choice remained is the magnitude of $|q_i|$ ($i = 4$, 5 and 6). Since Γ is determined from the intersection of the three circles, it is evident that an ill-conditioned situation will result when the radii of these circles become too large in comparison with the unit circle for the case of $|\Gamma| < 1$. On the other hand, the choice of $|q_i| < 0.5$ will result in similar problems as q_i is very near to the origin. Therefore, it appears that an optimum value for $|q_i|$ should be expected to lie in the range $0.5 \sim 1.5$. Computer simulations [9] show that the calibration techniques become less accurate if $|q_i| \cong 1$ and a decrease in the measurement accuracy has been verified when $|\Gamma| \cong |q_i|$.

2.4 Measurement Accuracy Estimation

It is convenient to visualize the six-port operation by means of a diagram in the complex plane as explained in section (2.2), where three circles are constructed and their intersection point gives the value of the measured reflection coefficient. The centers of the circles are primarily determined by the six-port characteristics and nominally independent of the reflection coefficient being measured. The circle radii, on the other hand , are proportional to the three normalized power readings P_6/P_3, P_5/P_3 and P_4/P_3.

In practice, due to measurement errors and detector noises, the three circles usually do not intersect at a common point. Their intersection will fall inside a triangle area as shown in figure (2.3). Therefore, how to assign the value of Γ from this triangle becomes the main task to enhance the measurement accuracy of the six-port technology.

For a wide-spread general utility, the preceding picture is only approximate. In fact, the centers of the three circles also have some functional dependence upon the detector readings. To evaluate the accuracy of a six-port junction, the reflection coefficient under test is expressed by the following equation (it will be proved in section (4.1)):

$$\Gamma = \frac{e - w}{cw - d} \tag{2.13}$$

where c, d and e are calibration parameters which are dependent on the six-port junction and power detectors, and w satisfies the following equations [22]:

$$|w|^2 = \frac{P_4}{P_3} \tag{2.14}$$

$$|w - m'|^2 = A'^2 \frac{P_5}{P_3} \tag{2.15}$$

and

$$|w - n'|^2 = B'^2 \frac{P_6}{P_3} \tag{2.16}$$

where m', n', A'^2 and B'^2 are also coefficients related to the calibration parameters of a six-port reflectometer.

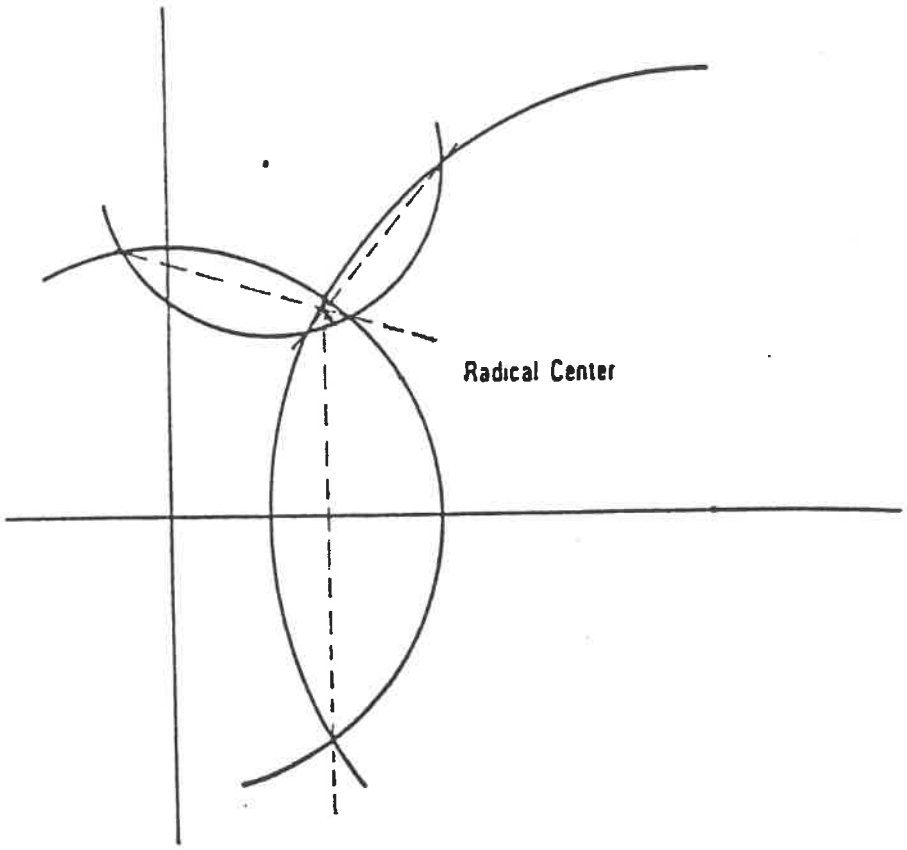

Figure 2.3: Confidence Area of Six-Port Reflectometry Measurements

In order to solve equations (2.14) $\sim$ (2.16), let

$$w = x + jy \tag{2.17}$$

$$m' = x_1 + jy_1 \tag{2.18}$$

$$n' = x_2 + jy_2 \tag{2.19}$$

thus, equations (2.14), (2.15) and (2.16) become

$$x^2 + y^2 = {r_0}^2 \tag{2.20}$$

$$(x - x_1)^2 + (y - y_1)^2 = {r_1}^2 \tag{2.21}$$

$$(x - x_2)^2 + (y - y_2)^2 = {r_2}^2 \tag{2.22}$$

where ${r_0}^2 = P_4/P_3$, ${r_1}^2 = {A'}^2 P_5/P_3$ and ${r_2}^2 = {B'}^2 P_6/P_3$. Subtracting (2.20) from (2.21) and (2.22) respectively, we can obtain a set of linear equations in terms of x and y. A solution of the above linear system gives

$$x = \frac{y_2\left({r_0}^2 - {r_1}^2 + {x_1}^2 + {y_1}^2\right) - y_1\left({r_0}^2 - {r_2}^2 + {x_2}^2 + {y_2}^2\right)}{2\left(x_1 y_2 - x_2 y_1\right)} \tag{2.23}$$

$$y = \frac{x_1\left({r_0}^2 - {r_2}^2 + {x_2}^2 + {y_2}^2\right) - x_2\left({r_0}^2 - {r_1}^2 + {x_1}^2 + {y_1}^2\right)}{2\left(x_1 y_2 - x_2 y_1\right)} \,. \tag{2.24}$$

Assume that the values of parameters $c, d, e, m', n', {A'}^2$ and ${B'}^2$ are known from calibration. Generally speaking, power detector readings P_3, P_4, P_5 and P_6 will differ from their true values. A maximum likelihood estimation of w

via a least square procedure is introduced to find a best estimator of Γ [24]. If the power meter error is assumed to be of Gaussian distribution, it can be shown [22] that the maximum likelihood estimations of P_3, P_4, P_5 and P_6 are minimizing the error function F as follows:

$$F = \sum_{i=3}^{6} \left(\frac{P_i - P_{it}}{\sigma_i} \right)^2 \tag{2.25}$$

where σ_i is the standard variance of the observed values of P_i and P_{it} is the assumed true power reading values which must satisfy equations (2.14), (2.15) and (2.16). In order to impose this constraint, it is convenient to retain P_{3t} as one of the independent variables and then eliminate P_{4t}, P_{5t} and P_{6t} from equation (2.25). The error related to these power detectors is:

$$\varepsilon_3 = P_3 - P_{3t} \,. \tag{2.26}$$

Substituting (2.26) into (2.14) $\sim$ (2.16), we obtain

$$\varepsilon_4 = P_4 - P_{3t} \left| w \right|^2 \tag{2.27}$$

$$\varepsilon_5 = P_5 - \frac{P_{3t} \left| w - m' \right|^2}{A'^2} \tag{2.28}$$

$$\varepsilon_6 = P_6 - \frac{P_{3t} \left| w - n' \right|^2}{B'^2} \,. \tag{2.29}$$

Therefore, equation (2.25) can be expressed in the following form

$$F = \sum_{i=3}^{6} \left(\frac{\varepsilon_i}{\sigma_i} \right)^2 \,. \tag{2.30}$$

At this point, it is only necessary to determine the value of P_{3t}, and then P_{4t}, P_{5t} and P_{6t} are easily deduced from P_{3t} and equations (2.27), (2.28) and

(2.29). The complete solution of this problem is given in [22].

It is noticed that the selection of the function to be minimized is only appropriate when the power meter error is assumed to have a Gaussian distribution. Sometimes the distribution of measurement errors or detector noises show a strong departure from Gaussianity. In this case, the maximum likelihood estimation will be not suitable and a nonlinear minimization is required, which will be difficult to apply in practice. A statistically based method to construct estimators of the reflection coefficient and to compare different six-port designs provides new development to analyse the accuracy of a six-port junction. The details of the method have been introduced in reference [23].

2.5 Conclusion

Basic principles of the six-port technique have been reported in this chapter. Analysis of a six-port reflectometer is developed to emphasize the importance of q_i point positions in designing six-port junction. Based on the significance of the q_i points, the design criterion of a six-port junction has been discussed. Finally, a method to increase the measuerment accuracy of a six-port reflectometer is presented.

Chapter 3

Design of the Wideband Six-Port Junction

3.1 Introduction

The fundamental characteristics of any microwave six-port reflectometer that determine the performance of the reflectometer in measurements are represented by the positions of the four q_i points in the complex plane. In the case of a six-port junction incorporating a reference port to monitor the incident power level, only three q_i points remain pertinent in designing this kind of six-port junctions.

Various proposed microwave six-port circuit configurations are based on the interconnection of several standard four port networks which enable broadband frequency coverage [11,24]. Nevertheless, these six-port circuit configurations

do not satisfy the optimal design goals suggested by Engen as we discussed in section (2.3) [11]. Some efforts have been focused to find simple six-port structures with an optimal q_i point distribution. Successful results have been obtained only in narrow frequency band [25,26,27].

3.2 Configuration of the Six-Port Junction

An integrated prefered six-port configuration with non-standard components is used in this design as shown in figure (3.1), where $PD1$ and $PD2$ are two-way equal power dividers, and Q_1, Q_2, Q_3 are hybrid bidirectional couplers with different coupling levels. It will be shown that an optimal distribution of the three q_i points is obtained by using two nonstandard directional couplers and one $3\,dB$ hybrid directional coupler. The phase compensation with frequency variations is provided by carefully choosing the lengths of the interconnections of transmission lines used in the six-port circuit. For analysis convenience, all of the components in this discussion are assumed to be lossless.

It is noticed that the port 3 is used to sample and to monitor the incident signal in the above six-port junction design. The relations between emergent waves at the four ports and the parameters of the six-port junction shown in figure (3.1) can be deduced by analysing the wave propagation inside the junc-

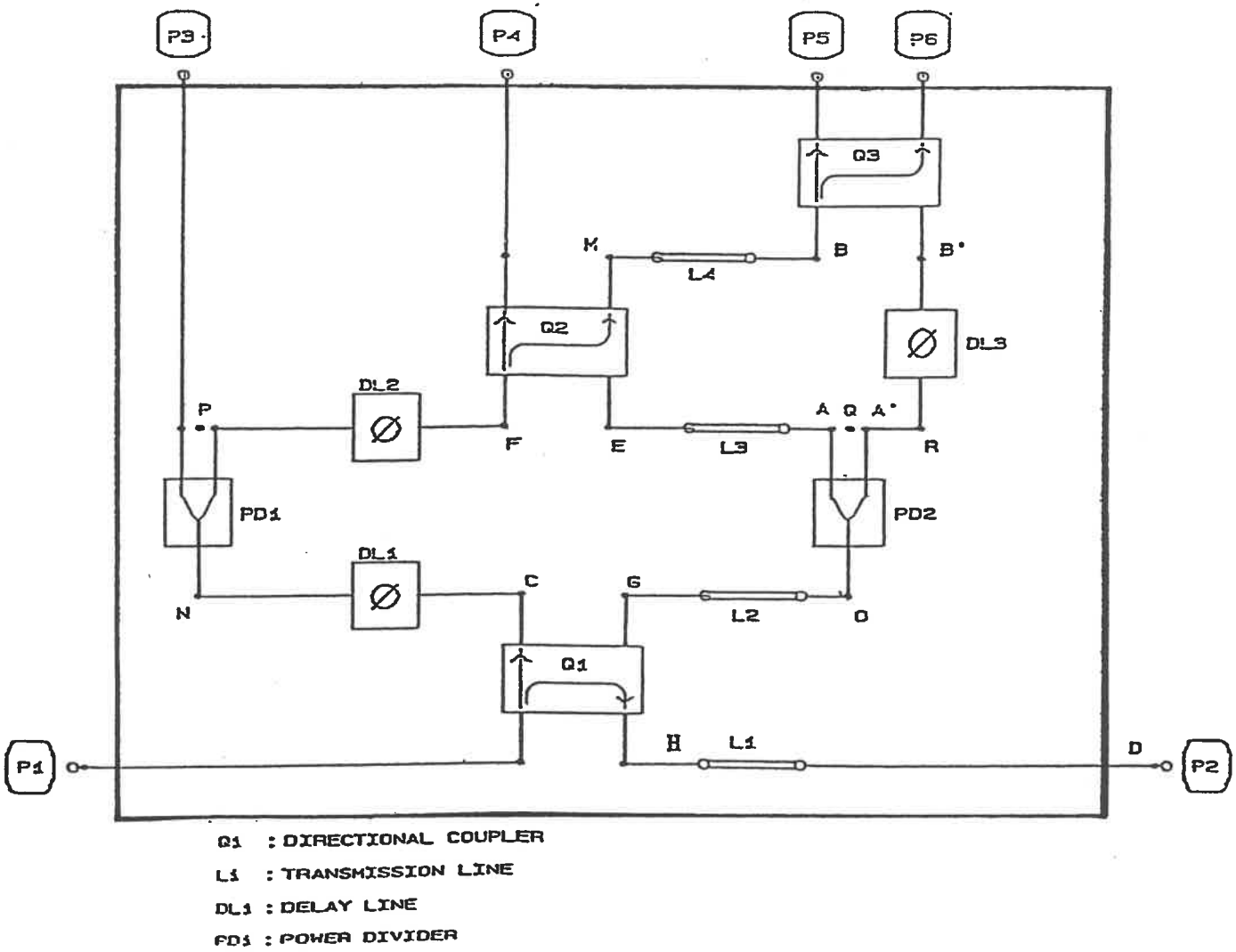

Figure 3.1: A Diagram of Designed Six-Port Junction

tion. The emergent waves at the four detecting ports are:

$$b_3 = \frac{t_1}{j\sqrt{2}c_1} b_2 e^{j(-\phi_2+\phi_3+\phi_5+\theta_p)} \tag{3.1}$$

$$b_4 = \frac{jt_1c_2}{\sqrt{2}} b_2 e^{j(\phi_2+2\theta+\phi_4+\phi_7+\phi_9+\theta_p)} \left[\Gamma - \frac{t_2}{c_1c_2} e^{j(-2\phi_2-\theta-\phi_4-\phi_7+\phi_8+\phi_6)}\right] \tag{3.2}$$

$$b_5 = \frac{t_1}{\sqrt{2}} b_2 e^{j(\phi_2+2\theta+\phi_4+\theta_p+\phi_{11}+\phi_8)} [t_2t_3 e^{j(\phi_7+\theta+\phi_{10}-\phi_8)} + jc_3]$$
$$\cdot \left\{\Gamma + \frac{c_2t_3 e^{j(-2\phi_2+\phi_3+\phi_6+\phi_{10}-\phi_4-\phi_8)}}{c_1[t_2t_3e^{j(\phi_7+\theta+\phi_{10}-\phi_8)} + jc_3]}\right\} \tag{3.3}$$

$$b_6 = \frac{t_1}{\sqrt{2}} b_2 e^{j(\phi_2+2\theta+\phi_4+\theta_p+\phi_{12}+\phi_8)} [t_3 + jt_2c_3 e^{j(\phi_7+\phi_{10}+\theta-\phi_8)}]$$
$$\cdot \left\{\Gamma + \frac{jc_2c_3e^{j(-2\phi_2+\phi_3+\phi_6+\phi_{10}-\phi_4-\phi_8)}}{c_1[t_3 + jt_2c_3e^{j(\phi_7+\phi_{10}+\theta-\phi_8)}]}\right\} \tag{3.4}$$

where $\Gamma = a_2/b_2$, a_2 and b_2 are the incident and reflected waves at the DUT port, θ represents the phase shift through a directional coupler, similarly θ_p is the phase shift through a power divider, c_1, c_2, c_3 and t_1, t_2, t_3 illustrate the coupling levels and transmitting levels of three directional couplers Q_1, Q_2, Q_3 respectively. Under ideal assumption, $c_i{}^2 + t_i{}^2 = 1$, ($i = 1, 2$ and 3) and ϕ_j ($j = 1, \ldots, 12$) represent effective electrical lengths of delay lines HD, CN, GO, PF, AE, $A'B'$, and MB as shown in figure (3.1) .

Comparing above equations with the basic six-port relation in formula (2.10), q_i points can be found as follows:

$$q_4 = \frac{t_2}{c_1\, c_2}\, e^{j(-2\phi_2-\theta-\phi_4-\phi_7+\phi_3+\phi_6)} \tag{3.5}$$

$$q_5 = -\frac{c_2\, t_3\, e^{j(-2\phi_2-\phi_4-\phi_8+\phi_3+\phi_6+\phi_{10})}}{c_1[t_2\, t_3\, e^{j(\phi_7+\phi_{10}+\theta-\phi_8)} + jc_3]} \tag{3.6}$$

$$q_6 = -\frac{jc_2\, c_3\, e^{j(-2\phi_2-\phi_4-\phi_8+\phi_3+\phi_6+\phi_{10})}}{c_1[t_3 + jt_2\, c_3\, e^{j(\phi_7+\phi_{10}+\theta-\phi_8)}]}\ . \tag{3.7}$$

Equations (3.5), (3.6) and (3.7) demonstrate that q_i points will be frequency invariant when the following equations are satisfied

$$\phi_3 + \phi_6 = 2\phi_2 + \phi_4 + \phi_7 + \theta \tag{3.8}$$

$$\phi_8 = \phi_7 + \phi_{10} + \theta\ . \tag{3.9}$$

Substituting equations (3.8) and (3.9) into equations (3.5), (3.6) and (3.7), we can express q_i simply as follows:

$$q_4 = \frac{t_2}{c_1 c_2} \tag{3.10}$$

$$q_5 = -\frac{c_2}{c_1(t_2 + jc_3/t_3)} \tag{3.11}$$

$$q_6 = -\frac{c_2}{c_1(t_2 - jt_3/c_3)}\ . \tag{3.12}$$

The three q_i points, therefore, depend entirely on the choice of the circuit components. Once the coupling levels of the three directional couplers are determined, the three q_i points will be fixed also. Considering the optimum design criterion : $|q_4| = |q_5| = |q_6|$, which are expected to lie within the range of $0.5 \sim 1.5$ and their arguments should differ by $120°$. The latter condition can be achieved, if

$$c_2 = \frac{\sqrt{2}}{\sqrt{3}} = 1.76\, dB \tag{3.13}$$

$$c_3 = \frac{1}{\sqrt{2}} = 3\, dB\,. \tag{3.14}$$

Now the magnitudes of q_i can be adjusted by the choice of c_1. It is clear from equation (3.10), (3.11) and (3.12) that the magnitudes of q_i points are inversely proportional to the coupling level of the first main directional coupler. That means the magnitudes of q_i points will be reduced as the coupling level c_1 increases. As mentioned in section (2.3), if $|q| \cong 1$ or $|q| \cong |\Gamma|$, a decrease in the measurement accuracy will occur. To avoid this problem, the three q_i points are pushed out of the unit circle in Γ plane in this six-port junction design. There are a number of possible variants of the value c_1 to keep the three q_i points out of the unit circle. Not apart from the optimum distribution suggested by Engen, the magnitudes of the q_i points become 1.54, when c_1 is chosen to be

$$c_1 = 0.45 = 6.75\,dB \tag{3.15}$$

Having determined all values of components based on the requirements of the q_i point distribution, the set of values of $|K_i|$ in equation (2.10), which in turn determine the relative power levels of the four signals at the four power detectors should be discussed to complete the design. Returning to equations (3.1) $\sim$ (3.4), it is found out that

$$|K_3| = \frac{t_1}{\sqrt{2}\,c_1} = 1.1 \tag{3.16}$$

$$|K_4| = \frac{t_1\,c_2}{\sqrt{2}} = 0.51 \tag{3.17}$$

$$|K_5| = \frac{t_1}{\sqrt{2}}\,|\,t_2\,t_3 + jc_3\,| = 0.51 \tag{3.18}$$

$$|K_6| = \frac{t_1}{\sqrt{2}}\,|\,t_3 + jt_2\,c_3\,| = 0.51\,. \tag{3.19}$$

The equality of $|K_4| = |K_5| = |K_6|$ displays the advantage obtained by the consideration of phase compensation of q_i points which minimize the requirement to the dynamic range of the four detectors. In such case the same quality power detectors with acceptable dynamic range ($50\,dB$) can be used at the four output ports. This circuit, therefore, provides also an optimal set of the values $|K_i|$ in terms of the power detector dynamic range.

So far, an optimum integrated six-port junction has been described attentively. It is noted that the operating frequency range of the six-port junction

depends mainly on the working bandwith of the components, i.e. power dividers and directional couplers. In this design, the expected frequency range should cover $2 \sim 18\,GHz$.

3.3 Directional Coupler Designs and Measurements

In order to construct a prefered wideband integrated six-port junction, as discribed in section (3.1), three hybrid directional couplers and two equal power dividers which cover a wide frequency range from 2 to $18\,GHz$ should be designed as the first step in designing a complete six-port circuit.

3.3.1 Wideband Directional Couplers with Tight Coupling Levels

A variety of physical configurations for directional couplers with tight coupling levels have been proposed and are used in microwave integrated circuits [28,29,30,31,32,33]. The common used types are branch-line hybrids, re-entrant structures [34], Lange couplers [30,35] and broadside coupled parallel lines or overlap coupled line configurations [33,36,37].

For increasing bandwidth and flatness of frequency responses, a single section of parallel lines should be expended by cascading multi-sections

[29,30,34,38,39]. Whenever multi-section couplers are fabricated for broad-band applications, a significant factor controlling their practical realization is the physical dimensions (i.e. the spacing between two coupling lines) of the middle coupling section. A method to solve this problem has been presented by Shelton in 1965 [29], namely tandem connection technique. It consists of several couplers with lower coupling values which are tandemly connected together in order to design the final coupler with a tight coupling level.

A wide band directional coupler with a slightly tighter coupling level (i.e. 6 dB coupler) can be obtained by suitably cascading broad-side coupled striplines (middle section) and overlap coupled parallel striplines (remaining sections) as shown in figure (3.2). For a 3 dB hybrid or an even more tighter coupler (e.g. 1.76 dB coupler) tandem connection technique must be applied.

3.3.2 Directional Coupler Designs

The 6.75 dB directional coupler can be achieved by using the configuration shown in figure (3.2). The 3 dB directional coupler is obtained by tandemly connecting two 8.34 dB directional couplers as shown in figure (3.4). The same configuration is used to obtain the 1.76 dB coupler from two 6.75 dB directional couplers.

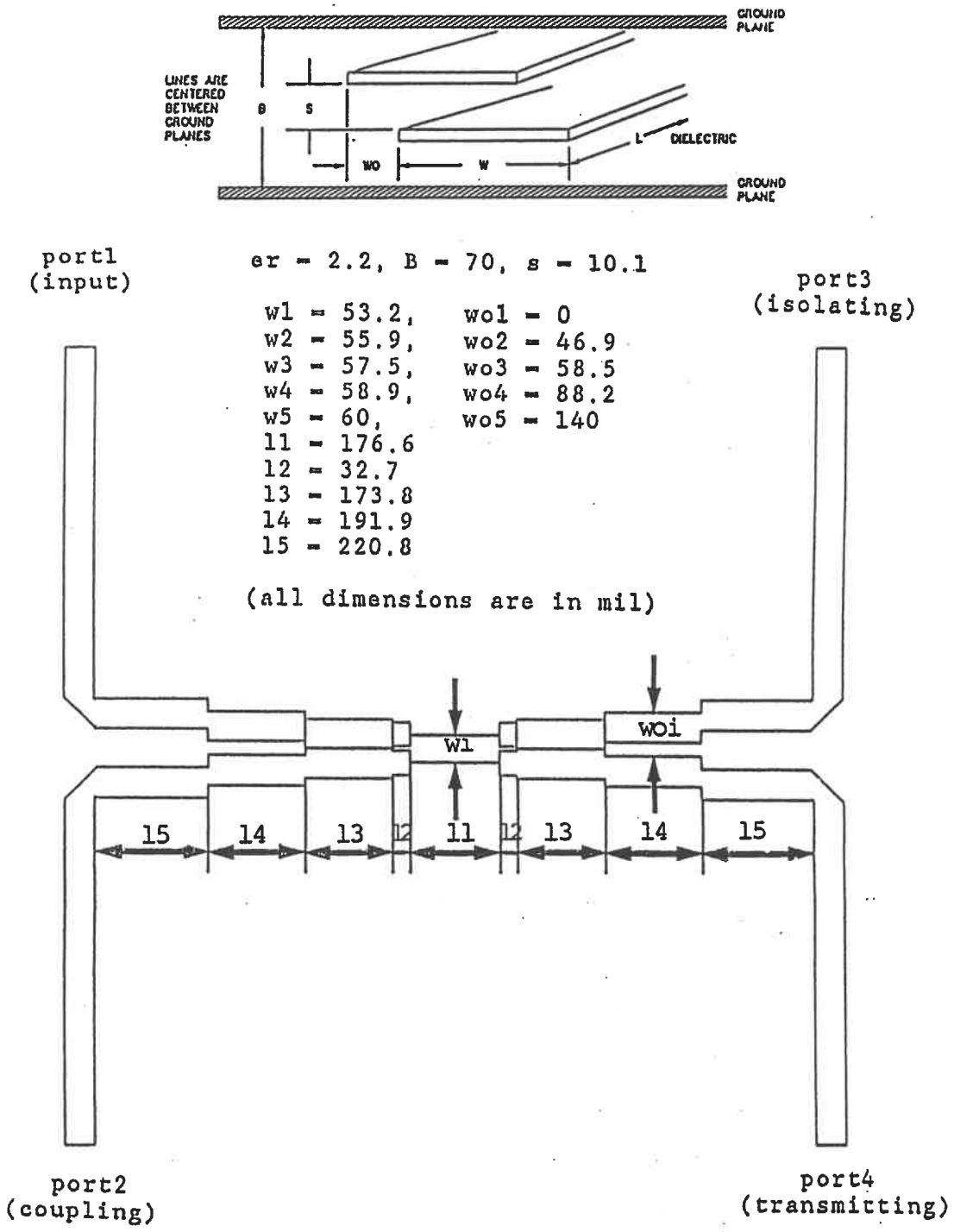

Figure 3.2: The Layout of the 6.75 dB Directional Coupler

For this kind of symmetrical multisection directional couplers, the design procedure is

1. Determine the required number of sections to cover frequency bandwidth $(2 \sim 18GHz)$ [40].

2. According to the coupling level required and the number of sections chosen, synthesize the even- and odd-mode impedances of the individual sections of the coupler by using a commecial software ' Linecalc[1] '[41].

3. Choose appropriately the substrate and its thickness in order to obtain a good performance at high frequency.

4. Based on the special configuration shown in figure (3.2) and the parameters of the substrate selected, calculate the dimensions of the individual sections by means of the even- and odd-mode impedances obtained above.

5. After all of sections connected together, adjust the final dimensions of the complete junction by 'trial and error' so that optimum characteristics, such as coupling level, reflection coefficient and directivity are achieved.

The substrate material is teflon with a dielectric constant of 2.30. The distance between the ground plates B is 1.778 millimeters (see figure (3.2)). The spacing of the center gap of the broad side coupling stripline configuration

[1]Linecalc : trade mark of ESSOF

should be as small as possible to minimize the effect caused by the nonsymmetrical location of the conductor strip lines with respect to the ground planes in the design of the power dividers. The power dividers which will be built up on the same substrate board contain resistors which are solded on two branches of the power dividers. The thickness of such resistors available in our labs is 0.254 mm. Therefore, the thickness of the middle layer substrate should be no less than 0.254 mm. In our design, this value is chosen to be 0.254 mm exactly.

After many iterations by using a ' Touchstone[2] ', a good performance directional coupler with coupling level $6.75\,dB$ has been obtained. The dimensions of the coupler have also been shown in figure (3.2). The simulation results of the coupler are shown in figure (3.3), where s_{11} represents the reflection coefficient, s_{21} stands for the coupling coefficient, s_{41} is the transmitting coefficient and s_{31} expresses the isolation coefficient.

The $3\,dB$ coupler is obtained by two suitably tandem connected $8.34\,dB$ couplers as illustrated in figure (3.4). The $8.34\,dB$ coupler is designed following the previous procedure. To meet the needs of the tandem connection, some stripline miters and transmission striplines with $50\,\Omega$ characteristic impedance must be added between the two less tight couplers. The final dimensions of the optimized $3\,dB$ coupler is also illustrated in figure (3.4). Figure (3.5) shows the

[2]Touchstone : trade mark of ESSOF

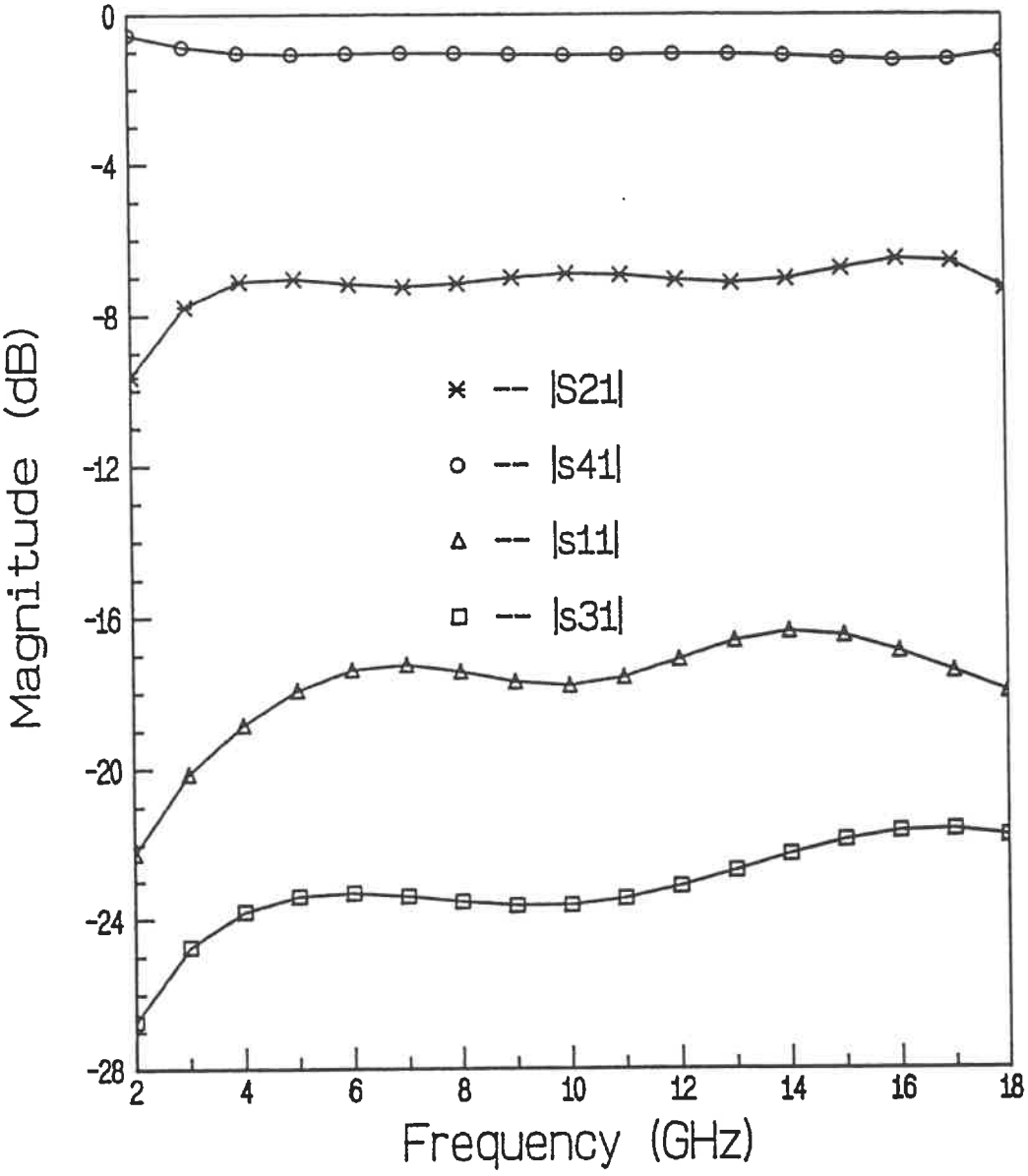

Figure 3.3: Simulation Results of the 6.75 dB Directional Coupler

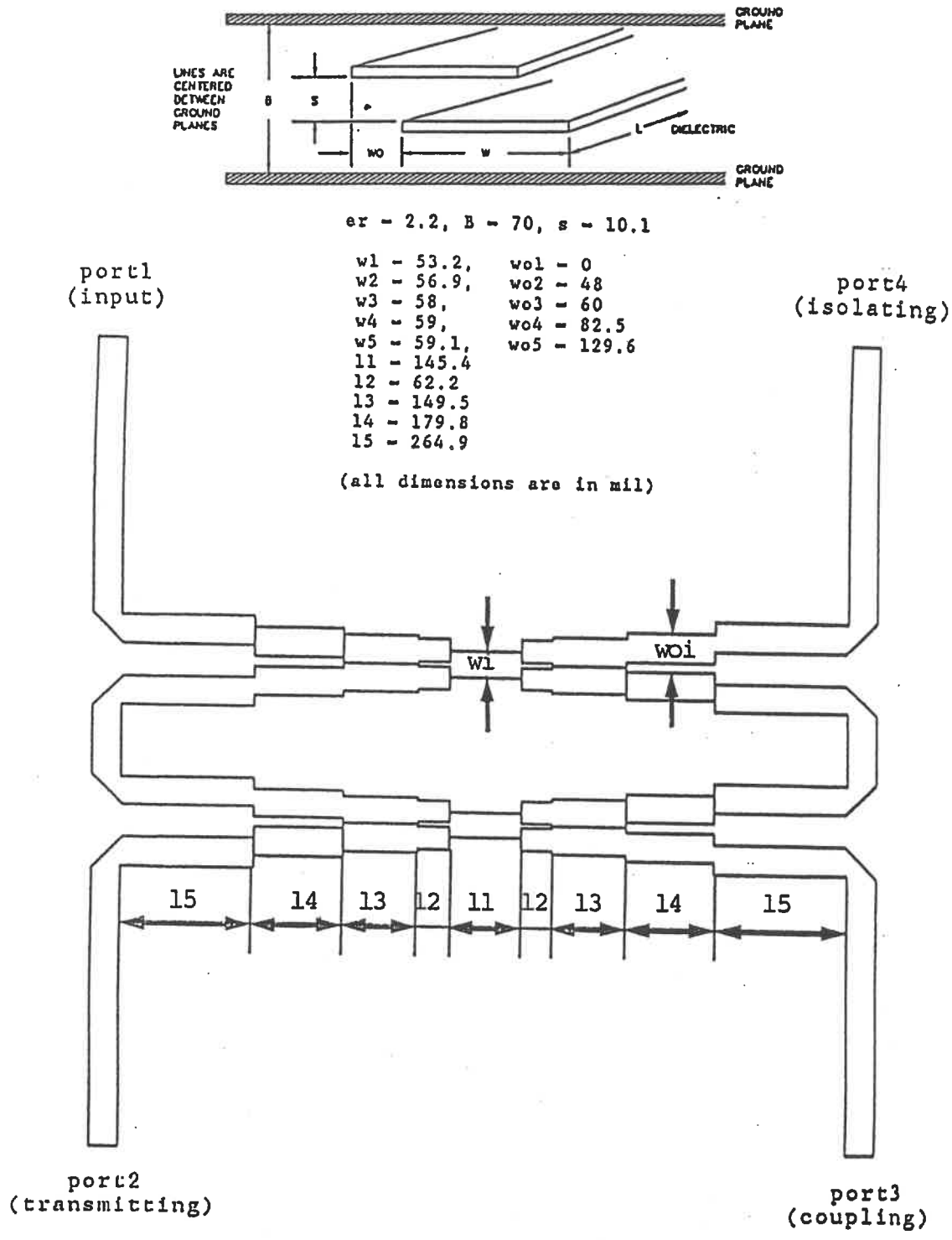

Figure 3.4: The Layout of the 3 dB Directional Coupler

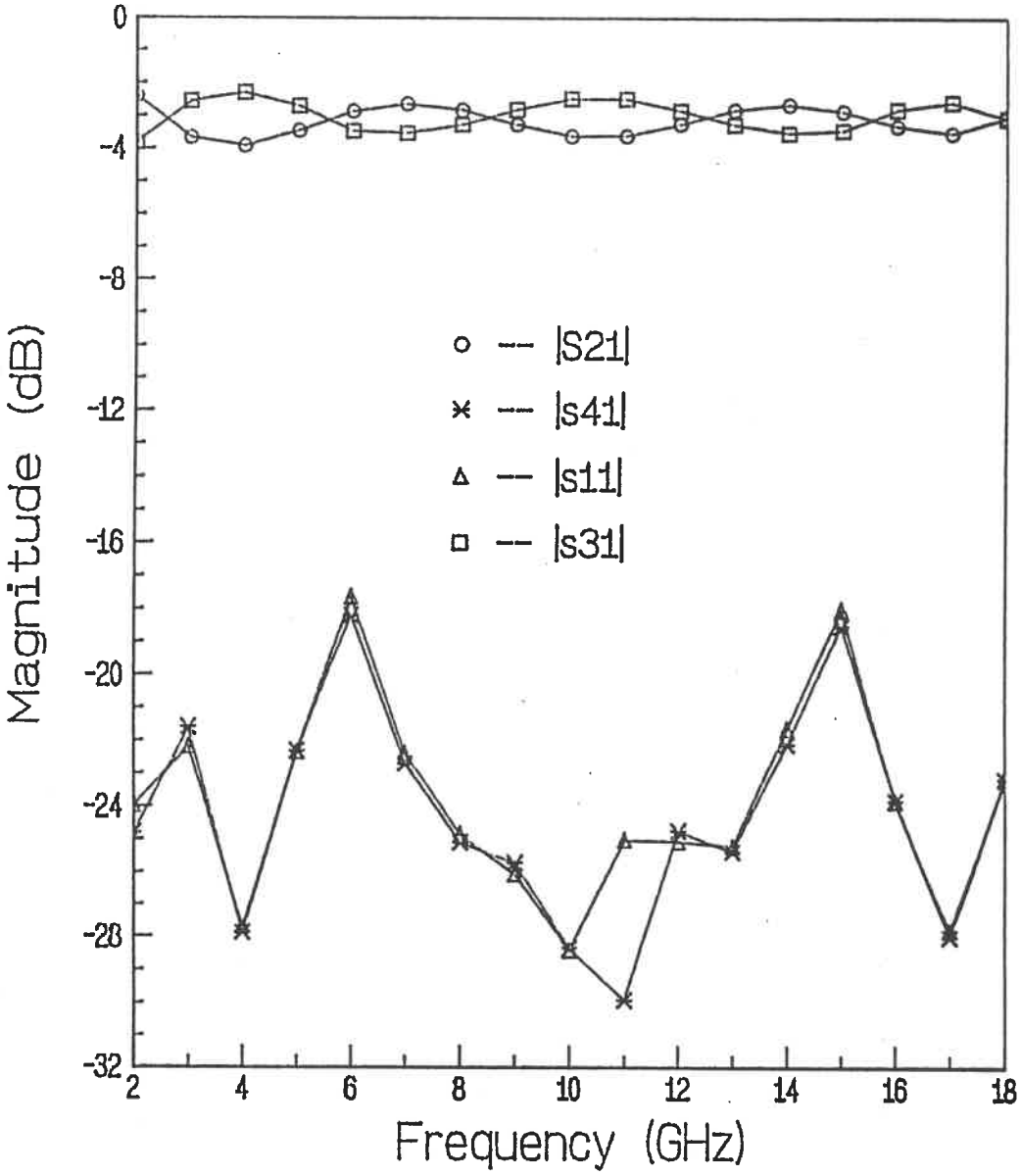

Figure 3.5: Simulation Results of the 3 dB Directional Coupler

simulation results of the $3\,dB$ coupler.

A similar approach can be taken to design a $1.76\,dB$ coupler which is composed of the same configuration as in figure (3.4). A single coupler with a little tighter coupling, i.e. $6.75\,dB$ in stead of $8.34\,dB$, should be designed first. The design procedure has been discussed before. The dimensions of each coupler in tandem section of the $1.76\,dB$ coupler are the same as that of the $6.75\,dB$ coupler as shown in figure (3.2). The simulation results of the designed $1.76\,dB$ coupler by using ' Touchstone ' is given in figure (3.6).

3.3.3 Manufacture and Test of CAD couplers

A block diagram of the measurement system used to test the designed six-port junction and its components is illustrated in figure (3.7). All of the instruments shown in figure (3.7) have wide operating frequency range which covers $2 \sim 18\,GHz$. A simple program has been made to establish the relations between these power ratios and to calculate the S parameter magnitudes of the tested coupler.

The measured magnitudes of S parameters of the $6.75\,dB$, $3\,dB$ and $1.76\,dB$ couplers are shown in figures (3.8), (3.9) and (3.10) respectively. Comparing with simulated results shown in figures (3.3), (3.5) and (3.6), it is obvious that,

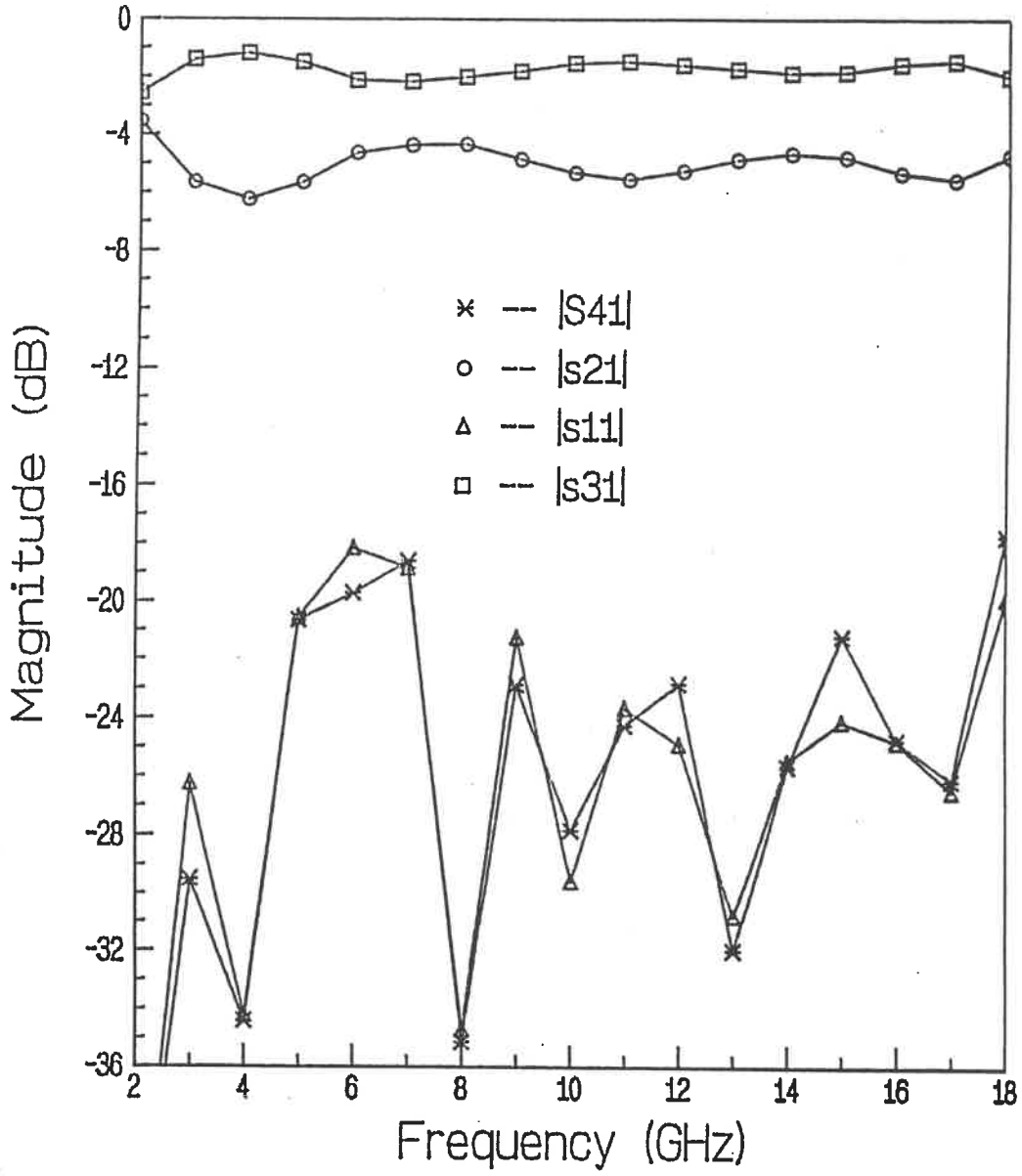

Figure 3.6: Simulation Results of the 1.76 dB Directional Coupler

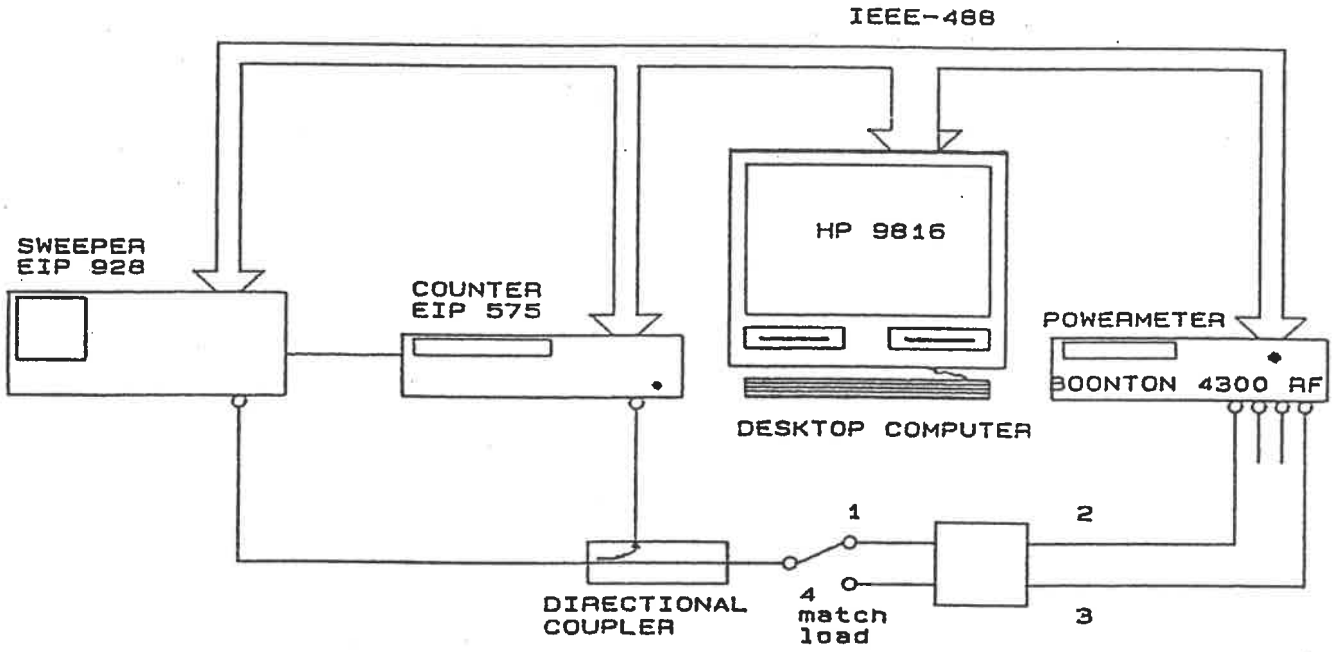

Figure 3.7: The Block Diagram of the Measurement System

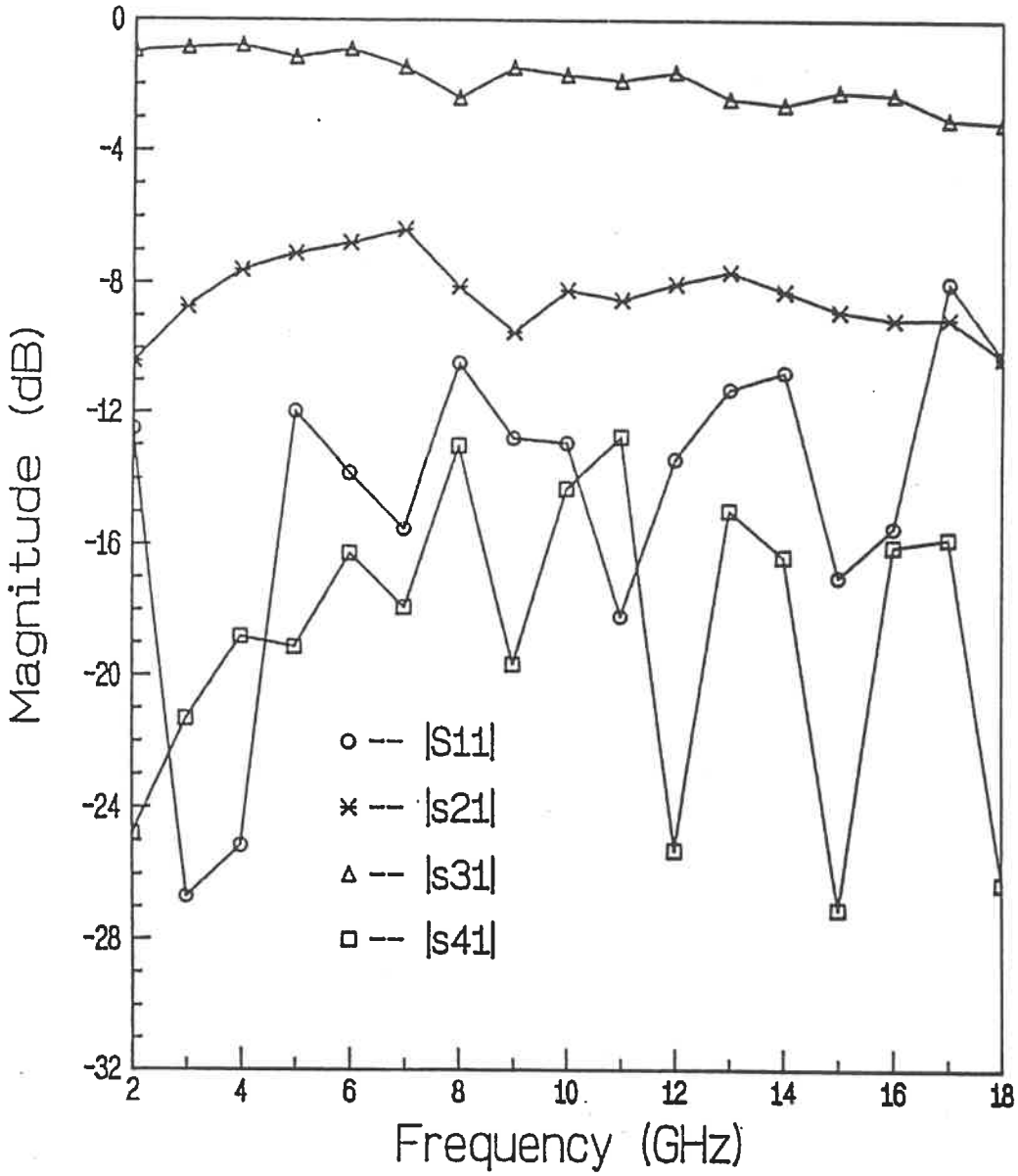

Figure 3.8: Measurement Results of the 6.75 dB Directional Coupler

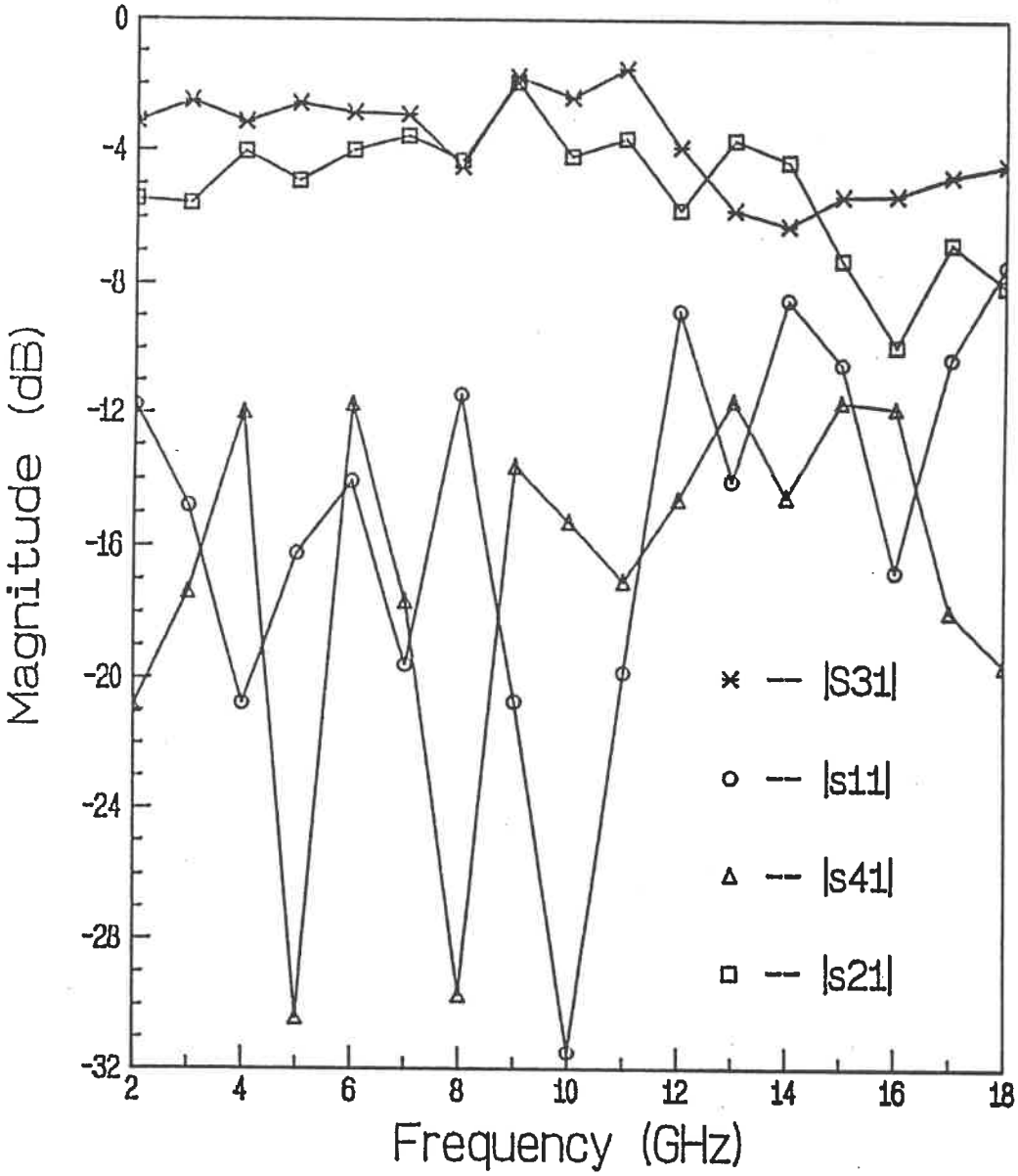

Figure 3.9: Measurement Results of the 3 dB Directional Coupler

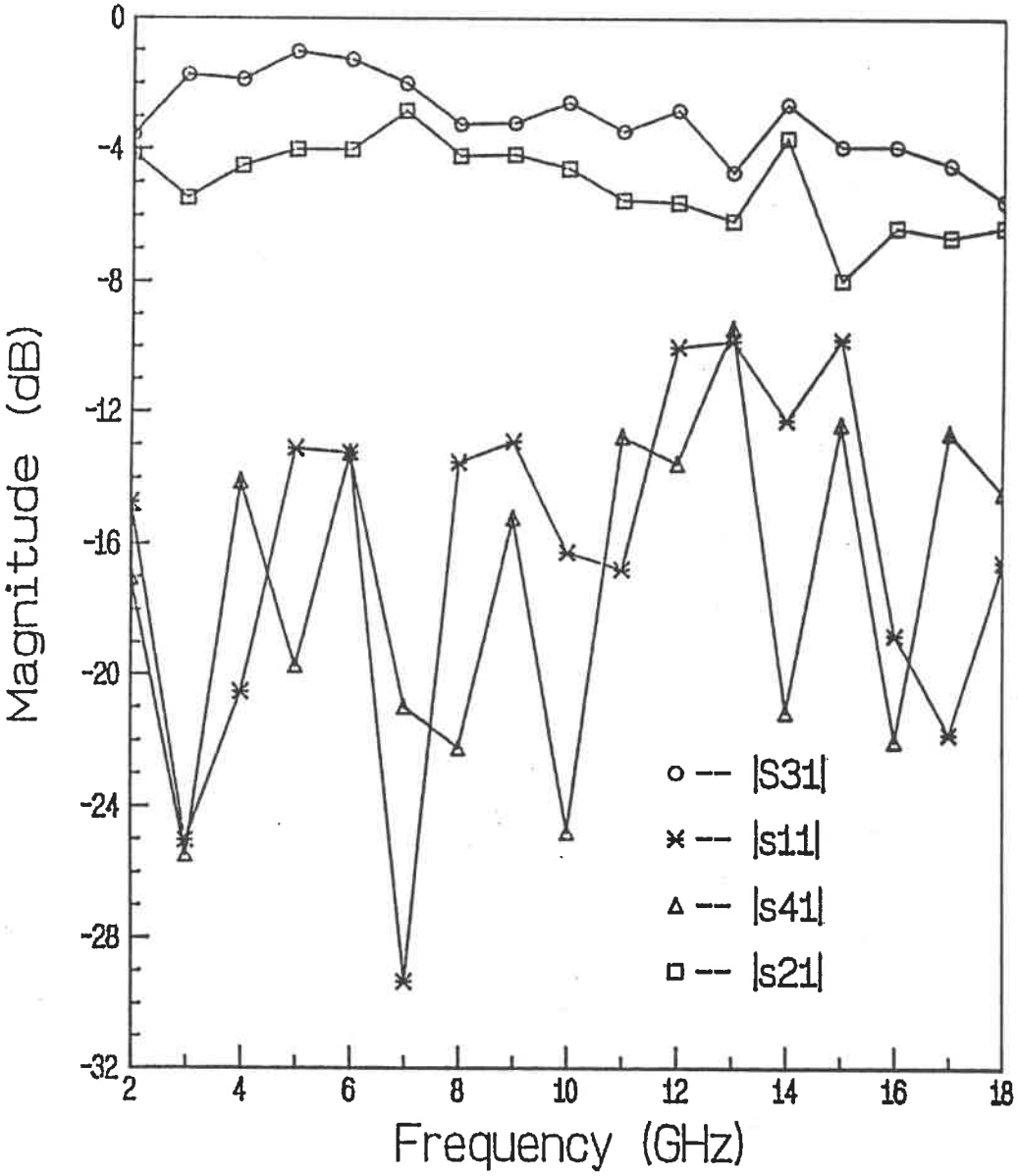

Figure 3.10: Measurement Results of the 1.76 dB Directional Coupler

at low frequencies the measured results are in excellent agreement with the simulated results obtained from ' Touchstone '. At high frequencies, especially above $15GHz$, the coupling level decreases gradually as the reflection coefficient increases. This can be explained by the fact that the radiation loss, the conductor loss and the dielectrical loss of an actual coupler increase with frequency and these effects are more serious above $15GHz$.

3.4 Designs and Measurements of Power Dividers

There are various kinds of microwave power dividers [42,43,44]. A useful broadband circuit for power division with equal phase characteristics at each of the output ports, as well as good isolation between the output ports, may be achieved through use of the series terminated, three port in-line power dividers first introduced by Wilkinson [42]. It consists of pairs of quarter-wave transmission lines terminated by resistors as illustrated in figure (3.11). As the number of individual sections increases, the bandwidth of the device increases also.

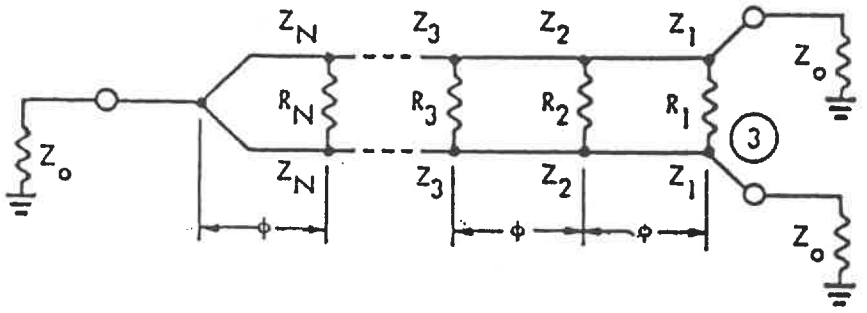

Figure 3.11: Electrical Configuration of a Multi-Section Wilkinson Two-Way Equal Power Divider

3.4.1 Design and Measurement of Stright Branch Line Wilkinson Power Dividers

The procedure of designing a Wilkinson power divider is quite similar to that of the coupler design. The first step is to decide the number of sections of the power divider. A seven-section with seven pairs of quarter-wavelength transmission lines is considered in this design. The impedances and the associated resistors of the individual sections should be determined according to reference [43]. Finally, the software ' Touchstone ' is used to optimize the power dividers in order to satisfy the design objectives.

Two kinds of power dividers are analysed in this thesis. The first kind consists of seven sections with quarter-wave length transmission lines and a right angle splitting as shown in figure (3.12). The second kind possesses the same configuration except that a 30° angle is used instead of the right angle splitting as illustrated in figure (3.13). The latter structure is expected to improve the input match. Measurements show that the characteristics of the structure with 30° angle splitting are improved comparing with the right angle one. Nevertheless, another problem arises. To achieve a high isolation between the output ports over the whole operating frequency range, the resistors must be very small, and the dimensions of resistors available in our labs are 1.52×1.27 mm. This means that the two branches of the power divider must be placed

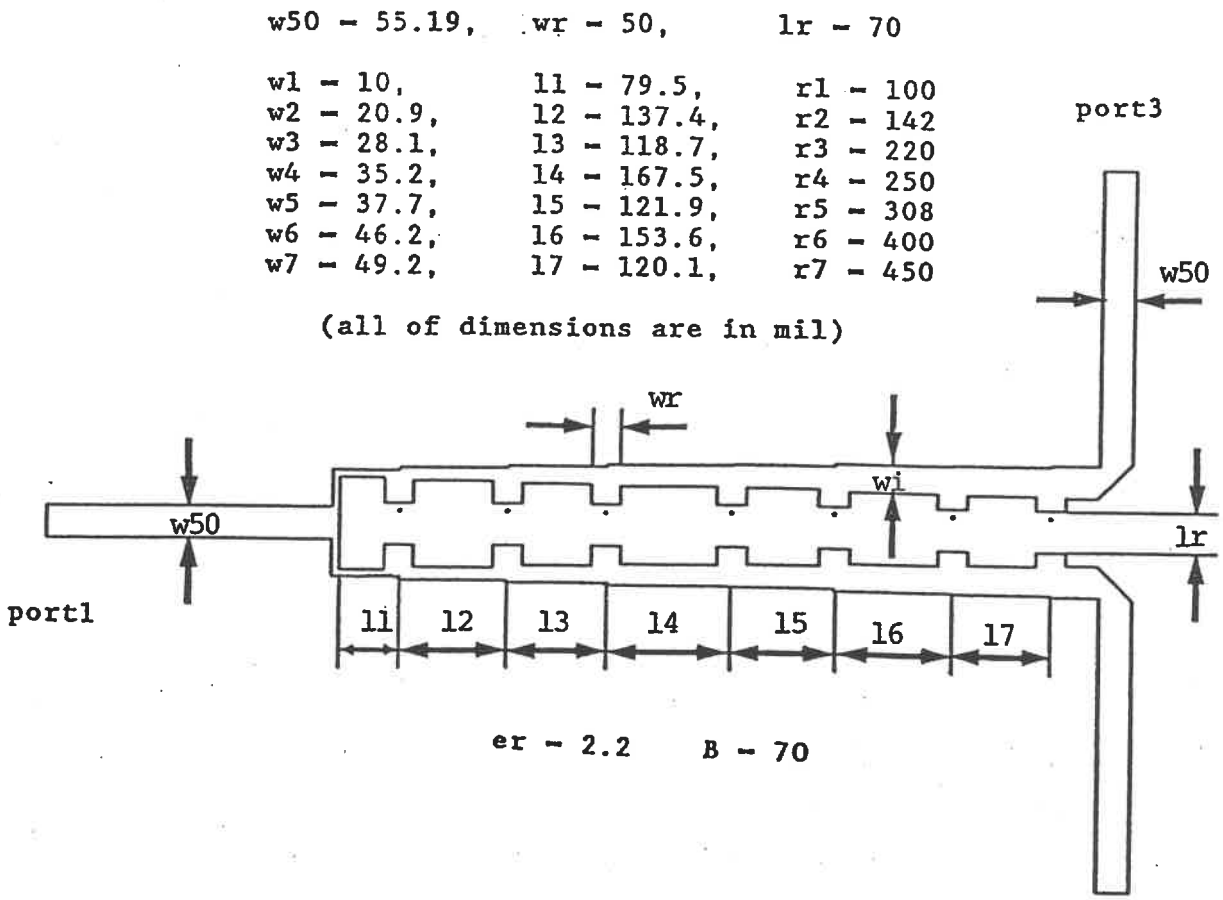

Figure 3.12: The Layout of the Wilkinson Power Divider with Input Right port2

Angle Splitting

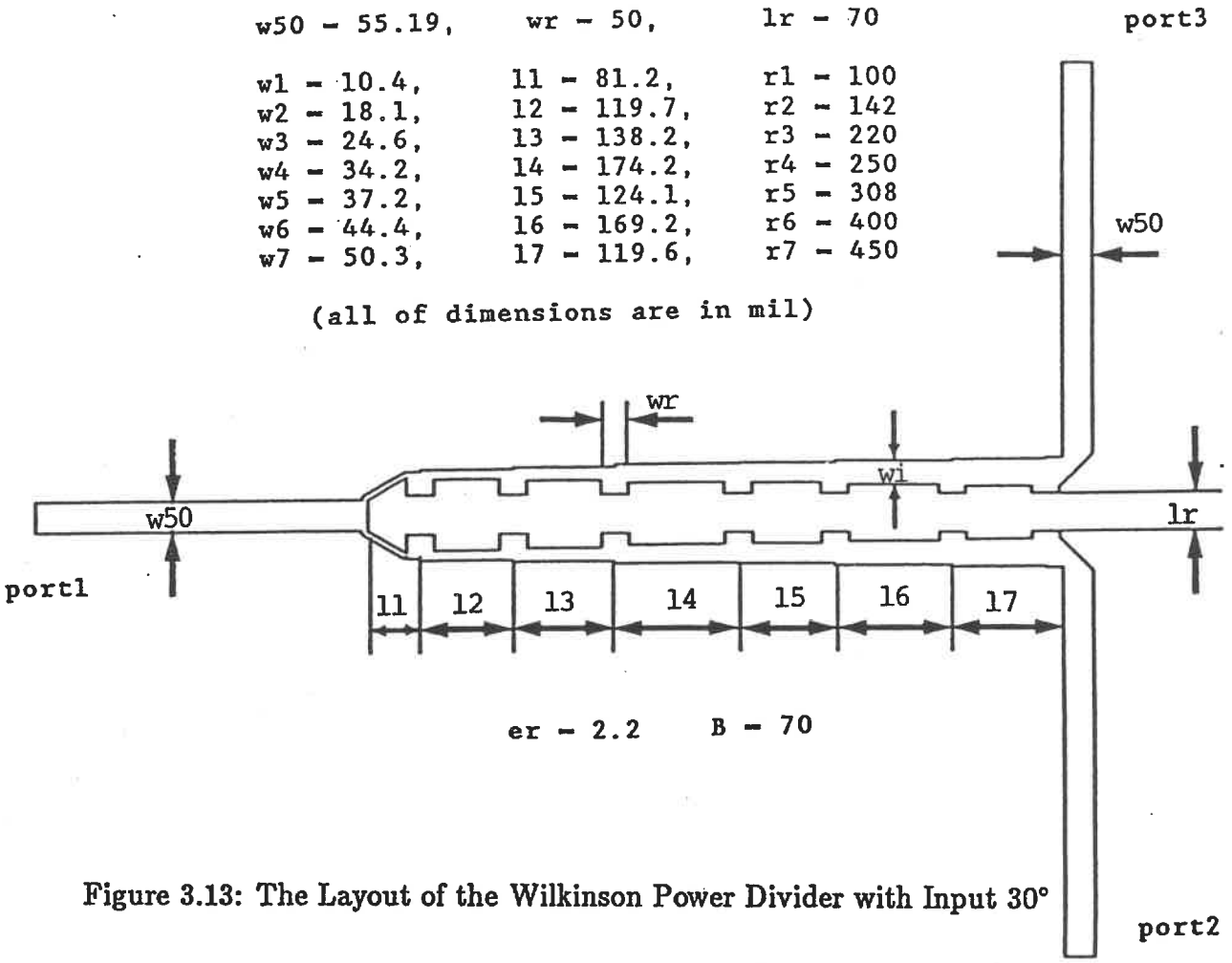

Figure 3.13: The Layout of the Wilkinson Power Divider with Input 30°

Angle Splitting

closely to each other in order to be connected to the resistors, and consequently the mutual couplings between the two branches arise. To avoid these unexpected couplings, the bridging transmission lines have been added between the parallel branches as shown in figure (3.13) to hold the resistors. The negative effects of such bridging lines are the degradation of the isolation between the two output ports. The S parameter amplitudes calculated by using ' Touchstone ' for these two configurations are presented in figure (3.14) and figure (3.15) respectively, where s_{32} represents the isolation between port 2 and 3 which is higher than 20 dB over the whole frequency band, s_{11} is the reflection coefficient at the input port (port 1), s_{21} and s_{31} stand for emergent waves from port 2 and 3 respectively.

Both power dividers have been built using the same manufacturing technique as that used to build the directional couplers. The measurement system used to characterize the directional couplers is also kept for testing power dividers. The measured S parameter amplitudes of the two kinds of power dividers are given in figure (3.16) and (3.17). Comparing these two responses, it can be deduced that 30 ° angle splitting power divider presents more flat responses over almost the whole frequency band and shows less reflection at high frequencies than the right angle splitting one. It is also noted that, the reflection coefficient $|s_{11}|$ and isolation between two output ports $|s_{32}|$ increase sharply after $15 GHz$. The reasons of this problem are probably: the effects of resistor dimensions (re-

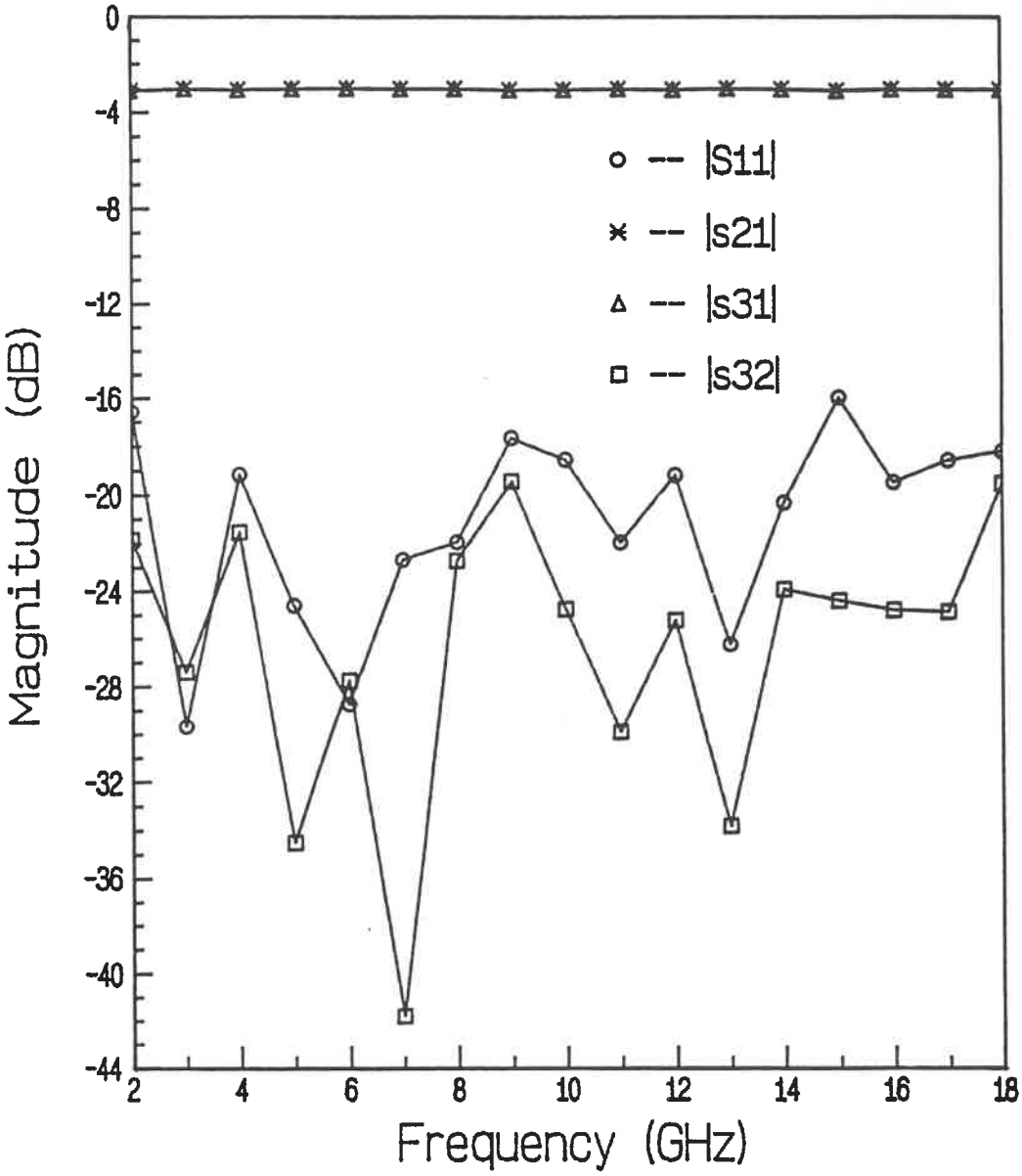

Figure 3.14: Simulation Results of the Right Angle Splitting Power Divider

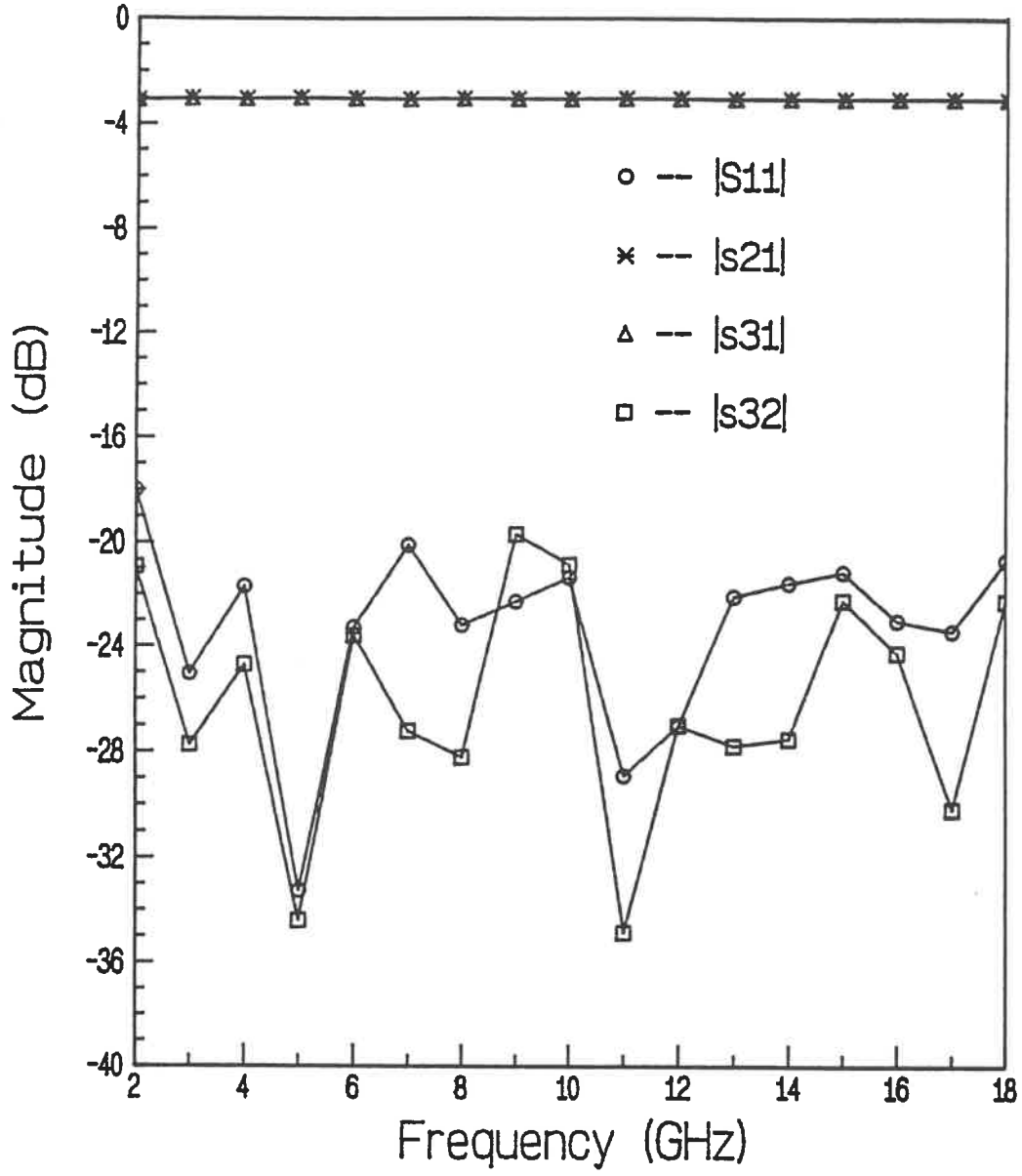

Figure 3.15: Simulation Results of the 30° Angle Splitting Power Divider

sistors should not be considered as lumped elements at high frequencies); the operating frequency range of the resistors; the length of bridging transmission lines for soldering the resistors and the effects of discontinuities introduced by T junctions between each section.

3.4.2 Design and Measurement of a Curved line Power Divider

The step discontinuities between each section of the branch transmision lines and the effects of the bridging lines at the end of each section in a common Wilkinson straight line power divider induce a degradation on its performance, specially at high frequency (i.e. higher than 15 GHz). A solution of this problem will be very attractive if the short bridging lines can be removed away, meanwhile the distances between the two branches of each section can be made large enough to neglect the couplings between them. Fortunately, this solution can be realized when the straight branch lines of each section are bent into half-circles [45,46]. Consequently, bridging lines disappear as shown in figure (3.18). We shall see that in this configuration the bridging lines for soldering the terminating resistors are replaced by the intersection of the two adjacent curved lines, the distances between the two branches of each section are increased and the discontinuity between each section is reduced also.

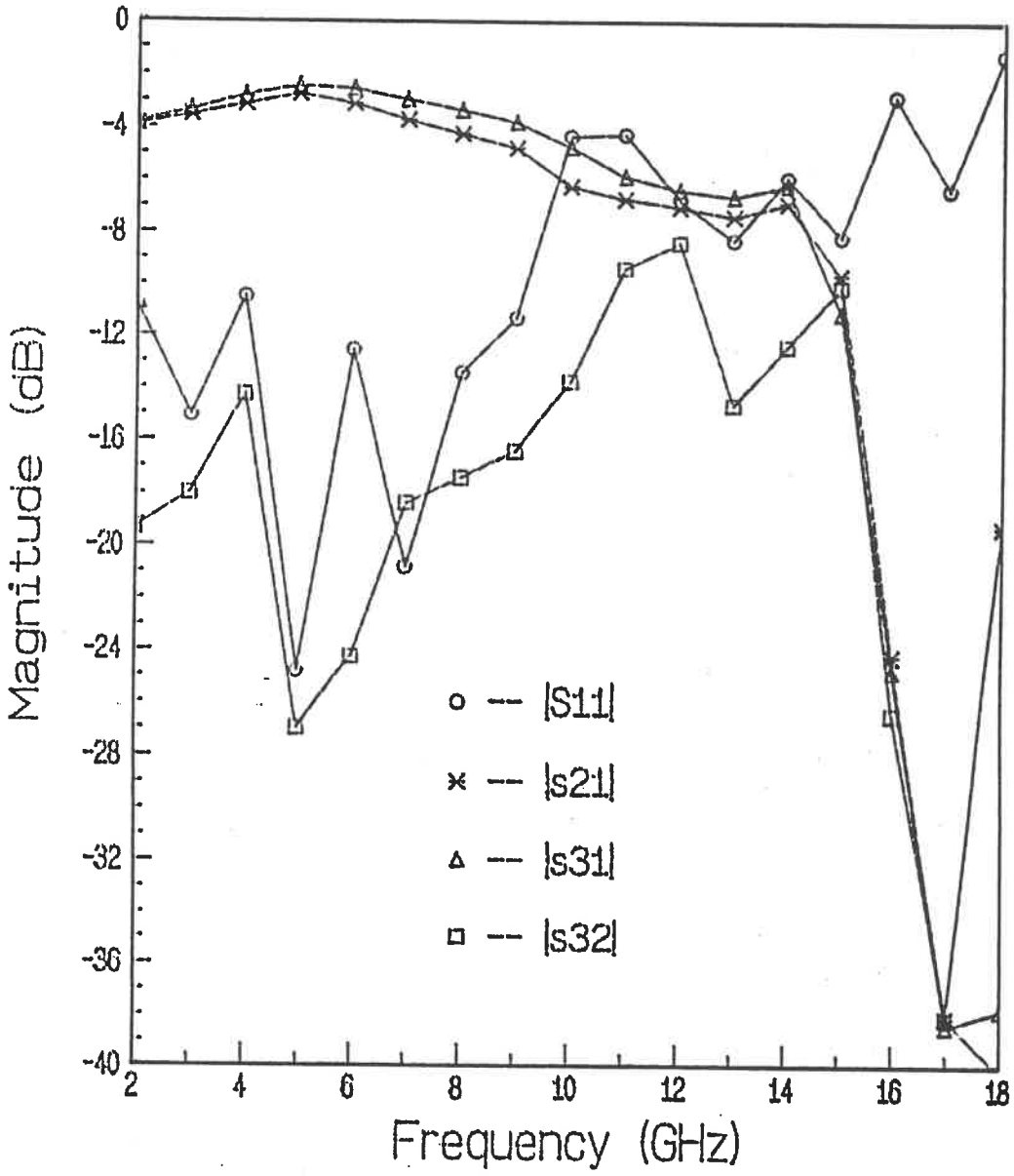

Figure 3.16: Measurement Results of the Right Angle Splitting Power Divider

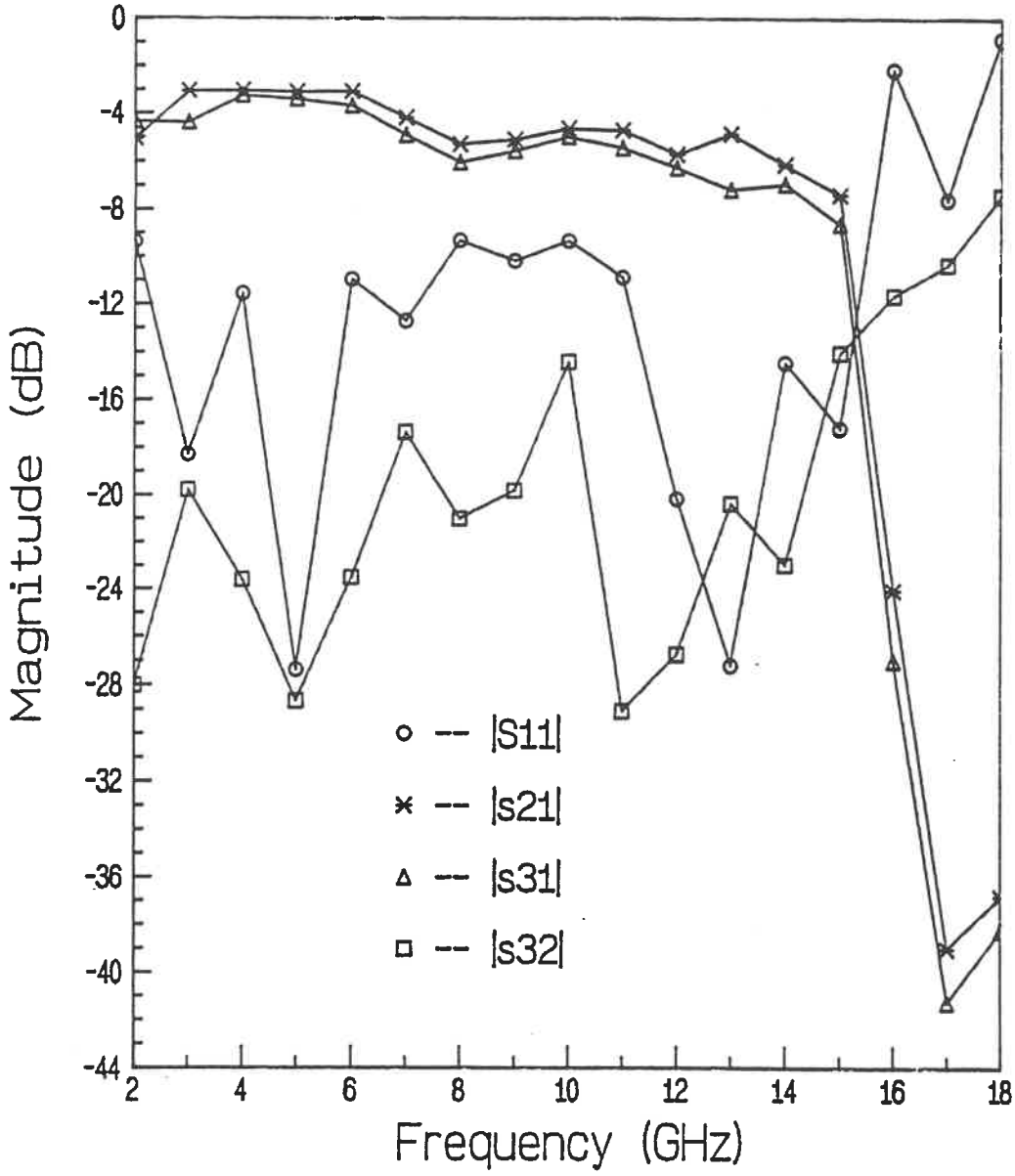

Figure 3.17: Measurement Results of the 30° Angle Splitting Power Divider

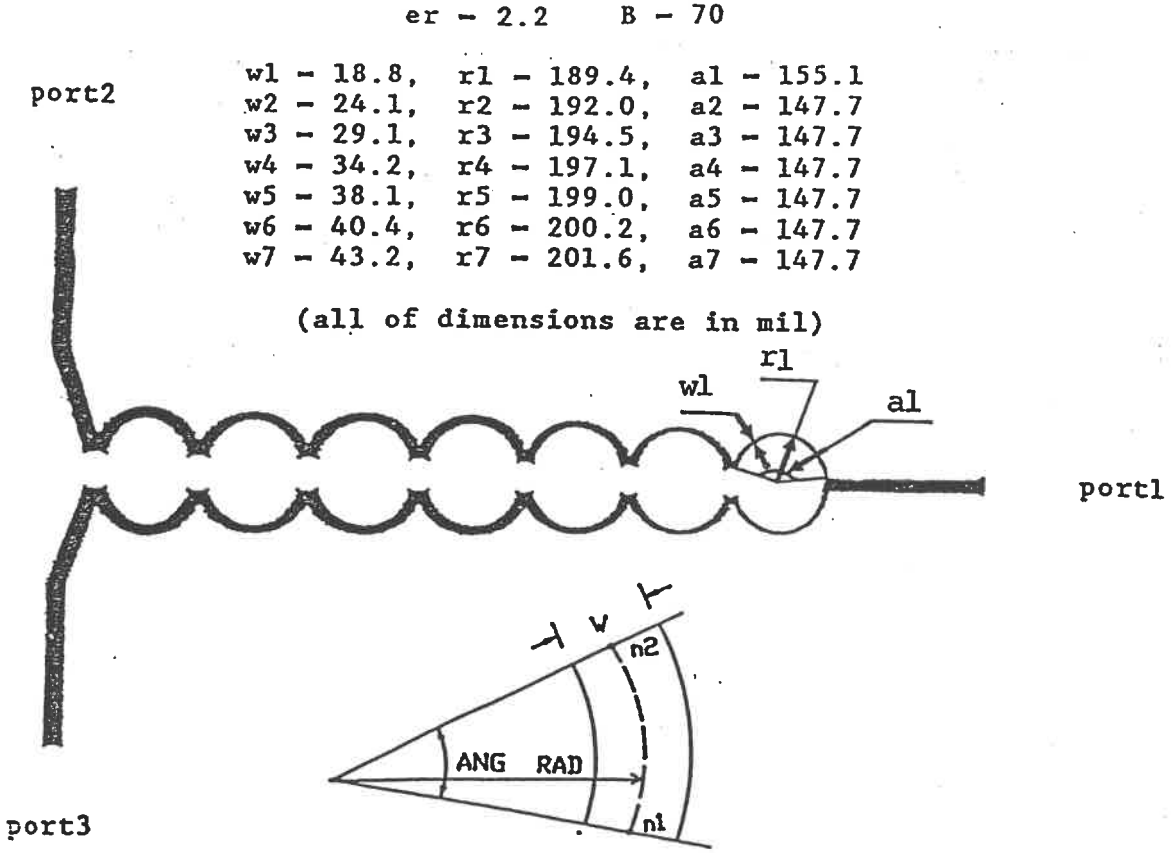

Figure 3.18: The Layout of the Curved Line Wilkinson Power Divider

The values of the impedances and resistors for each section of the curved line power divider are selected to be the same as the values of the stright line power dividers recommended in reference [43]. The physical length of a curved branch in the CAD model is taken to be equal to the median path of the half-circle as shown in figure (3.18). The electrical lengths of the curved line configuration remain initially the same as the straight line configuration because there is no special means to calculate the physical dimensions of the curved stripline by ' Linecalc '. First analysed results of this structure by ' Touchstone ' shows that it is not as well as expected in broadband performances. Optimization techniques are applied again to obtain a good performance. The simulation of S parameter amplitudes after numerous optimizations and the corresponding measurement results are illustrated in figures (3.19) and (3.20) respectively.

Comparing the measured S parameter amplitudes of the straight line power divider with 30° angle splitting in figure (3.17) with that of the curved line one in figure (3.20), it is noted that the reflection coefficient of the curved line structure is not improved much more than the configuration of straight lines, but the isolation between the two output ports of the curved line power divider is much better than the straight line one, and it is even better than the CAD simulated results. This indicates that the simulation models are not effective enough. This result is reasonable since the short soldering lines are eliminated so that the terminating resistors can be connected to the branches directly.

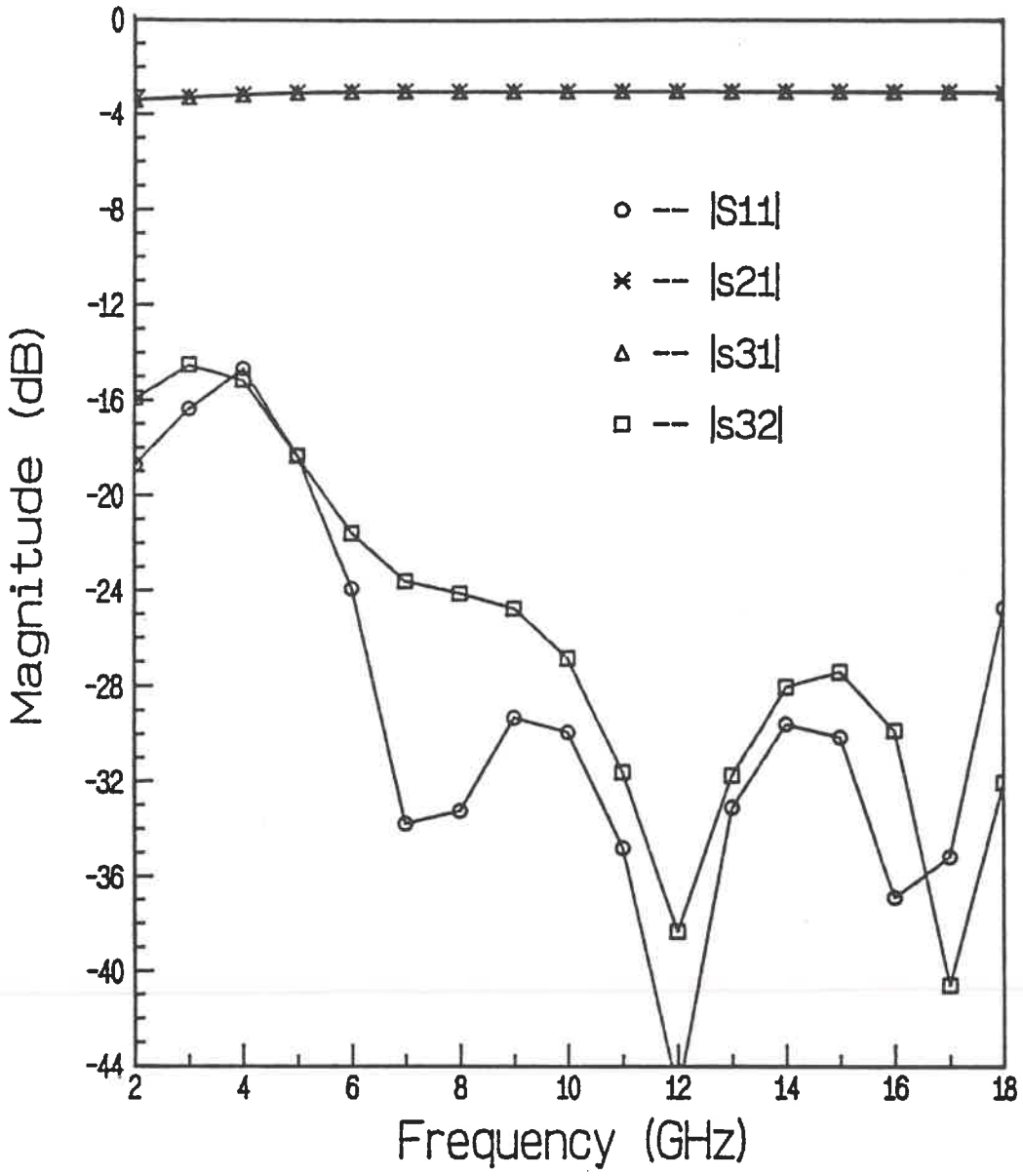

Figure 3.19: Simulation Results of the Curved Line Power Divider

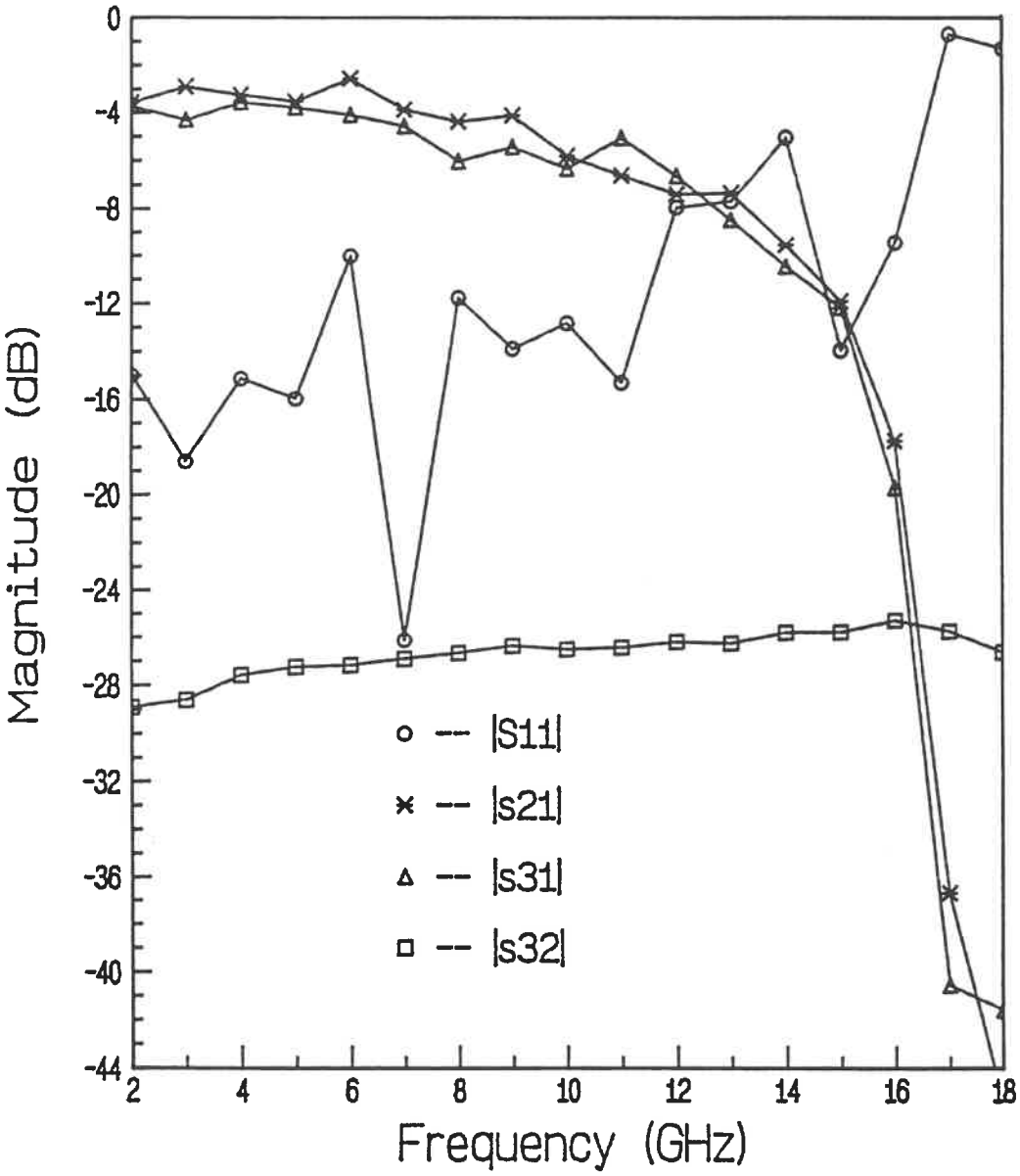

Figure 3.20: Measurement Results of the Curved Line Power Divider

The high reflection coefficients of Wilkinson power dividers with both straight branches and curved branches at high frequencies are caused by many factors. The dimensions of the resistors available are not small enough so that they no longer behave like lumped resistors (their physical lengths are comparable with the wave length of the signal at high frequencies above $15\,GHz$) [45].

3.5 The Complete Integrated Six-Port Junction

In the last two sections , three directional couplers and two power dividers required to build the optimal six-port junction are designed and tested. In this section, we will discuss the interconnection of these components according to the optimal topology shown in figure (3.1) by using $50\,\Omega$ transmission lines and bends.

To make the q_i points fixed with frequency variations and distributed symmetrically in the complex plane by $120°$, two important conceptual equations which involve the lengths of several transmission lines must be satisfied in terms of electrical length requirements as illustrated in figure (3.1)

$$CNPF = HD + DHGOAE \tag{3.20}$$

$$A'B' = AEMB\,. \tag{3.21}$$

In addition to the above two equations, the following three equations must be taken into account to deal with the physical connections of the different components constituting the six-port junction shown in figure (3.1)

$$NCGO = PFEQ \tag{3.22}$$

$$EAA'R = MBB' \tag{3.23}$$

$$ME = B'R\,. \tag{3.24}$$

Since the coupled lines of the three couplers locate in two different layers, the positions of all components and transmission lines at each layer must be determined carefully to avoid the unexpected intercross between top and bottom layers. The layout of the six-port junction is illustrated in figure (3.21). The layouts of the top and bottom layers are shown in figures (3.22) and (3.23) respectively. The important dimensions of the six-port junction which determine the characteristics of the phase compensations are included in six equations as shown in figure (3.22). The meaning of the symbols used in these equations are explained in the following:

l_{abcd} : physical length in mil of the fraction line *abcd*

$l_{3031} = 600$

$l_{1112} = 580$

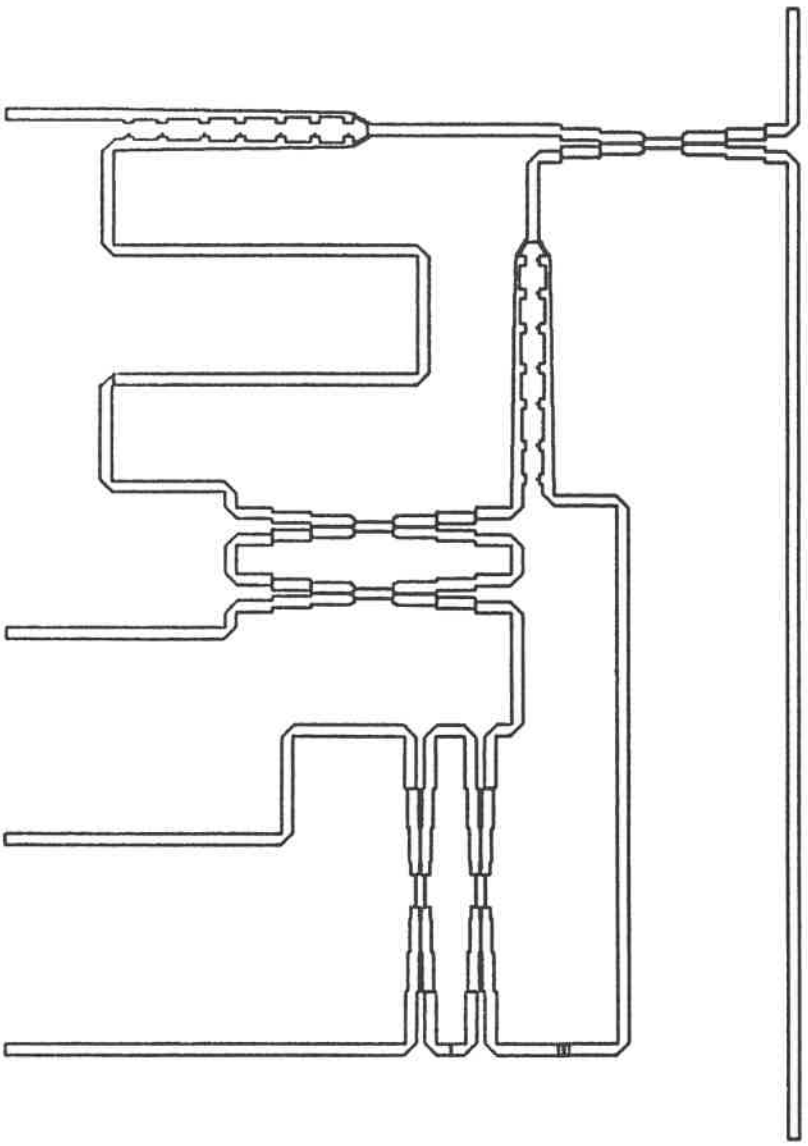

Figure 3.21: The Layout of the *CAD* Six-Port Junction

$l_{3435} = 400$

$l_{0920} = 500$

$l_{3940} = 500$

$l_{econ} = 1756$: effective electrical length of the connector at the port DUT

$l_{eb} = 43.9$: effective electrical length of the stright angle bend

$l_{ecoui}, (i = 1, 2)$: effective electrical length of the i^{th} coupler

$l_{ecou1} = 1278$

$l_{ecou2} = 3252$

$w50 = 55.2$: width of the $50\,\Omega$ transmission line

$wo5 = 140$: offset width of the 5^{th} section for the first coupler

$l_{coui}, (j = 2, 3)$: physical length of the j^{th} coupler

$l_{cou2} = 1546$

$l_{cou3} = 1730$

$l_{pdv} = 1363$: physical length of the power divider

$w_{pdv} = 98.6$: width of the inner outline of the power divider

```
12122 = 13031+lecon-11112-2*leb+(lecou1+3*w50-wo5-lcou2)/2
10405 = 11112+lcou2-lpdv+(w50+wpdv)/2
12324 = lpdv+13435+wo5-2*10920-(7*w50+wpdv)/2
14748 = (lecou2-2*leb-wcou2-lcou3-wpdv)/2
14950 = wcou2+13940-2*w50+lcou3
15152 = (14748+wpdv+2*w50)/2
```

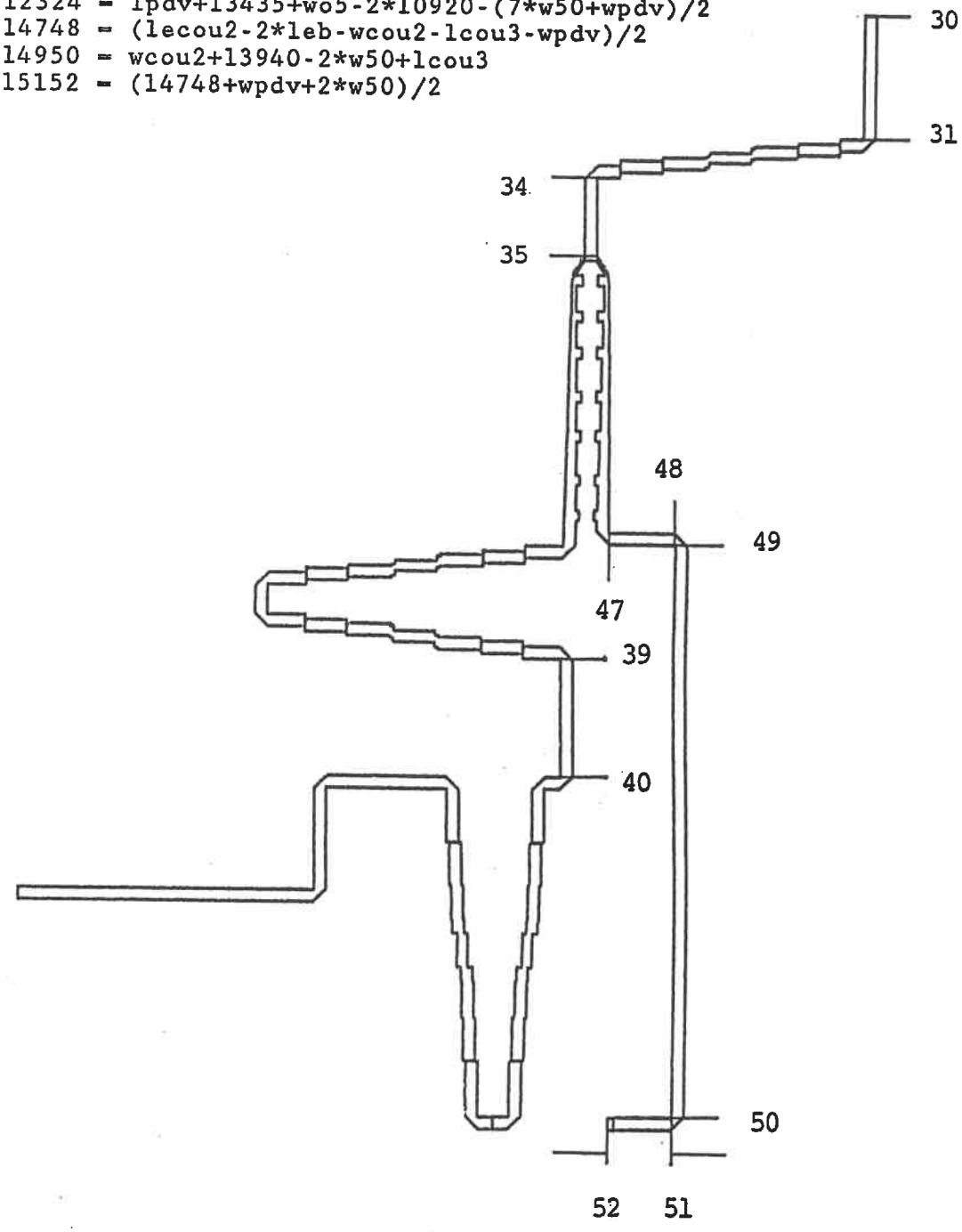

Figure 3.22: The Layout of the Top Layer of the Six-Port Junction

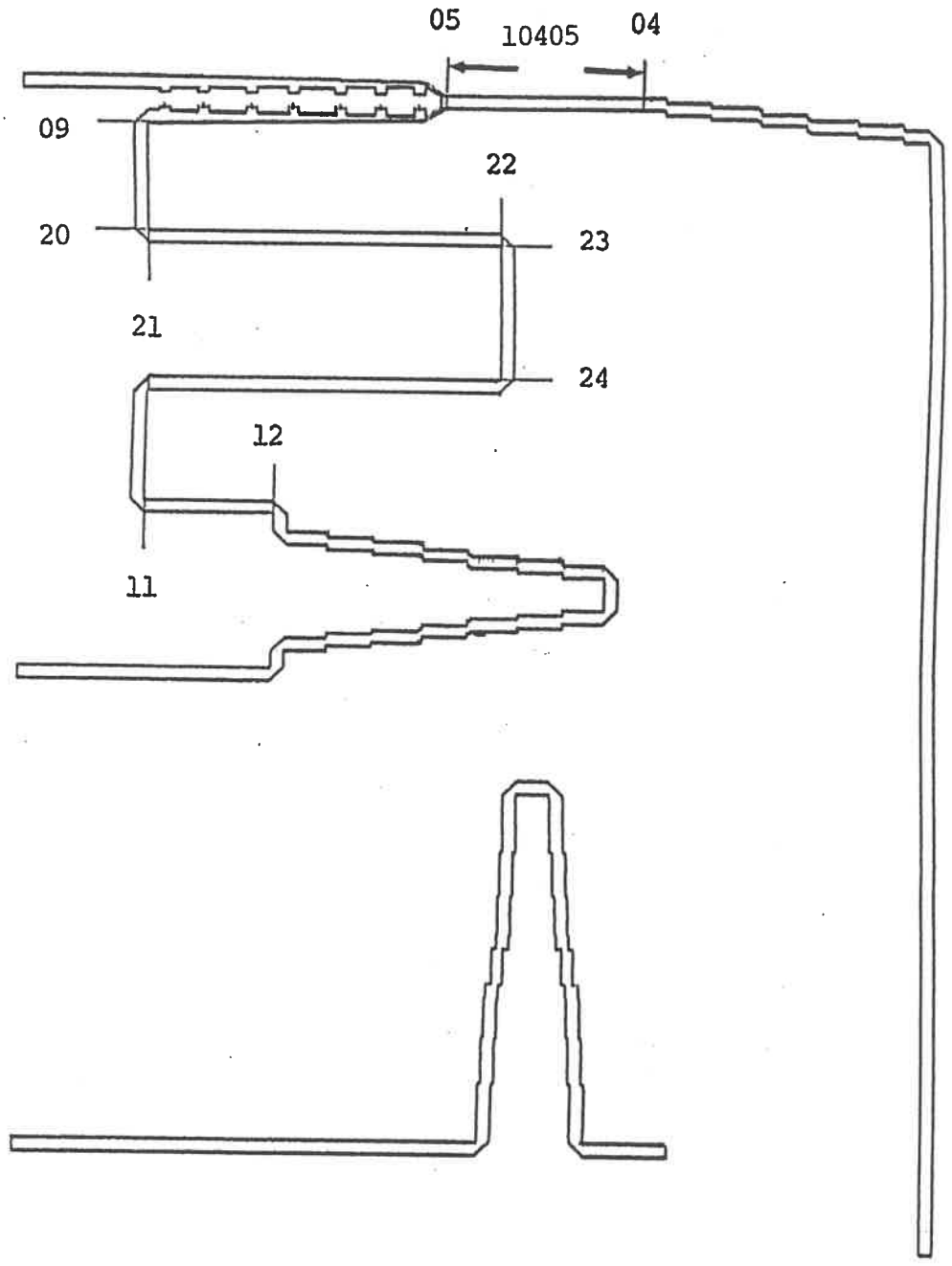

Figure 3.23: The Layout of the Bottom Layer of the Six-Port Junction

$w_{cou2} = 694.4$: width of the outer outline of the second coupler

A tapered via hole with finite metal thickness is unavoidable and must be used to transmit a RF signal from the bottom to the upper layers as shown in figure (3.21). The dimensions of the hole should be as small as possible in order to push its intrinsic resonance frequency higher than $18\,GHz$.

The complete junction can be simulated by ' Touchstone '. As it will be explained later that there is a disagreement between the theoretical analysis and practical measurement of the six-port above $12\,GHz$. For the convenience of comparing these two results, the frequency range of our six-port junction is cut down below $12\,GHz$. The final characteristics of the junction in terms of S parameters are obtained through optimizations. The variations of the q_i point positions with frequency are mostly concerned for our design objective. When output ports of the six-port junction are matched to each power detector, it is shown [47] that the q_i points can be expressed as a function of the six-port scattering parameters as follows:

$$q_i = \frac{s_{i1}}{s_{22}s_{i1} - s_{21}s_{i2}} \quad , \quad \text{for } i = 3,\ 4,\ 5 \text{ and } 6\ .$$

If the junction incorporates a reference port (in our case, it is port 3) to monitor the forward signal ($s_{32} \cong 0$), and the measuring port mismatch is not excessive ($s_{22} \cong 0$), then q_3 becomes infinite as discussed before.

The amplitudes and phases of three q_i points are calculated in terms of a $APC-7$ to N type connector by using the above equations over frequency range $2 \sim 12\,GHz$ and are illustrated in figures (3.24) and (3.25). It is clear that there are some small ripples of the three q_i point positions with frequency variations. This perturbation is caused by many reasons, such as

1. fluctuations of the coupling factors and power dividing levels with frequency;

2. the mismatch of different components at the input and the output ports;

3. the phase unbalance at the output of the couplers and power dividers;

4. the finite directivity of the couplers and the finite isolation between the two branches of the power dividers.

3.6 Conclusion

Three directional couplers ($1.76\,dB$, $3\,dB$ and $6.75\,dB$) and two power dividers have been designed, built and tested. The optimal six-port junction is obtained by connecting the above components and using 50Ω transmission lines. Simulation results show that this six-port junction has the following important advantages: the three q_i points are distributed symmetrically in the complex plane and their positions change little with signal frequency variations

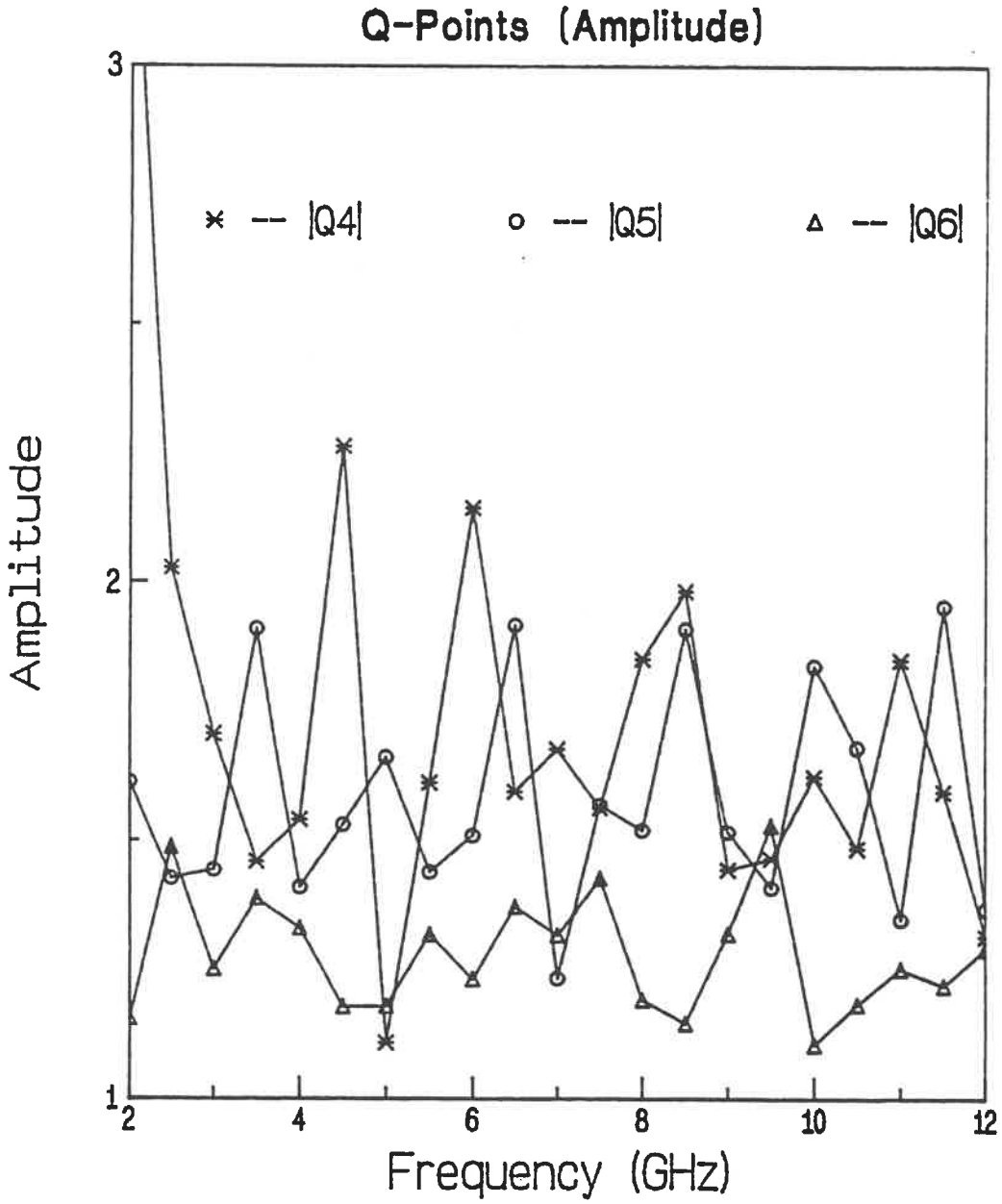

Figure 3.24: Simulation Amplitude Results of the Q_i Point Variations over $2 \sim 12GHz$ Frequency Band with a APC-7 to N Connector

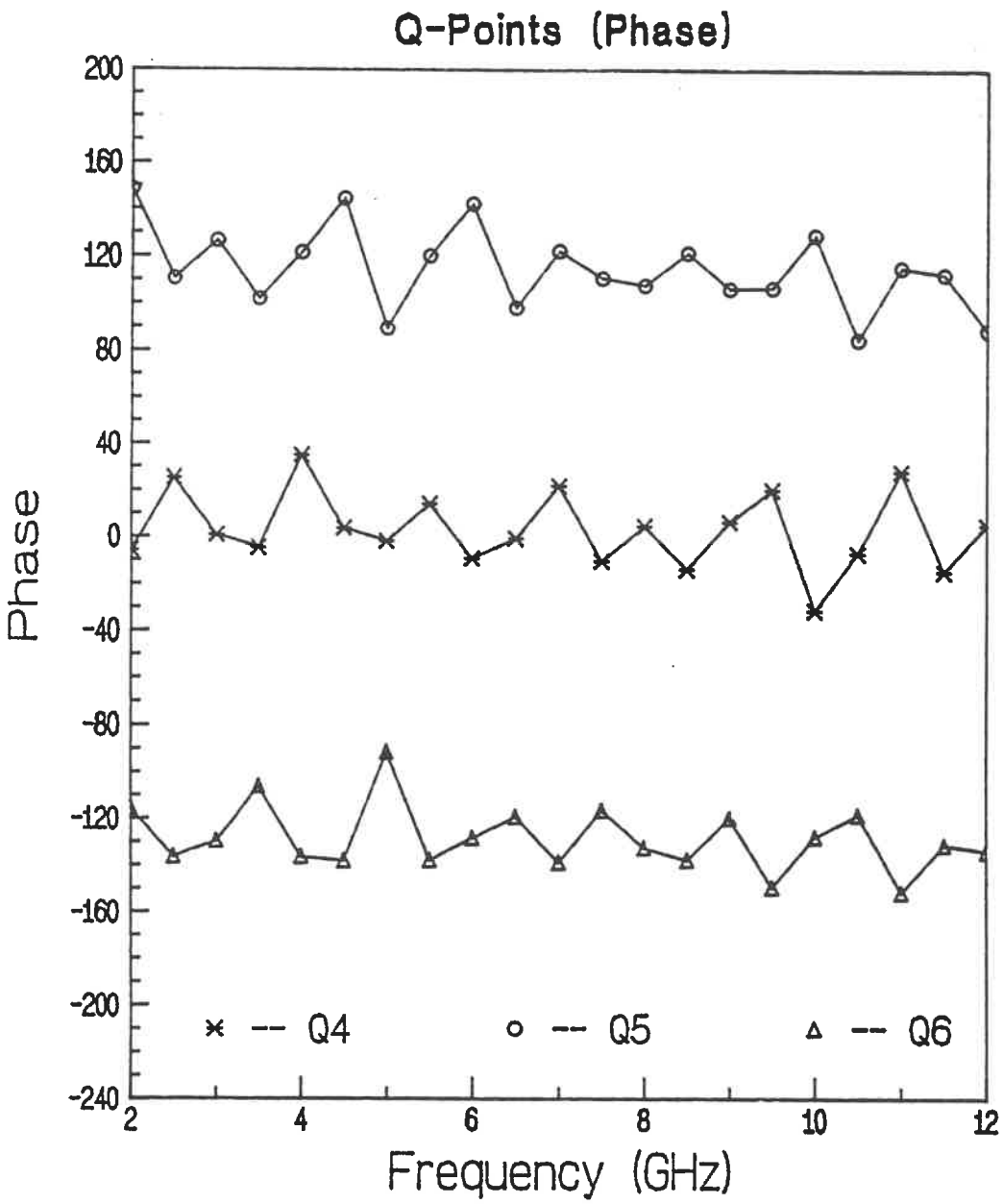

Figure 3.25: Simulated Results of the Phase of the Q_i Point Variations over $2 \sim 12GHz$ Frequency Band with a APC-7 to N Connector

over very large bandwidth ($2 \sim 12 GHz$). This feature minimizes the number of frequency points at which the reflectometer must be calibrated, it also reduces the effect of the frequency instability of the signal source on calibration and measurement results.

Chapter 4

Calibration of Six-Port Reflectometers

4.1 Introduction

Various methods for calibrating a six-port reflectometer have been presented in the past [10,48,49,50,51,52]. The most important differences between these methods are the number of calibrating standards required, the restrictions on the type of standards and the amount of computational effort needed to find the calibrating parameters.

Each method has its own advantages and drawbacks. For example, the calibration using four offset short circuits [10] assumes that in each case $|\Gamma| = 1$. In practice there is loss associated with the short-circuit element (with its offsetting line), but the calibration procedure does not include this information.

Moreover, the use of only reactive calibrating standards leads to reduced confidence in measurements of Γ near the center of the Smith Chart.

4.2 Calibration of the Wide-band Six-Port Reflectometer

To calibrate the designed six-port junction, the method first proposed by Engen [53] and later developed in details by Hodgetts and Griffin [21] is chosen. This method is based on the use of sliding terminations [22] and permits the calibration problem to be separated into two distinct steps. In the first, the six-port is reduced to an equivalent nominal four port reflectometer. This requires the determination of five of the eleven constants which describe the nominal four-port reflectometer. The second part of the problem is to determine the six real (or three complex) parameters, which define the reference plane (error box). This approach has several advantages, i.e.

1. it is not necessary to determine all eleven constants simultaneously;
2. only $3\frac{1}{2}$ known standard impedances are required. In addition, a number of different unknown impedances (at lest 10) are needed;
3. it provides a convenient method of exploiting the redundancy which is inherent in this method.

Details about the algorithm can be found in reference [21]. For the convenience of discussion about the calculations of q_i point positions in the next section, some equations are repeated in the following. The relation between power detector readings and the reflection coefficient of the DUT has been deduced in section (2.1). After the normalization of equation (2.10) by P_3, it gives

$$w_i{}^2 = \frac{P_i}{P_3} = \frac{|d_i\,\Gamma + e_i|^2}{|c\,\Gamma + 1|^2} \quad , \quad i = 4,\ 5 \text{ and } 6 \tag{4.1}$$

where

$$c = -\frac{1}{q_3} \quad , \quad d_i = -\frac{K_i}{K_3\,q_3} \quad , \quad e_i = \frac{K_i\,q_i}{K_3\,q_3} \ .$$

Equation (4.1) can be rewritten as follows:

$$w_K = \frac{d_K\,\Gamma + e_K}{c\,\Gamma + 1} \quad , \quad K = i - 3 \tag{4.2}$$

Solving Γ from these equations, we have

$$\Gamma = \frac{e_1 - w_1}{c\,w_1 - d_1} = \frac{e_2 - w_2}{c\,w_2 - d_2} = \frac{e_3 - w_3}{c\,w_3 - d_3} \ . \tag{4.3}$$

Writing $Q_K = |w_K|^2$ and eliminating Γ from equation (4.3), the following three equations are obtained:

$$Q_1 = |w_1|^2 \quad , \quad A^2\,Q_2 = |w_1 - m|^2 \quad , \quad B^2\,Q_3 = |w_1 - n|^2 \tag{4.4}$$

with

$$A = \left|\frac{c\,e_1 - d_1}{c\,e_2 - d_2}\right| \quad , \quad B = \left|\frac{c\,e_1 - d_1}{c\,e_3 - d_3}\right|$$

$$m = \frac{d_1 e_2 - d_2 e_1}{c\, e_2 - d_2} \quad , \quad n = \frac{d_1 e_3 - d_3 e_1}{c\, e_3 - d_3}$$

where complex numbers m and n can be written as follows:

$$m = M cos\mu + jM sin\mu \quad , \quad n = N cos\nu + jN sin\nu \quad , \quad M, N > 0 . \tag{4.5}$$

Using equation (4.5), one can define

$$p \equiv |m - n|^2 \quad , \quad q \equiv |n|^2 = N^2 \quad , \quad r \equiv |m|^2 = M^2 . \tag{4.6}$$

The embedded reflection coefficient w is related to the reflection coefficient Γ as follows:

$$w = \frac{d\,\Gamma + e}{c\,\Gamma + 1} \tag{4.7}$$

where c, d and e are the error box parameters. These parameters are functions of ${Q_K}^S$ and ${\Gamma_K}^S$. ${Q_K}^S$ are ratios of the power readings P_K/P_3 corresponding to the reflection coefficients of standard impedances ${\Gamma_K}^S$ used in error box calibration procedures. The vector w can be calculated from the five real parameters A^2, B^2, p, q, r and three power ratios Q_K observed for any subsequently connected load. The relation between w and w_1 can be expressed as follows [21],

$$w = w_1(cos\mu - jsin\mu) . \tag{4.8}$$

Substituting equation (4.8) into equation (4.2), one can obtain that $d = d_1(cos\mu - jsin\mu)$ and $e = e_1(cos\mu - jsin\mu)$.

However, the five real parameters A^2, B^2, p, q and r which characterize a nominal four port reflectometer can be found by observing the power ratios corresponding to ten (or more) impedances. The VRC of such impedance must be different and not need to be explicitly known [21]. The procedure to obtain the five real parameters is to solve a set of equations by the standard least square method. It is not necessary to display every details of this procedure, since it has been explained very clealy in reference [21].

At low frequency measurements, the ten different impedance loads can be easily provided by a sliding short circuit and some known standards, i.e. a match load, a short circuit and an open circuit [53]. However, for high frequency applications, there is no sliding short circuit available above 10 GHz. In order to obtain the required number of load terminations at high frequency range, the long line theory [54] is applied. The idea of the theory is that various different impedances along a circle in the Γ plane with its radius equal to or less than unity over the operating frequency range can be obtained by means of a section of delay transmission line, an attenuator and an open / a short circuit termination. A key problem of this theory is to avoid each impedance value from coinciding with another over the whole operating frequency range. The theory originally presented by Hoer [54] serves for ' Thru-Reflect-Line ' (TRL) or ' Thru-Short-Delay ' (TSD) calibration methods. The phase shift caused by

a transmission line (through) is $e^{-j\beta l}$, where l is the physical length of the line. The length of the transmission line should be chosen so that the value of its electrical length must not be or not near multiples of 180°, otherwise the system used to solve the parameters characterizing the six-port reflectometer becomes ill-conditioned. In our case, we expect that the section of delay transmission line plays a role as a phase shifter to replace a sliding short circuit over freqency range $2 \sim 18\,GHz$. The phase shift caused by the line is $e^{-j2\beta l}$ instead of $e^{-j\beta l}$ in the ' through ' situation. Therefore, some equations proved by Hoer in [54] to calculate the length of the transmission line and the phase shift resulted from this line must be modified correspondingly.

Let the calibration frequency step be Δf, the phase shift over each Δf through the transmission line is,

$$\Delta\phi = 2\beta l = 24\, l\, \Delta f \sqrt{\epsilon_r} \tag{4.9}$$

where l represents the length of the line in centimeter, Δf is the calibration frequency step in gigahertz, $\Delta\phi$ expresses the phase shift in degree caused by the delay line at each frequency step, ϵ_r stands for the dielectrical constant of the medium in the transmission line.

If the line length is chosen so that the phase shifts nearest to 180° (denoted by ϕ_{min}) satisfy the following relation,

$$\Delta\phi = 2\phi_{min} \tag{4.10}$$

where

$$\phi_{min} = 90°/(1+n) \ , \ n = 0, 1, 2 \ldots \tag{4.11}$$

and selecting the starting frequency f_1 for the calibration to be one of the following points

$$f_1 = \frac{\Delta f}{2} + n_1 \Delta f \ , \ n_1 = 0, 1, \ldots \tag{4.12}$$

It can be proved that the effective phase shifts nearst to 180° at all frequencies of measurement will be equal to or grater than ϕ_{min} [54]. From equations (4.9) and (4.10) we can obtain:

$$\Delta f = \frac{\phi_{min}}{12\, l \sqrt{\epsilon_r}} \tag{4.13}$$

Hence, the length of the transmission line can be determined by

$$l = \frac{\phi_{min}}{12\, \Delta f \sqrt{\epsilon_r}} \ . \tag{4.14}$$

There are several available values of ϕ_{min} and their relevant lengths of the transmission line from equations (4.11) and (4.14), when n is an integer ($n = 0, 1, 2 \ldots$). In our calibration procedure, $\phi_{min} = 90°$ and the corresponding length of the transmission line $l \cong 6.6$ cm have been chosen.

By adopting this technique, thirteen standards have been obtained and are grouped as following:

1. A match load, an open circuit and a short circuit.

2. An open circuit and a short circuit plus this delay line, which produces two values along the unit circle in the Γ plane with $90°$ phase different from open circuit and the short circuit as shown in figure (4.1).

3. An open circuit and a short circuit with a $3\,dB$ attenuator, which provides two points on the circle $|\Gamma| = 0.707$.

4. An open circuit and a short circuit with a $3\,dB$ attenuator plus the delay line, the situation is the same as case 2 except that the two points are located on the circle $|\Gamma| = 0.707$.

5. An open circuit and a short circuit with a $6\,dB$ attenuator.

6. An open circuit and a short circuit with a $6\,dB$ attenuator plus the delay line.

The choice of the standards according to the above method ensures that the calibration system to be solved is well-conditioned. Consequently no singularity over the whole operating frequency band is expected. The distribution of the impedances on the complex plane obtained from the thirteen standards is shown in figure (4.1).

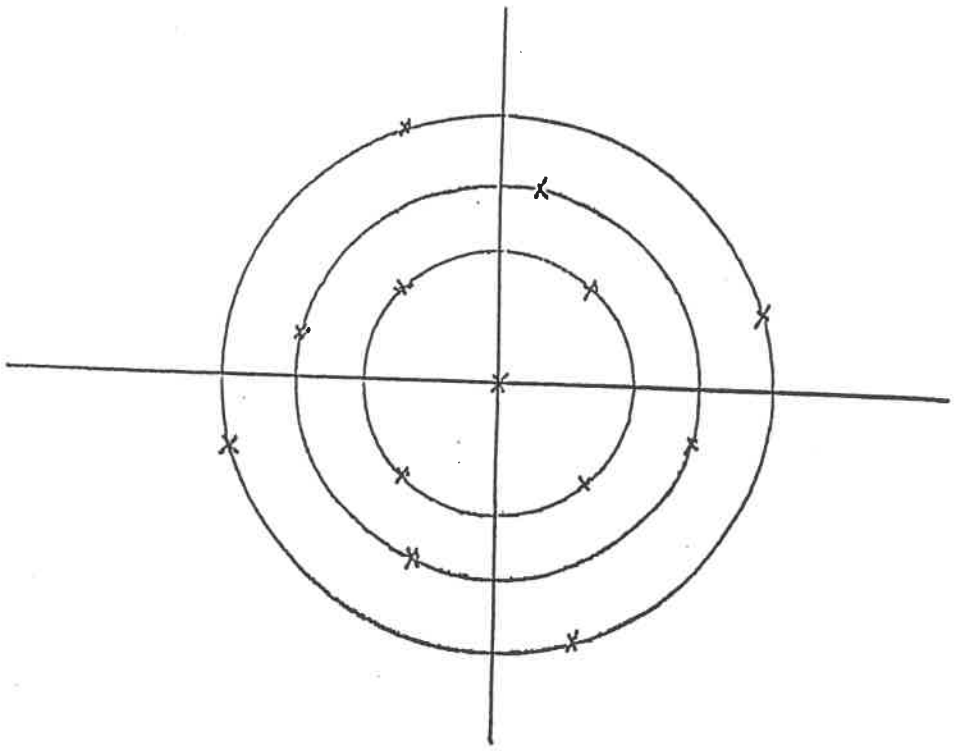

Figure 4.1: Impedance Distribution of Thirteen Calibration Standards on the Complex Plane

The six-port reflectometer discussed before is calibrated by means of this method over frequency range of $2 \sim 12\,GHz$. After the calibration, the designed six-port junction is used to measure an open/short circuit (Wiltron Co. model 22A50). The measurement results of this open/short circuit by using the six-port junction are compared with the calculation result as shown in figure (4.2) and (4.3). The measurement result of the six-port circuit displays a very good agreement with the numerical calculation.

4.3 Calculation of q_i Points

The variations of the q_i point positions with frequency are most concerned in this design. An interesting result from a computer simulation has been discussed in section (3.4). After the calibration of a six-port junction, its q_i point positions over the operating frequency range can be calculated from the calibration parameters.

It is noticed that equations (4.4) express three circles in w_1 plane, their centers are 0, m and n respectively. The solution for these equations of w_1 is given geometrically by the intersection of the three circles. That means, in fact, it is w_1 not Γ that will be determined by the intersection of three circles. However, w is related to Γ via a bilinear transformation. Solving Γ from equation

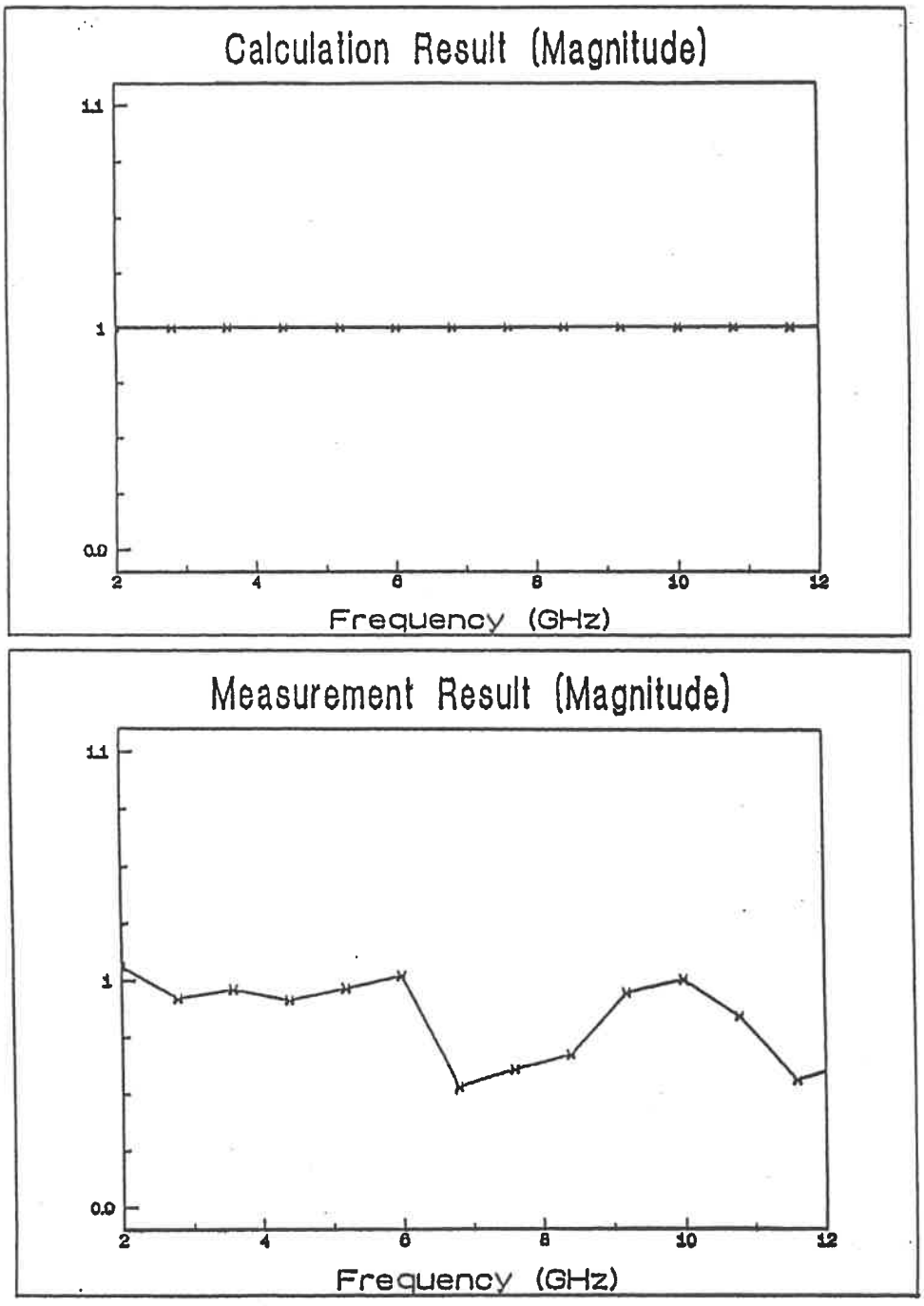

Figure 4.2: Measurement and Calculation Results of an Offset Short Circuit

(Wiltron Co. Model: 22*A*50) over $2 \sim 12GHz$ (Amplitude)

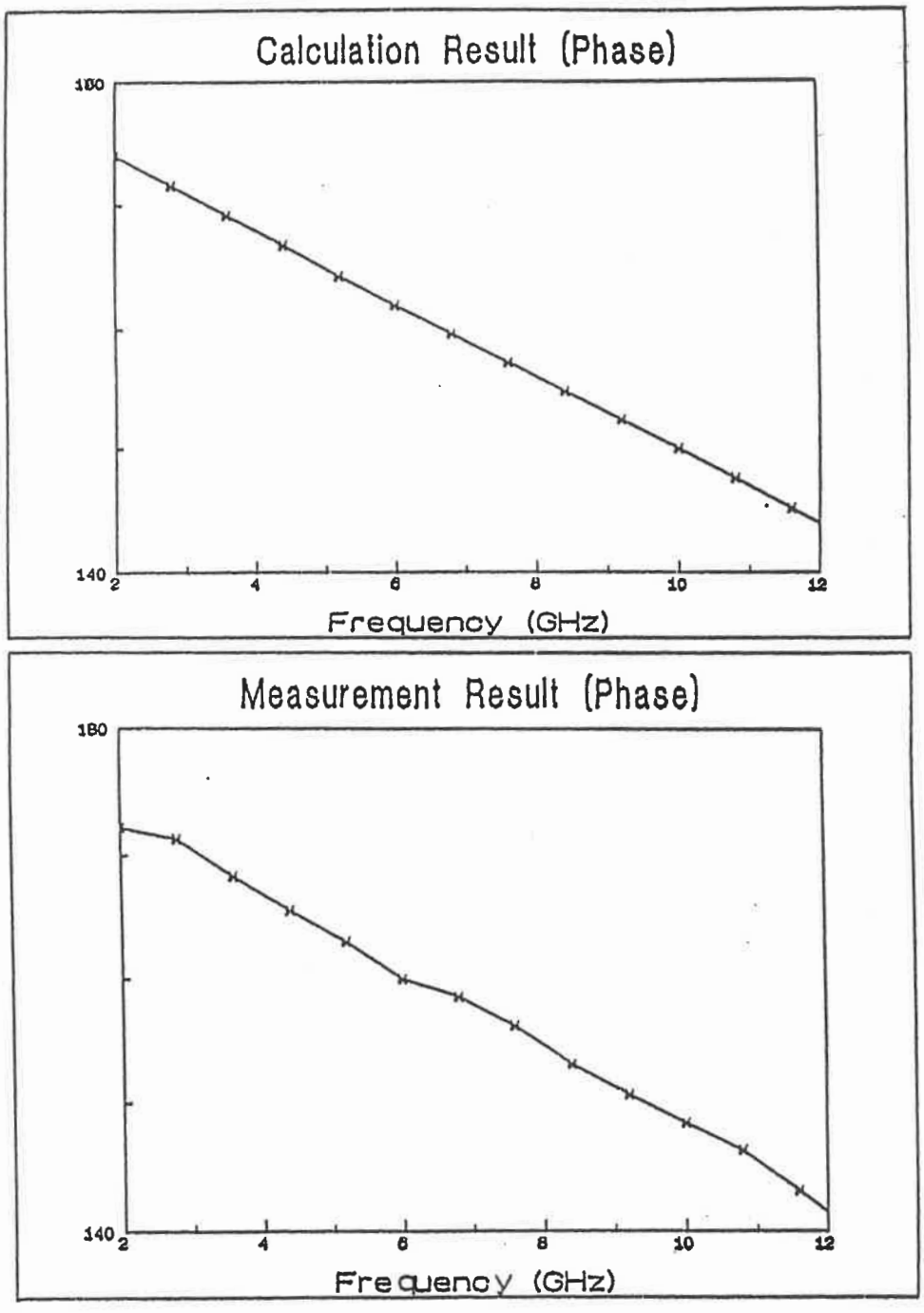

Figure 4.3: Measurement and Calculation Results of an Offset Short Circuit (Wiltron Co. Model: 22A50) over $2 \sim 12GHz$ (Phase)

(4.8), we can get

$$\Gamma = \frac{e - w}{cw - d} \tag{4.15}$$

A well known property of any bilinear transformation is that circles are mapped into circles, which indicates that any point on w plane can be mapped into an unique position on Γ plane by the equation (4.14). It gives an hint that the three q_i points on Γ plane can be obtained from the centers of the three circles on w plane by means of the bilinear transformation.

The w plane is achieved by rotating the w_1 plane with an angle μ degree along the counterclockwise direction as shown in equation (4.7). So the centers of the three circles denoted by cc_1, cc_2 and cc_3 respectively on w plane will be obtained easily by multiplying 0, m, n to the rotating factor $(cos\mu - jsin\mu)$, therefore

$$cc_1 = 0 \tag{4.16}$$

$$cc_2 = m\,(cos\mu - jsin\mu) = M \tag{4.17}$$

$$cc_3 = n\,(cos\mu - jsin\mu) = Ncos\,(\mu - \nu) + jNsin\,(\mu - \nu) \tag{4.18}$$

$$cos\,(\mu - \nu) = -\frac{(p - q - r)}{2\sqrt{qr}}$$

$$sin\,(\mu - \nu) = \pm\sqrt{1 - cos^2\,(\mu - \nu)}$$

The sign in the last equation can be determined according to reference [21] by using a $\frac{1}{2}$ standard load. It should be noted that cc_1, cc_2 and cc_3 represent the q_i points in w plane. By mapping the w plane to Γ plane using equation (4.14), three q_i points in Γ plane can be calculated from the measured values

$$q_4 = -\frac{e}{d} \tag{4.19}$$

$$q_5 = \frac{e - M}{cM - d} \tag{4.20}$$

$$q_6 = \frac{e - N\left[cos\left(\mu - \nu\right) + jsin\left(\mu - \nu\right)\right]}{cN\left[cos\left(\mu - \nu\right) + jsin\left(\mu - \nu\right)\right] - d} \tag{4.21}$$

The variations of q_i points of the designed six-port junction over frequency range $2 \sim 12\,GHz$ calculated by equations (4.18) $\sim$ (4.20) are given in figures (4.5) and (4.6) respectively. It is noticed that the phase of the measured q_i points of the six-port junction shown in figure (4.6) is not compensated so well as the result from the computer analysis in figure (3.25). This deviation is caused by the different types of connectors used in measurements and in analysis. A connector from $APC-7$ to N type is taken into account in computer analysis. However, connector from $APC-7$ to SMA type is utilized in the manufacture and in measurements. The two types of connectors have different electrical lengths, therefore, they will produce different phase shifts

in the circuit. A section of lossless transmission line with the same length as the difference between the two connectors can be added in measurements so that the same compensated condition as in the computer analysis can be achieved. To avoid this accurate manufacture, the equivalent electrical length of the connector ($APC-7$ to SMA) used in measurements is exchanged with that ($APC-7$ to N) used in computer analyses to verify the identity between measurements and computer analyses. New simulation results using $APC-7$ to SMA connector are illustrated in figure (4.4). Comparing figure (4.4) and (4.6), similar responses are obtained. This confirms the success in designing the six-port junction according to the objective goals.

The magnitudes of the q_i points of the designed six-port junction shown in figure (4.5) mainly concentrate between 1 and 2. At a few exceptional frequencies, the measured magnitudes of q_i exceed 2 and this might result from the via hole in the circuit. However, these points of large magnitudes will not influence the measurement properties of the six-port because they can be corrected by the calibration.

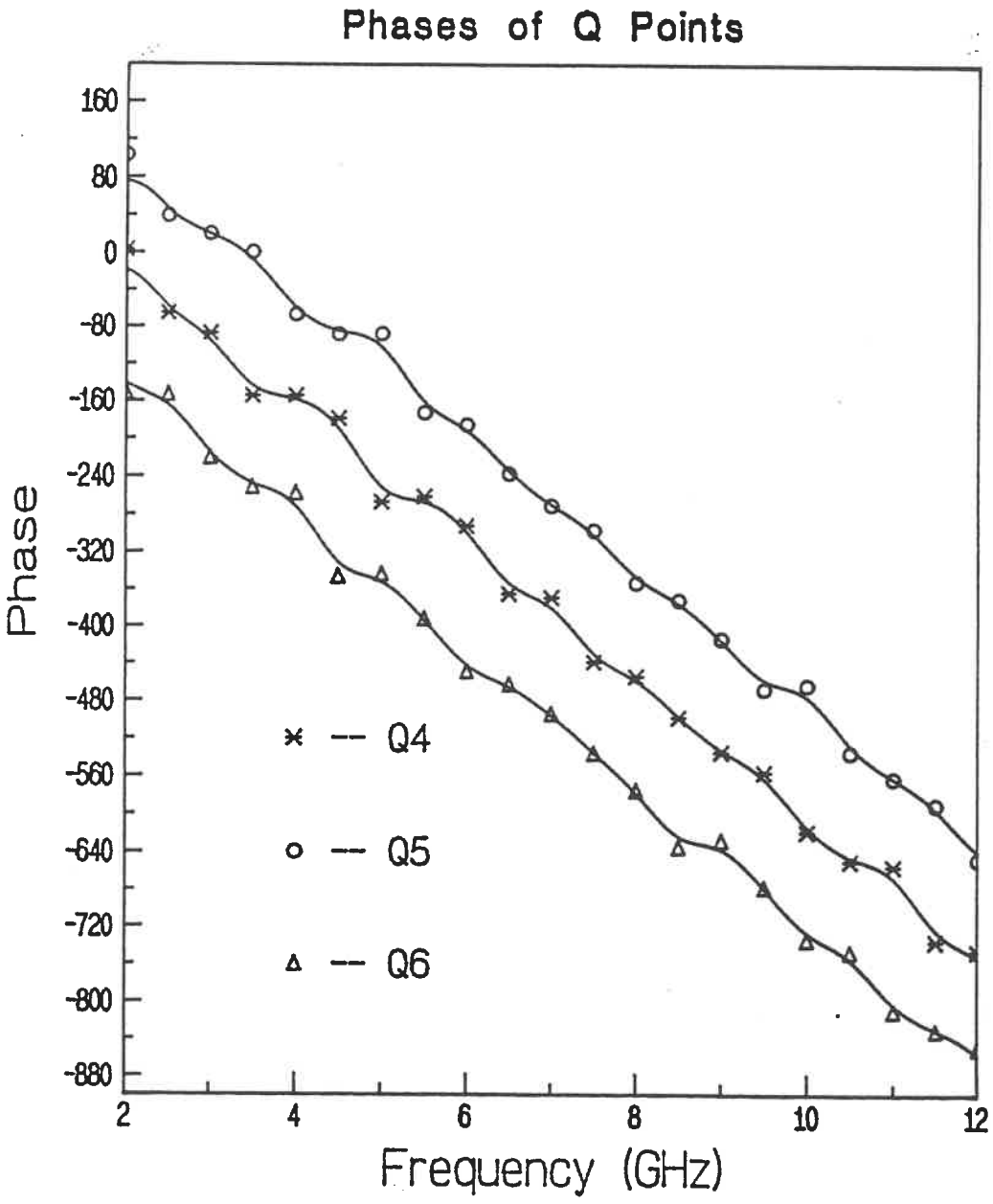

Figure 4.4: Simulated Results of the Phase of the Q_i Point Variations over $2 \sim 12GHz$ Frequency Range with a APC-7 to SMA Connector

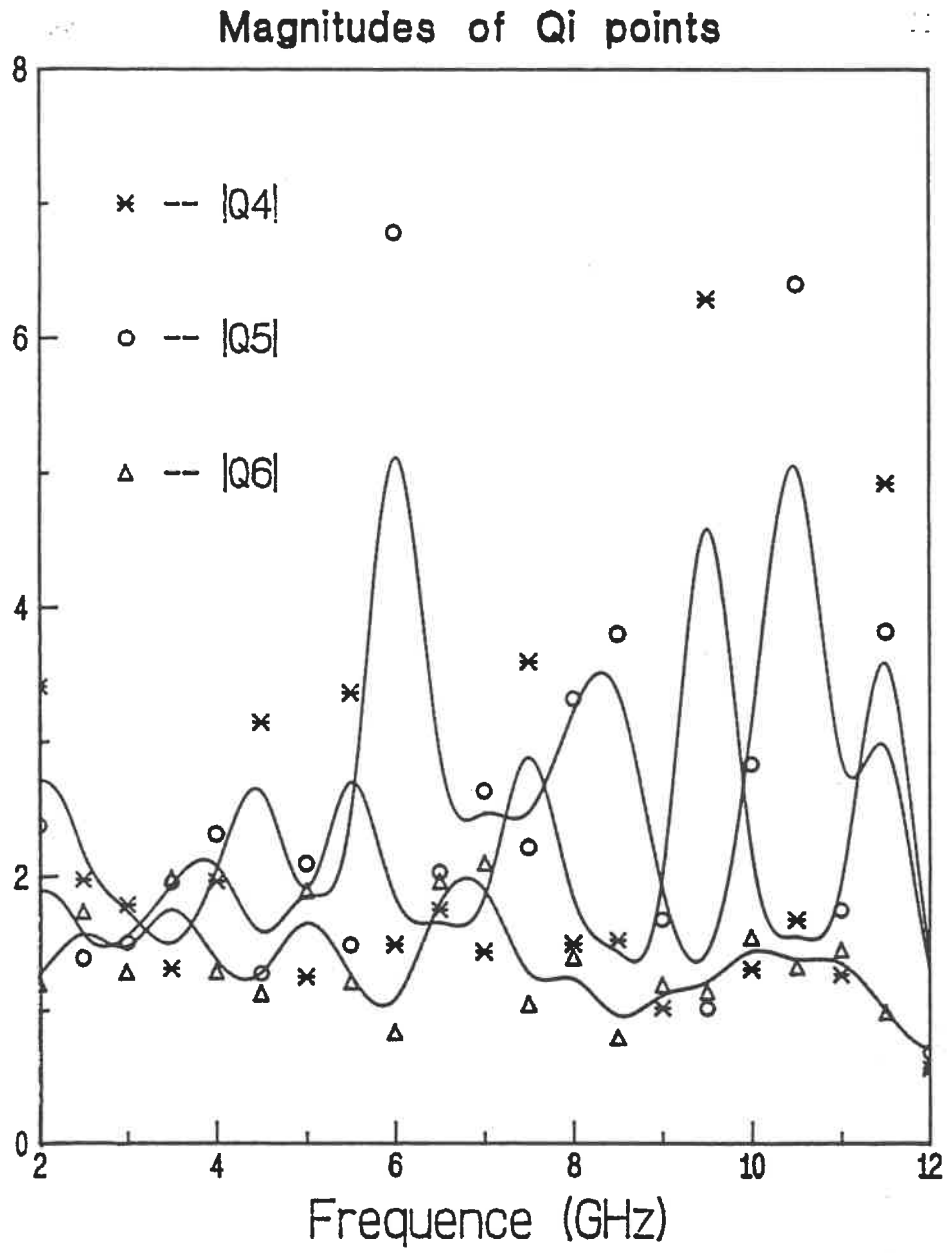

Figure 4.5: Measured Results of the Amplitude of the Q_i Point Variations over $2 \sim 12GHz$ Frequency Range with a APC-7 to SMA Connector

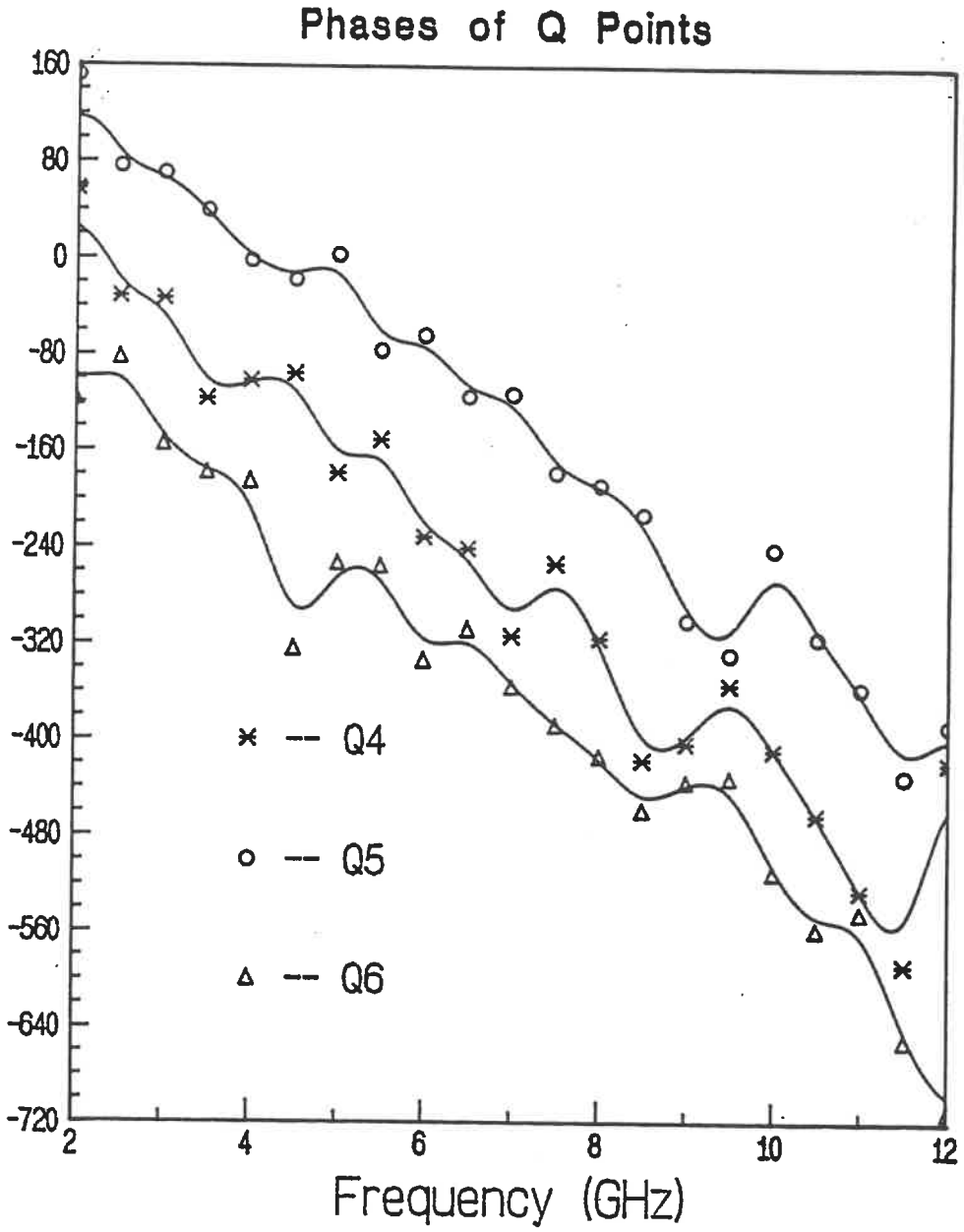

Figure 4.6: Measured Results of the Phase of the Q_i Point Variations over $2 \sim 12GHz$ Frequency Range with a APC-7 to SMA Connector

4.4 Conclusion

It is concluded that a compensated six-port junction has been designed, fabricated and tested. By applying the long line theory and mapping principles, the agreement between computer analysis results and measurement results has been verified. In order to reduce the deviations between the analysis and measurement, a better manufacture technology is required.

Chapter 5

Conclusion

This thesis describes the procedures for the design, the manufacture, the measurement and the calibration of a wideband six-port junction over a wide frequency band. Solutions to the problems encountered in the designing procedure are discussed in detail. The main contributions of this thesis can be summarized as follows:

1. Wideband couplers covering a frequency range of $2 \sim 18\,GHz$ with very tight coupling levels ($1.76\,dB$ and $3\,dB$ respectively) have been designed, built and measured successfully. The small deviations between CAD results and measurement data are explained.

2. Three different Wilkinson power dividers, i.e. a right angle splitting power divider, a $30°$ angle splitting power divider and a curved line power divider, operating in a frequency range of $2 \sim 15\,GHz$ have been designed,

built and measured with satisfactory results. It has been found out that the 30° angle splitting power divider presents a better input match than the right angle one. In addition, the curved line power divider gives a very good isolation between its two output ports (better than $-25\,dB$ over a frequency range of $2 \sim 15\,GHz$). Due to this property, the curved line power divider could be very useful for certain special applications, such as balanced amplifier designs.

3. Since there is no available effective sliding short circuit above $10\,GHz$ to provide the required number of impedance loads for the calibration over the frequency range of $2 \sim 18\,GHz$, the long line theory [54] has been modified to solve this problem. The designed six-port junction operating over the frequency range of $2 \sim 12\,GHz$ was calibrated by using this improved theory. The final calibration results have confirmed the improvements.

4. Mathematical expressions to calculate q_i points of a six-port junction based on Hodgetts and Griffin's calibration method has been found. These formulas (obtained by the bilinear transformation concept) derive the q_i point calculation procedure from calibration parameters. The q_i point positions of the designed six-port junction have been calculated by using the above expressions. The results are comparable to those obtained by

computer simulations.

Finally, it was found that the designed six-port junction presents very little phase sensitivity to the frequency variations over $2 \sim 12GHz$. Computer simulation results and experimental measurement analysis display a very good agreement over the complete frequency band. This kind of six-port junction is suitable for swept frequency measurements and microwave pulse measurements.

Recommendations

We have already discussed different configurations of Wilkinson power dividers in section 3.4. The measurement results for three kinds of Wilkinson power dividers have shown large reflections above $15\,GHz$. This phenomenon is caused by many factors. Two of them are very important and further work might worth to be done in these respects.

Firstly, the resistors with smaller dimensions or integrated stripline resistors should be used. If the dimensions of resistors are not small enough in comparision to the wave length, the resistors will no longer behave like lumped components. Their resonance frequencies may be comparable to the signal frequency, therefore, give rise to some problems at high frequencies.

Secondly, an input signal is transmitted to the two branches of a Wilkinson power divider by a $50\,\Omega$ transmission line via a symmetrical T junction. Both the discontinuity of the T junction and mismatching between the transmission line ($50\,\Omega$) and the first branch ($95\,\Omega$) contribute the negative responses to such power dividers at the high frequency range. The following efforts could provide improvements to the problems. 1) Design a special matching network which will compensate the reflections at high frequency range and remain the good performances of the power divider under $12\,GHz$. 2) Develop a better model

of T junction at high frequency by advanced methods, i.e. various numerical methods, in stead of the available model in ' Touchstone '.

In addition, the connection between two layers of the six-port junction should be payed much attention to obtain good behaviour. The diameter of the hole for the connection should be as small as possible. If both problems of the discontinuity of power dividers and the connection between the two layers of the junction can be solved well, the designed six-port reflectometer can be expected to operate over the frequency range of $2 \sim 18\,GHz$.

References

[1] P. L. Somlo and J. D. Hunter, **Microwave Impedance Measurement** IEE Electrical Measurement series2 , 1985

[2] P. I. Somlo , **Band-Limited Deconvolution of Locating Reflectometer Results** , IEEE Trans. on MTT, vol. MTT-27, No. 2, 1976, pp128–135

[3] J. R. Andrews and W. L. Gans , **Time Domain Automatic Network Analyser** Mesure, L'onde Electrique , 1975, 55, pp569–574

[4] W. Littlr , **An NBS Developed Automatic Network Analyzer** CPEM , 1976

[5] **Automating The PH 8410 B Microwave Network Analyzer** Application Note 221 A, June 1980

[6] G. F. Engen and C. A. Hoer , **Application of an Arbitrary Six-Port Junction to Power Measurement Problems** IEEE Trans. on MI, vol. MI-21, 1972, pp470–474

[7] C. A. Hoer, **The Six-Port Coupler: A New Approach to Measuring Voltage, Current, Power, Impedance and Phase** IEEE Trans. on IM, vol. IM-21, 1972, pp466–470

[8] G. F. Engen, **The Six-Port Reflectometer: An Alternative Network Analyzer** IEEE Trans. on IM, vol. IM-21, 1972 , pp1075–1080

[9] A. E. Bailey, **Microwave Measurement** IEE Electrical Measurement series3 , 1985

[10] Shihe Li and R. G. Bosisio, **Calibration of Multiport Reflectometers by Means of Four Open / Short Circuits** IEEE Trans. on MTT, vol. MTT-30, July 1982, pp1085–1090

[11] G. F. Engen, **An Improved Circuit for Implementing the Six-Port Technique of Microwave Measurements** IEEE Trans. on MTT, vol. MTT-25, Dec. 1977, pp1080–1083

[12] E. J. Griffin, **Six-Port Reflectometer Circuit Comprising Three Directrional Coupler** Electron Lett. 1982, pp491–493

[13] M. D. Rafal and W. T. Joines, **Optimizing the Design of the Six-Port Junction** IEEE MTT-S Digest, 1980, pp437–439

[14] E. J. Griffin, G. J. Slack and L. D. Hill, **Broadband Six-Port Reflectometer Junction** Electron Lett. 1983, pp921–922

[15] Z. H. Feng, **Broadband Dielectric Waveguide Coupler and Six-Port Network** IEEE MTT-S Digest, 1986, pp237–240

[16] M. Malkomes and R. Walsdorf, **Integrated Fin-Line 6-Ports for MM-Wave Network Analyzers** IEEE MTT-S Digest, 1986, pp669–671

[17] I. Ohta, **A New Six-Port Microwave Network: Six-Port Magic Junction** IEEE Trans. on MTT, vol. MTT-36, May 1988, pp859–864

[18] L. Kaliouby and R. G. Bosisio, **A New Method for Six-Port Swept Frequency Automatic Network Analysis** IEEE Trans. on MTT, vol. MTT-32, Dec. 1984, pp1678–1682

[19] C. A. Hoer, **Using Six-Port and Eight-Port Junctions to Measure Active and Passive Circuit Parameters** NBS Tech. Note 673, 1975

[20] G. F. Engen, **The Six-Port Measurement Technique — A Status Report** Microwave Journal, 1978, 21, ,pp18–89

[21] T. E. Hodgetts and E. J. Griffin, **A Unified Treatment of the Theory of Six-Port Reflectometer Calibration Using the Minimum of Standards** Royal Signals and Radar Establishment, Malvern Report No. 83003

[22] G. F. Engen, **A Least Square Solution for Use in the Six-Port Measurement Technique** IEEE Trans. on MTT, vol. MTT-28, Dec. 1980, pp1473–1477

[23] M. Berman, P. I. Somlo and M. J. Buckley, **A Comparative Statistical Study of Some Proposed Six-Port Junction Designs** IEEE Trans. on MTT, vol. MTT-35, Nov. 1987, pp971–977

[24] H. M. Cronson and L. Susman, **A Six-Port Automatic Network Analyzer** IEEE Trans. on MTT, vol. MTT-25, Dec. 1977, pp1086–1091

[25] R. J. Collier and N. A. El-Deeb, **On the Use of a Microstrip Three-Line System as a Six-Port Refelectometer** IEEE Trans. on MTT, vol. MTT-27, Oct. 1979, pp847–853

[26] A. L. Cullen, S. K. Judah and F. Nikravesh, **Impedance Measurement Using a Six-Port Directional Coupler** IEE proc., vol. 127, part H, No. 2, April 1980, pp92–98

[27] E. R. B. Hansson and G. P. Riblet, **An Ideal Six-Port Network Consisting of a Matched Reciprocal Lossless Five-Port and a Perfect Directional Coupler** IEEE Trans. on MTT, vol. 31, March 1983 pp284–289

[28] P. R. Ikäläinen and G. L. Matthaei, **Wide-Band Forward-Coupling Microstrip Hybrids with High Directivity** IEEE Trans. on MTT,

vol. MTT-35, Aug. 1987, pp719–725

[29] R. Shelton, J. Wolf and R. Van Wagoner, **Tandem Couplers and Phase Shifters for Multi-Octave Bandwidth** Microwaves, April 1965, pp14–19

[30] J. Lange, **Interdigitated Stripline Quadrature Hybrid** IEEE Trans. on MTT, vol. MTT-17, Dec. 1969, pp1150–1151

[31] Yusuke Tajima and Susumu Kamihashi, **Multiconductor Couplers** IEEE Trans. on MTT, vol. MTT-26, Oct. 1978, pp795–801

[32] S. Wang, F. Ghannouchi and R. G. Bosisio, **A Wideband Microstrip Coupler with Tight Coupling Level** Microwave Journal Apr. 1990

[33] S. B. Cohn, **Characteristic Impedances of Broad-Side Coupled Strip Transmission Lines** IRE Trans. MTT, Nov. 1960, pp633–637

[34] G. L. Matthaei, L. Young and E. M. T. Jones, **Microwave Filters, Impedance-Matching Networks and Coupling Structures** New York, McGraw-Hill, 1964, Dedham, MA: Artech House, 1980

[35] V. Rizzoli and A. Lipparin, **The Design of Interdigitated Couplers for MIC Applications** IEEE Trans. on MTT, vol. MTT-26, Jan. 1978, pp7–15

[36] Harlan Howe, **Stripline Circuit Design** Artech House, 1974

[37] J. P. Shelton, **Impedances of Offset Parallel-Coupled Strip Transmission Lines** IEEE Trans. on MTT, vol. MTT-14, Jan. 1966, pp7–15

[38] L. Young, **Parallel Coupled Lines and Directional Couplers** Dedham, MA: Artech House, 1972

[39] R. K. Hoffman, **Handbook of Microwave Integrated Circuits** Artech House, 1983

[40] E. G. Cristal and L. Young, **Theory and Tables of Optimum Symmetrical TEM-Mode Coupled-Transmission-Line Directional Couplers** IEEE Trans. on MTT, vol.MTT-13, No. 5, Sep. 1965 pp544–558

[41] K. C. Gupta, R. Garg and R. Chadha, **Computer-Aided Design of Microwave Circuits** Artech House, 1981

[42] E. J. Wilkinson, **A N-Way Hybrid Power Divider** IRE Trans. on MTT, vol. MTT-8, Jan. 1960, pp116–118

[43] S. B. Cohn, **A Class of Broadband Three-Port TEM-Mode Hybrids** IEEE Trans. on MTT, vol. MTT-16, Feb. 1968, pp110–116

[44] R. B. Ekinge, **A New Method of Synthesizing Matched Broad-Band TEM-Mode Three-Ports** IEEE Trans. on MTT, vol. MTT-19, Jan. 1971, pp81–88

[45] M. Hamadallah, **Microstrip Power Dividers at mm-Wave Frequencies** Microwave Journal, July 1988, pp115–127

[46] C. Q. Li, S. H. Li and R. G. Bosisio, **CAD/CAM Design of an Improved Wideband Wilkinson Power Divider** Microwave Journal, Nov. 1984, pp125–135

[47] F. Ghannouchi, Ph. D. Thesis, **Mesures micro-ondes assistés par ordinateur utilisant un nouveau corrélateur six-port** Ecole Polytechnique de Montréal, 1987

[48] J. D. Hunter and P. I. Somlo, **An Explicit Six-Port Calibration Method Using Five Standards** IEEE Trans. on MTT, vol. MTT-33, Jan. 1985, pp69–72

[49] G. P. Riblet and E. R. B. Hansson, **A Spects of the Calibration of a Single Six-Port Using a Load and Offset Reflection Standards** IEEE Trans. on MTT, vol. MTT-30, 1982, pp2120–2125

[50] P. I. Somlo and J. D. Hunter, **A Six-Port Reflectometer and its Complete Characterization by Convenient Calibration Procedures** IEEE Trans. on MTT, vol. MTT-30, Feb. 1982, pp186–192

[51] D. Woods, **Analysis and calibration Theory of the General Six-Port Reflectometer Employing Four Amplitude Detectors** Proc. IEE vol. 126, Feb. 1979, pp221–228

[52] F. M. Ghannouchi and R. G. Bosisio, **An Alternative Explicit Six-Port Matrix Calibration Formalism Using Five Standards** IEEE Trans. on MTT, vol. MTT-36, March 1988, pp494–498

[53] G. F. Engen, **Calibrating the Six-Port Reflectometer by Means of Sliding Terminations** IEEE Trans. on MTT, vol. MTT-26, Dec. 1978, pp951–957

[54] C. A. Hoer, **Choosing Line Lengths for Calibrating Network Analyzers** IEEE Trans. on MTT, vol. MTT-31, Jan. 1983, pp76–78

[55] R. Larose, F. M. Ghannouchi and R. G. Bosisio, **A New Multi-Harmonic Load-Pull Method for Nonlinear Device Characterization and Modeling** IEEE MTT-S, 1990

Appendix A

There are many programs have been made by the author in different softwares in order to simulate, optimize, calibrate and calculate required parameters of components of the six-port junction. All programs used in the above research work are enclosed and exlpained in this appendix.

The programs listed in this appendix will organize the same order as they appeared in the previous chapters. The files of these programs will be displayed after their names and short explainations about their locations, their functions and their utilizations in the following pages.

The purpose of this file is to simulate a 6.75 dB stripline hybrid coupler by using broadside and cascaded offside structures over $2 \sim 18\,GHz$. The substrate is made by teflon. The definition of all dimensions and layout of the

coupler in this file have been shown in figure 3.2.

This file is used to simulate a 3 dB stripline hybrid coupler by tandemly connected two 8.34 dB hybrid couplers. The detailed dimensions and the layout of the coupler have been given in figure 3.4.

This file is used to simulate a 1.76 dB stripline hybrid coupler by the same configuration as 3 dB hybrid explained above.

The file is used to simulate a two-way stripline Wilkinson equal power divider with seven sections and right angle splitting input over frequency range 2-18 GHz. The dimensions and the layout of this kind of power divider are shown in figure 3.12.

This file is used to simulate a two-way stripline Wilkinson equal power divider with seven sections and 30° angle splitting input over frequency range 2-18 GHz. The dimensions and the layout of this kind of power divider are shown in figure 3.13.

Touchstone File No. 6 — pdvs13.ckt (page A 15)

This file allows to simulate a two-way stripline Wilkinson equal power divider with seven sections and curved line branch over frequency range 2-18 GHz. The dimensions and the layout of this kind of power divider are shown in figure 3.18.

Touchstone File No. 7 — spjw9.ckt (page A 19)

The file is used to simulate the complete six-port junction with phase compensation over $2 \sim 12\,GHz$. The final dimensions and the layout of this six-port junction are shown in figures 3.21, 3.22 and 3.23 respectively.

Program No. 8 — q_simu (page A 24)

This program is used to calculate the distribution of three complex q_i points from simulation results.

Program No. 9 — circle_sin (page A 25)

This program is designed to plot the distribution curves of three q_i points of the six-port junction by simulation results on Smith Chart.

Program No. 10 — calibrat.for (page A 36)

The objective of this program is to calibrate the six-port reflectometer by using thirteen standards.

Program No. 11 — qpnts_w (page A 42)

This program proceeds the calculation of the q_i points from calibration parameters obtained by program 10.

All of the programs presented here are stored in directories /users/wang/ or /eesof/users/wang/ of HP-300. The MICAD files which give the layouts of all components and the six-port junction are also stored in these directories with the same names as TOUCHSTONE files except the extention is .dwg in stead of .ckt.

```
        TOUCHSTONE FILE No. 1

!name: /users/wang/scou69.ckt
!purpose:   Simulate a 6.75 dB hybrid coupler with stripline.
var
        w1#  5    53.17566          55
        w2#  10   55.94775          57
        w3#  25   57.54633          59
        w4#  30   58.89824          60
        w5#  40   59.99735          61
        w6#  15   46.98273          48
        w7#  20   58.54716          85
        w8#  40   88.21836         120
        w9#  80   139.99373         140
        l1#  100  176.58426        600
        l2#  30   32.71959         400
        l3#  100  173.77057        400
        l4#  30   191.89558         400
        l5#  100  220.87592         400
        s1=10.1
eqn
        w50=58.16
        x11=w6/2
        x12=-x11
        x21=(w7-w6)/2
        x22=-x21
        x31=(w8-w7)/2
        x32=-x31
        x41=(w9-w8)/2
        x42=-x41
ckt
        ssub er=2.30    b=71.1  t=1.0    rho=0
soclin 45 46 36 35  w^w5  wo^w9  s^s1 l^l5  w1=0   w2=0   w3=0   w4=0
soclin 35 36 32 31  w^w4  wo^w8  s^s1 l^l4  w1^x41 w2^x42 w3=0   w4=0
soclin 31 32 02 01  w^w3  wo^w7  s^s1 l^l3  w1^x31 w2^x32 w3=0   w4=0
soclin 01 02 03 04  w^w2  wo^w6  s^s1 l^l2  w1^x21 w2^x22 w3=0   w4=0
sbclin 04 03 05 06  w^w1  s^s1   l^l1       w1^x11 w2^x12 w3^x12 w4^x11
soclin 06 05 07 08  w^w2  wo^w6  s^s1 l^l2  w1=0   w2=0   w3^x22 w4^x21
soclin 08 07 09 10  w^w3  wo^w7  s^s1 l^l3  w1=0   w2=0   w3^x32 w4^x31
soclin 10 09 37 38  w^w4  wo^w8  s^s1 l^l4  w1=0   w2=0   w3^x42 w4^x41
soclin 38 37 47 48  w^w5  wo^w9  s^s1 l^l5  w1=0   w2=0   w3=0   w4=0
def4p  45 46 47 48  amp

freq
        sweep   2   18   1
grid
        range   2   18   1
opt
        range   2   18   1
        couple db[s31]=-1.76   2
!       couple db[s11]<-18
        couple db[s41]<-18
```

```
        TOUCHSTONE FILE No. 2

!name:  /users/wang/scou39.ckt
!purpose:   Simulate a 3 dB hybrid coupler with stripline by tandem
!           connection technique.
var
        w1#  5    53.17566         55
        w2#  10   56.89228         57
        w3#  25   57.98434         59
        w4#  30   58.97050         60
        w5#  40   59.07040         61
        w6#  15   47.99568         48
        w7#  20   60.03483         85
        w8#  40   82.52119        120
        w9#  80   129.62764        140
        l1#  100  145.45259       600
        l2#  30   62.17291        400
        l3#  100  149.48808       400
        l4#  30   179.84398        400
        l5#  100  194.90436        400
        s1=10.1
eqn
        w50=58.16
        x11=w6/2
        x12=-x11
        x21=(w7-w6)/2
        x22=-x21
        x31=(w8-w7)/2
        x32=-x31
        x41=(w9-w8)/2
        x42=-x41
        w61=-w6
        w71=-w7
        w81=-w8
        w91=-w9
ckt
        ssub er=2.30    b=71.1  t=1.0    rho=0
soclin 45 46 36 35  w^w5  wo^w9  s^s1 l^15  w1=0   w2=0   w3=0   w4=0
soclin 35 36 32 31  w^w4  wo^w8  s^s1 l^14  w1^x41 w2^x42 w3=0   w4=0
soclin 31 32 02 01  w^w3  wo^w7  s^s1 l^13  w1^x31 w2^x32 w3=0   w4=0
soclin 01 02 03 04  w^w2  wo^w6  s^s1 l^12  w1^x21 w2^x22 w3=0   w4=0
sbclin 04 03 05 06  w^w1  s^s1   l^11       w1^x11 w2^x12 w3^x11 w4^x12
soclin 06 05 07 08  w^w2  wo^w61 s^s1 l^12  w1=0   w2=0   w3^x21 w4^x22
soclin 08 07 09 10  w^w3  wo^w71 s^s1 l^13  w1=0   w2=0   w3^x31 w4^x32
soclin 10 09 37 38  w^w4  wo^w81 s^s1 l^14  w1=0   w2=0   w3^x41 w4^x42
soclin 38 37 47 48  w^w5  wo^w91 s^s1 l^15  w1=0   w2=0   w3=0   w4=0
def4p  45 46 47 48  amp

        slin   10       11  w^w50 l=70
        smiter 11       12  w^w50
        slin   12       13  w^w50 l=70
        def2p  10       13  conc

        amp    01 02 03 04
        conc   11       01
        conc   02       12
        conc   03       13
        conc   14       04
        def4p  11 12 14 13  part

        part   01 02 03 04
```

```
        part   03 05 06 02  flip
        slin   11       01  w^w50    l=500
        slin   05       55  w^w50    l=500
        slin   06       66  w^w50    l=500
        slin   04       44  w^w50    l=500
        def4p  11 55 66 44  couple
out
        couple db[s21] gr1
        couple db[s41] gr1
        couple db[s11] gr1
        couple db[s31] gr1
        couple ang[s21] gr2
        couple ang[s41] gr2
        couple ang[s31] gr2
freq
        sweep   2   18   1
grid
        range   2   18   1
opt
        range   2   18   1
        couple db[s31]=-1.76   2
!       couple db[s11]<-18
        couple db[s41]<-18
```

```
        TOUCHSTONE FILE No. 3

!name:  /users/wang/scou19.ckt
!purpose:   Simulate a 1.76 dB hybrid coupler with stripline by tandem
!           connection technique.
var
        w1#  5    53.17566         55
        w2#  10   55.94775         57
        w3#  25   57.54633         59
        w4#  30   58.89824         60
        w5#  40   59.99735         61
        w6#  15   46.98273         48
        w7#  20   58.54716         85
        w8#  40   88.21836        120
        w9#  80   139.99373        140
        l1#  100  176.58426       600
        l2#  30   32.71959        400
        l3#  100  173.77057       400
        l4#  30   191.89558        400
        l5#  100  220.87592        400
        s1=10.1
eqn
        w50=58.16
        x11=w6/2
        x12=-x11
        x21=(w7-w6)/2
        x22=-x21
        x31=(w8-w7)/2
        x32=-x31
        x41=(w9-w8)/2
        x42=-x41
        w61=-w6
        w71=-w7
        w81=-w8
        w91=-w9
ckt
        ssub er=2.30    b=71.1  t=1.0    rho=0
soclin 45 46 36 35  w^w5  wo^w9  s^s1 l^15  w1=0   w2=0   w3=0   w4=0
soclin 35 36 32 31  w^w4  wo^w8  s^s1 l^14  w1^x41 w2^x42 w3=0   w4=0
soclin 31 32 02 01  w^w3  wo^w7  s^s1 l^13  w1^x31 w2^x32 w3=0   w4=0
soclin 01 02 03 04  w^w2  wo^w6  s^s1 l^12  w1^x21 w2^x22 w3=0   w4=0
sbclin 04 03 05 06  w^w1  s^s1   l^11       w1^x11 w2^x12 w3^x11 w4^x12
soclin 06 05 07 08  w^w2  wo^w61 s^s1 l^12  w1=0   w2=0   w3^x21 w4^x22
soclin 08 07 09 10  w^w3  wo^w71 s^s1 l^13  w1=0   w2=0   w3^x31 w4^x32
soclin 10 09 37 38  w^w4  wo^w81 s^s1 l^14  w1=0   w2=0   w3^x41 w4^x42
soclin 38 37 47 48  w^w5  wo^w91 s^s1 l^15  w1=0   w2=0   w3=0   w4=0
def4p  45 46 47 48  amp

        slin   10       11  w^w50 l=70
        smiter 11       12  w^w50
        slin   12       13  w^w50 l=70
        def2p  10       13  conc

        amp    01 02 03 04
        conc   11       01
        conc   02       12
        conc   03       13
        conc   14       04
        def4p  11 12 14 13  part

        part   01 02 03 04
```

```
        part   03 05 06 02  flip
        slin   11       01  w^w50    l=500
        slin   05       55  w^w50    l=500
        slin   06       66  w^w50    l=500
        slin   04       44  w^w50    l=500
        def4p  11 55 66 44  couple
out
        couple db[s21] gr1
        couple db[s41] gr1
        couple db[s11] gr1
        couple db[s31] gr1
        couple ang[s21] gr2
        couple ang[s41] gr2
        couple ang[s31] gr2
freq
        sweep   2   18   1
grid
        range   2   18   1
opt
        range   2   18   1
        couple db[s31]=-1.76   2
!       couple db[s11]<-18
        couple db[s41]<-18
```

```
        TOUCHSTONE FILE No. 4

!name:  /eesof/users/wang/pdvs.ckt
!purpose: Simulate an two-way equal Wilkinson power divider in stripline with
!seven section and right angle splitting  over frequency range 2-18 GHz.

var
        l11#  60   79.53388     700
        l22#  100  137.44058     600
        w11#  10   10.00320       60
        w22#  15   20.89998       45
        w33#  20   28.10320       45
        w44#  30   35.22472       50
        w55#  35   37.69623       50
        w66#  40   46.21544       53
        w77#  40   49.18617       53
        l33#  100  118.68668     600
        l44#  100  167.50681     700
        l55#  100  121.90446     600
        l66#  100  153.64542     600
        l77#  100  120.12370     600
        l2#   50   50.01918       300
        r1=100
        r2=142
        r3=220
        r4=250
        r5=308
        r6=400
        r7=450
eqn
        w50=54.16
        s=(w50+w11)/2+l2
        l3=s-35-w22/2
        l4=s-35-w33/2
        l5=s-35-w44/2
        l6=s-35-w55/2
        l7=s-35-w66/2
        l8=s-35-w77/2
        l9=s-35-w50/2
ckt
        ssub    er=2.30     b=71.1   t=1.0    rho=0.0
        slin    1    2      w^w50        l=50
        stee    3   14  2   w1^w11       w2^w11          w3^w50
        slin    3    4      w^w11        l^l2
        sbend   5    4      w^w11        ang=90
        slin    5    6      w^w11        l^l11
        stee    6    7  8   w1^w11       w2^w22          w3=50
        slin    8   11      w=50         l^l3
        res     11  12      r^r1
        slin    12  13      w=50         l^l3
        slin    14  15      w^w11        l^l2
        sbend   15  16      w^w11        ang=90
        slin    16  17      w^w11        l^l11
        stee    18  17  13  w1^w22       w2^w11          w3=50

        slin    7   19      w^w22        l^l22
        stee    19  20  21  w1^w22       w2^w33          w3=50
        slin    21  24      w=50         l^l4
        res     24  25      r^r2
        slin    25  26      w=50         l^l4
        slin    18  27      w^w22        l^l22
```

```
        stee    28   27   26   w1^w33        w2^w22        w3=50

        slin    20   29        w^w33         l^133
        stee    29   30   31   w1^w33        w2^w44        w3=50
        slin    31   34        w=50          l^15
        res     34   35        r^r3
        slin    35   36        w=50          l^15
        slin    28   37        w^w33         l^133
        stee    38   37   36   w1^w44        w2^w33        w3=50

        slin    30   39        w^w44         l^144
        stee    39   40   41   w1^w44        w2^w55        w3=50
        slin    41   44        w=50          l^16
        res     44   45        r^r4
        slin    45   46        w=50          l^16
        slin    38   47        w^w44         l^144
        stee    48   47   46   w1^w55        w2^w44        w3=50

        slin    40   49        w^w55         l^155
        stee    49   50   51   w1^w55        w2^w66        w3=50
        slin    51   54        w=50          l^17
        res     54   55        r^r5
        slin    55   56        w=50          l^17
        slin    48   57        w^w55         l^155
        stee    58   57   56   w1^w66        w2^w55        w3=50

        slin    50   59        w^w66         l^166
        stee    59   60   61   w1^w66        w2^w77        w3=50
        slin    61   64        w=50          l^18
        res     64   65        r^r6
        slin    65   66        w=50          l^18
        slin    58   67        w^w66         l^166
        stee    68   67   66   w1^w77        w2^w66        w3=50

        slin    60   69        w^w77         l^177
        stee    69   70   71   w1^w77        w2^w50        w3=50
        slin    71   74        w=50          l^19
        res     74   75        r^r7
        slin    75   76        w=50          l^19
        slin    68   77        w^w77         l^177
        stee    78   77   76   w1^w50        w2^w77        w3=50
        def3p   1    70   78   amp
out
        amp     db[s32]   gr1
        amp     db[s11]   gr1
        amp     db[s22]   gr1
        amp     db[s31]   gr1
freq
        sweep   2    18    1
grid
        range   2    18    1
opt
        range   2    18    1
        amp     db[s32]<-20
        amp     db[s11]<-18
        amp     db[s22]<-18
        amp     db[s31]=-3.01    2
```

```
        TOUCHSTONE FILE No. 5

!name:  /eesof/users/wang/pdvs2.ckt
!purpose: Simulate an two-way equal Wilkinson power divider in stripline with
!seven section and 30 degree angle splitting  over frequency range 2-18 GHz.

var
        lm #  80   81.22088     700
        l22#  100  119.74888     600
        w11#  10   10.42927       70
        w22#  15   18.10150      45
        w33#  20   24.59375      45
        w44#  30   34.23678      50
        w55#  35   37.17457      55
        w66#  40   44.42837      60
        w77#  40   50.34691      65
        l33#  80   138.21889     600
        l44#  100  174.20088     700
        l55#  100  124.08887     600
        l66#  100  169.23085     600
        l77#  100  119.60981     600
        r1=230
        r2=130
        r3=230
        r4=300
        r5=460
        r6=600
        r7=460
eqn
        w50=55.19
!       lm=l11+50
        s=(w50+w11)/2+0.500*lm
        l3=s-35-w22/2
        l4=s-35-w33/2
        l5=s-35-w44/2
        l6=s-35-w55/2
        l7=s-35-w66/2
        l8=s-35-w77/2
        l9=s-35-w50/2
ckt
        ssub    er=2.20     b=70.1   t=1.0    rho=0.0
        slin    1    2      w^w50       l=50
        stee    3   14  2   w1^w11      w2^w11          w3^w50
        sbend   90   3      w^w11       ang=30
        sbend   4   90      w^w11       ang=30
        slin    4    5      w^w11       l^lm
        sbend   6    5      w^w11       ang=30
        stee    6    7  8   w1^w11      w2^w22          w3=50
        slin    8   11      w=50        l^l3
        res     11  12      r^r1
        slin    12  13      w=50        l^l3
        sbend   14  91      w^w11       ang=30
        sbend   91  15      w^w11       ang=30
        slin    15  16      w^w11       l^lm
        sbend   16  17      w^w11       ang=30
        stee    18  17  13  w1^w22      w2^w11          w3=50

        slin    7   19      w^w22       l^l22
        stee    19  20  21  w1^w22      w2^w33          w3=50
        slin    21  24      w=50        l^l4
        res     24  25      r^r2
```

```
        slin    25  26      w=50        l^14
        slin    18  27      w^w22       l^122
        stee    28  27  26  w1^w33       w2^w22        w3=50

        slin    20  29      w^w33       l^133
        stee    29  30  31  w1^w33       w2^w44        w3=50
        slin    31  34      w=50        l^15
        res     34  35      r^r3
        slin    35  36      w=50        l^15
        slin    28  37      w^w33       l^133
        stee    38  37  36  w1^w44       w2^w33        w3=50

        slin    30  39      w^w44       l^144
        stee    39  40  41  w1^w44       w2^w55        w3=50
        slin    41  44      w=50        l^16
        res     44  45      r^r4
        slin    45  46      w=50        l^16
        slin    38  47      w^w44       l^144
        stee    48  47  46  w1^w55       w2^w44        w3=50

        slin    40  49      w^w55       l^155
        stee    49  50  51  w1^w55       w2^w66        w3=50
        slin    51  54      w=50        l^17
        res     54  55      r^r5
        slin    55  56      w=50        l^17
        slin    48  57      w^w55       l^155
        stee    58  57  56  w1^w66       w2^w55        w3=50

        slin    50  59      w^w66       l^166
        stee    59  60  61  w1^w66       w2^w77        w3=50
        slin    61  64      w=50        l^18
        res     64  65      r^r6
        slin    65  66      w=50        l^18
        slin    58  67      w^w66       l^166
        stee    68  67  66  w1^w77       w2^w66        w3=50

        slin    60  69      w^w77       l^177
        stee    69  70  71  w1^w77       w2^w50        w3=50
        slin    71  74      w=50        l^19
        res     74  75      r^r7
        slin    75  76      w=50        l^19
        slin    68  77      w^w77       l^177
        stee    78  77  76  w1^w50       w2^w77        w3=50
        def3p   1   70  78  amp
out
        amp     db[s32]   gr1
        amp     db[s11]   gr1
        amp     db[s22]   gr1
        amp     db[s31]   gr1
freq
        sweep   2   18    1
grid
        range   2   18    1
opt
        range   2    8    1
        amp     db[s32]<-20
        amp     db[s11]<-18
        amp     db[s22]<-18
        amp     db[s31]=-3.01   2
        range   8   14    1
        amp     db[s32]<-20     2
```

```
amp     db[s11]<-20     2
amp     db[s22]<-20     2
amp     db[s31]=-3.01   4
range    14   18    1
amp     db[s32]<-20     3
amp     db[s11]<-20     3
amp     db[s22]<-20     3
amp     db[s31]=-3.01   6
```

```
        TOUCHSTONE FILE No. 6

!name:  /eesof/users/wang/pdvs13.ckt
!purpose: Simulate an two-way equal Wilkinson power divider in stripline with
!seven section and curve line branch over frequency range 2-18 GHz.
dim
ang deg

var
        w11 # 10 18.84462 35
        w22 # 15 24.07305 35
        w33 # 20 29.05625 40
        w44 # 25 34.23674 45
        w55 # 30 38.08396 50
        w66 # 35 40.36448 55
        w77 # 40 43.16020 60
        r0  # 50 179.99767 250
        w50=    55.19
        wres=100
        r11 = 350
        r22 = 300
        r33 = 250
        r44 = 400
        r55 # 200 328.10034 500
        r66 # 200 253.21495 500
        r77 # 300 405.40640 500
        r88 # 300 463.87314 500
        r99 # 300 421.74271 500

eqn
   !    r0=300/pi
        ww0= wres/2
        w01= wres/2
        w02= wres/2
        w03= wres/2
        w04= wres/2
        w05= wres/2
        w06= wres/2
        w07= wres/2
        w08= wres/2
        w011=w50/2
        l50= (w50-59.05511)/2
        r1= r0 +w11/2
        r2= r0 +w22/2
        r3= r0 +w33/2
        r4= r0 +w44/2
        r5= r0 +w55/2
        r6= r0 +w66/2
        r7= r0 +w77/2
        r8= r0 +w88/2
        r9= r0 +w99/2
        r10=r0 +w50/2
        c=(w50/2)/(r1-w11/2)
        a10=(c+c^3/6+3*c^5/40+15*c^7/336)*180/pi
        a=ww0/(r0)
        a0=(a+a^3/6+3*a^5/40+15*a^7/336)*180/pi
        a1=180-a10-a0
        a2=180-2*a0
        a3=180-2*a0
        a4=180-2*a0
        a5=180-2*a0
```

```
a6=180-2*a0
a7=180-2*a0
a8=180-2*a0
a9=180-2*a0
a11= a1+a10
wl10=r1-(r1-w11/2)*cos((180-a1)/2)
wl20=r2-(r2-w22/2)*cos((180-a2)/2)
wl30=r3-(r3-w33/2)*cos((180-a3)/2)
wl40=r4-(r4-w44/2)*cos((180-a4)/2)
wl50=r5-(r5-w55/2)*cos((180-a5)/2)
wl60=r6-(r6-w66/2)*cos((180-a6)/2)
wl70=r7-(r7-w77/2)*cos((180-a7)/2)
wl80=r8-(r8-w88/2)*cos((180-a8)/2)
wl1=wl10+wl20
wl2=wl20+wl30
wl3=wl30+wl40
wl4=wl40+wl50
wl5=wl50+wl60
wl6=wl60+wl70
wl7=wl70+wl80
ww01=0!(wres-50)/2
ckt
 ssub    er=2.20     b=70.1   t=1.0    rho=0.0
 slin    1    2      w^w50       l^r1
 stee 102 101 2 w1^w11 w2^w11 w3^w50
 sbend    101  103  w^w11 ang^a9
 sbend    104  102  w^w11 ang^a9
 scurve 103 13     w^w11   ang^a1   rad^r1
 scurve 21 23 w^w22 ang^a2 rad^r2
 scurve 31 33 w^w33 ang^a3 rad^r3
 scurve 41 43 w^w44 ang^a4 rad^r4
 scurve 51 53 w^w55 ang^a5 rad^r5
 scurve 61 63 w^w66 ang^a6 rad^r6
 scurve 71 73 w^w77 ang^a7 rad^r7
 scurve 81 83 w^w88 ang^a8 rad^r8
 scurve 91 93 w^w99 ang^a9 rad^r9
 stee 21 13 15 w1^w22 w2^w11 w3=50      a1^a0 a2^a0
 stee 31 23 25 w1^w33 w2^w22 w3=50      a1^a0 a2^a0
 stee 41 33 35 w1^w44 w2^w33 w3=50      a1^a0 a2^a0
 stee 51 43 45 w1^w55 w2^w66 w3=50        a1^a0 a2^a0
 stee 61 53 55 w1^w66 w2^w55 w3=50      a1^a0 a2^a0
 stee 71 63 65 w1^w77 w2^w66 w3=50     a1^a0 a2^a0
 stee 81 73 75 w1^w88 w2^w77 w3=50     a1^a0 a2^a0
 stee 91 83 85 w1^w99 w2^w88 w3=50     a1^a0 a2^a0
 stee 111 93 95 w1^w50 w2^w99 w3=50    a1^a0 a2^a0
 slin 111 113 w^w50 l^r10
 scurve 14 104     w^w11   ang^a1   rad^r1
 scurve 24 22 w^w22 ang^a2 rad^r2
 scurve 34 32 w^w33 ang^a3 rad^r3
 scurve 44 42 w^w44 ang^a4 rad^r4
 scurve 54 52 w^w55 ang^a5 rad^r5
 scurve 64 62 w^w66 ang^a6 rad^r6
 scurve 74 72 w^w77 ang^a7 rad^r7
 scurve 84 82 w^w88 ang^a8 rad^r8
 scurve 94 92 w^w99 ang^a9 rad^r9
 stee 14 22 16 w1^w11 w2^w22 w3=50       a1^a0 a2^a0
 stee 24 32 26 w1^w22 w2^w33 w3=50       a1^a0 a2^a0
 stee 34 42 36 w1^w33 w2^w44 w3=50        a1^a0 a2^a0
 stee 44 52 46 w1^w44 w2^w55 w3=50      a1^a0 a2^a0
 stee 54 62 56 w1^w55 w2^w66 w3=50      a1^a0 a2^a0
 stee 64 72 66 w1^w66 w2^w77 w3=50      a1^a0 a2^a0
```

```
          stee 74 82 76 w1^w77 w2^w88 w3=50      a1^a0 a2^a0
          stee 84 92 86 w1^w88 w2^w99 w3=50      a1^a0 a2^a0
          stee 94 112 96 w1^w99 w2^w50 w3=50     a1^a0 a2^a0
          slin 114 112 w^w50 l^r10
          slin 15 19 w=50  l^ww01
          slin 25 29 w=50  l^ww01
          slin 35 39 w=50  l^ww01
          slin 45 49 w=50  l^ww01
          slin 55 59 w=50  l^ww01
          slin 65 69 w=50  l^ww01
          slin 75 79 w=50  l^ww01
          slin 85 89 w=50  l^ww01
          slin 95 99 w=50  l^ww01
          slin 16 18 w=50  l^ww01
          slin 26 28 w=50  l^ww01
          slin 36 38 w=50  l^ww01
          slin 46 48 w=50  l^ww01
          slin 56 58 w=50  l^ww01
          slin 66 68 w=50  l^ww01
          slin 76 78 w=50  l^ww01
          slin 86 88 w=50  l^ww01
          slin 96 98 w=50  l^ww01
     !    res 15 16 r^r11 spac l=50
     !    res 25 26 r^r22 spac l=50
     !    res 35 36 r^r33 spac l=50
     !    res 45 46 r^r44 spac l=50
     !    res 55 56 r^r55 spac l=50
     !    res 65 66 r^r66 spac l=50
     !    res 75 76 r^r77 spac l=50
          res 18 19 r^r11 spac l=50
          res 28 29 r^r22 spac l=50
          res 38 39 r^r33 spac l=50
          res 48 49 r^r44 spac l=50
          res 58 59 r^r55 spac l=50
          res 68 69 r^r66 spac l=50
          res 78 79 r^r77 spac l=50
          res 88 89 r^r88 spac l=50
          res 98 99 r^r99 spac l=50
 def3p 1  113 114  amp
out
        amp    db[s32]  gr1
        amp    db[s11]  gr1
        amp    db[s22]  gr1
        amp    db[s13]  gr1
freq
        sweep   2   18   1
grid
        range   2   18   1
opt
        range   2   18   1
        amp    db[s32]<-20     1
        amp    db[s11]<-25     1
        amp    db[s22]<-20     1
        amp    db[s31]=-3.01   5
        range   8   14   1
        amp    db[s32]<-25     3
        amp    db[s11]<-30     2
        amp    db[s22]<-20     2
!       amp    db[s31]=-3.01   6
        range   14  18   1
!       amp    db[s32]<-18     4
```

```
        amp     db[s11]<-25     3
        amp     db[s22]<-20     3
!       amp     db[s31]=-3.01   6
```

```
        TOUCHSTONE FILE No. 7

!name:  /eesof/users/wang/spjw9.ckt
!purpose: Simulate a complete six-port junction with phase compensation over
!         2-12 GHz.

var
        w50 = 55.19
        wp1 = 10.2
        wp2 = 18.4
        wp3 = 25.5
        wp4 = 34.2
        wp5 = 37.0
        wp6 = 44.4
        wp7 = 50.3
        lp1 = 85.4
        lp2 = 125.1
        lp3 = 129.0
        lp4 = 159.8
        lp5 = 136.7
        lp6 = 168.8
        lp7 = 123.9
        w1 = 47.8
        w2 = 52.5
        w3 = 54.0
        w4 = 55.0
        w5 = 55.3
        wo2 = 42.6
        wo3 = 60.8
        wo4 = 93.9
        wo5 = 140.0
        l1 = 201.1
        l2 = 17.0
        l3 = 209.6
        l4 = 201.8
        l5 = 110.1
        s1 = 10.1
        w11 = 45.2
        w22 = 52.6
        w33 = 53.4
        w44 = 55.0
        w55 = 55.9
        wo22 = 45
        wo33 = 57.2
        wo44 = 76.2
        wo55 = 101.7
        l11 = 169.7
        l22 = 66.2
        l33 = 177.5
        l44 = 205.4
        l55 = 197.2
        l3031#  400  600.00096   700
        l3435#  300  400.85773   600
        l3940#  200  495.10242   700
        l1112#  450  578.23846   800
        l0920#  300  487.96359   700
eqn
        sp = (w50+wp1)/2+0.5*lp1
        lp11 = sp-35-wp2/2
        lp22 = sp-35-wp3/2
        lp33 = sp-35-wp4/2
```

```
lp44 = sp-35-wp5/2
lp55 = sp-35-wp6/2
lp66 = sp-35-wp7/2
lp77 = sp-35-w50/2
lecon = 1756
leb = 43.9
lpdv = lp1+lp2+lp3+lp4+lp5+lp6+lp7+wp1+400
wpdv = 2*sp-w50                                                    !6
wcou2 = (wo5+w50)*2+280+24
lcou2 = l1+2*(l2+l3+l4+l5)+140+2*w50+12
lcou3 = l11+2*(l22+l33+l44+l55)+140+2*w50+12
lecou1 = l1+2*(l2+l3+l4+l5)
lecou2 = 3252
x11 = wo2/2
x12 = -x11
x21 = (wo3-wo2)/2
x22 = -x21
x31 = (wo4-wo3)/2
x32 = -x31
x41 = (wo5-wo4)/2
x42 = -x41
wo21 = -wo2
wo31 = -wo3
wo41 = -wo4
wo51 = -wo5
x311 = wo22/2
x312 = -x311
x321 = (wo33-wo22)/2
x322 = -x321
x331 = (wo44-wo33)/2
x332 = -x331
x441 = (wo55-wo44)/2
x442 = -x441
wo221 = -wo22
wo331 = -wo33
wo441 = -wo44
wo551 = -wo55
l1394 = l1112+550
l2122 = l3031+lecon-l1112-2*leb+(lecou1+3*w50-wo5-lcou2)/2+9
l0405 = l1112+lcou2-lpdv+(w50+wpdv)/2+5
l2324 = lpdv+l3435+wo5-2*l0920-(7*w50+wpdv)/2-5
l4748 = (lecou2-2*leb-wcou2-lcou3-wpdv)/2
l4950 = wcou2+l3940-2*w50+lcou3+15
l5152 = (l4748+wpdv+2*w50)/2+6
ckt
ssub   er=2.20     b=70.1  t=1.0   rho=0.0
stee   3   14  1   w1^wp1  w2^wp1  w3^w50          !power divider
sbend  90   3      w^wp1   ang=30
sbend  4   90      w^wp1   ang=30
slin   4    5      w^wp1   l^lp1
sbend  6    5      w^wp1   ang=30
stee   6    7  8   w1^wp1  w2^wp2  w3=50
slin   8   11      w=50    l^lp11
res    11  12      r=100                spac l=60
slin   12  13      w=50    l^lp11
sbend  14  91      w^wp1   ang=30
sbend  91  15      w^wp1   ang=30
slin   15  16      w^wp1   l^lp1
sbend  16  17      w^wp1   ang=30
stee   18  17  13  w1^wp2  w2^wp1  w3=50
slin   7   19      w^wp2   l^lp2                   !the second one
```

```
        stee   19  20  21  w1^wp2  w2^wp3  w3=50
        slin   21  24      w=50    l^lp22
        res    24  25      r=142                  spac l=60
        slin   25  26      w=50    l^lp22
        slin   18  27      w^wp2   l^lp2
        stee   28  27  26  w1^wp3  w2^wp2  w3=50
        slin   20  29      w^wp3   l^lp3                    !the third one
        stee   29  30  31  w1^wp3  w2^wp4  w3=50
        slin   31  34      w=50    l^lp33
        res    34  35      r=200                  spac l=60
        slin   35  36      w=50    l^lp33
        slin   28  37      w^wp3   l^lp3
        stee   38  37  36  w1^wp4  w2^wp3  w3=50
        slin   30  39      w^wp4   l^lp4                    !the fouth one
        stee   39  40  41  w1^wp4  w2^wp5  w3=50
        slin   41  44      w=50    l^lp44
        res    44  45      r=230                  spac l=60
        slin   45  46      w=50    l^lp44
        slin   38  47      w^wp4   l^lp4
        stee   48  47  46  w1^wp5  w2^wp4  w3=50
        slin   40  49      w^wp5   l^lp5                    !the fivth one
        stee   49  50  51  w1^wp5  w2^wp6  w3=50
        slin   51  54      w=50    l^lp55
        res    54  55      r=300                  spac l=60
        slin   55  56      w=50    l^lp55
        slin   48  57      w^wp5   l^lp5
        stee   58  57  56  w1^wp6  w2^wp5  w3=50
        slin   50  59      w^wp6   l^lp6                    !the sixth one
        stee   59  60  61  w1^wp6  w2^wp7  w3=50
        slin   61  64      w=50    l^lp66
        res    64  65      r=400                   spac l=60
        slin   65  66      w=50    l^lp66
        slin   58  67      w^wp6   l^lp6
        stee   68  67  66  w1^wp7  w2^wp6  w3=50
        slin   60  69      w^wp7   l^lp7                    !the seventh
        stee   69  70  71  w1^wp7  w2^w50  w3=50
        slin   71  74      w=50    l^lp77
        res    74  75      r=450                   spac l=60
        slin   75  76      w=50    l^lp77
        slin   68  77      w^wp7   l^lp7
        stee   78  77  76  w1^w50  w2^wp7  w3=50
        slin   70      80  w^w50   l=50
        slin   78      79  w^w50   l=50
        def3p  1   80  79  pdv

soclin 45 46 36 35 w^w5 wo^wo5 s^s1 l^l5 w1=0   w2=0   w3=0   w4=0
soclin 35 36 32 31 w^w4 wo^wo4 s^s1 l^l4 w1^x41 w2^x42 w3=0   w4=0  !coupler1
soclin 31 32 02 01 w^w3 wo^wo3 s^s1 l^l3 w1^x31 w2^x32 w3=0   w4=0
soclin 01 02 03 04 w^w2 wo^wo2 s^s1 l^l2 w1^x21 w2^x22 w3=0   w4=0
sbclin 04 03 05 06 w^w1        s^s1 l^l1 w1^x11 w2^x12 w3^x11 w4^x12
soclin 06 05 07 08 w^w2 wo^wo2 s^s1 l^l2 w1=0   w2=0   w3^x21 w4^x22
soclin 08 07 09 10 w^w3 wo^wo3 s^s1 l^l3 w1=0   w2=0   w3^x31 w4^x32
soclin 10 09 37 38 w^w4 wo^wo4 s^s1 l^l4 w1=0   w2=0   w3^x41 w4^x42
soclin 38 37 47 48 w^w5 wo^wo5 s^s1 l^l5 w1=0   w2=0   w3=0   w4=0
        def4p  45 46 47 48  coupl1
        slin   10       11  w^w50  l=70           !coupler2
        smiter 11       12  w^w50
        slin   12       13  w^w50  l=70
        def2p  10       13  conc                 !bend for tendam connection
        coupl1 01 02 03 04
        conc   11       01
```

```
       conc   02       12
       conc   03       13
       conc   14       04
       def4p  11 12 14 13  part
       part   01 02 03 04
       part   03 05 06 02  flip
       def4p  01 05 06 04  coupl2
soclin 45 46 36 35 w^w55 wo^wo55 s^s1 l^155 w1=0  w2=0  w3=0  w4=0 !coupler3
soclin 35 36 32 31 w^w44 wo^wo44 s^s1 l^144 w1^x441 w2^x442  w3=0  w4=0
soclin 31 32 02 01 w^w33 wo^wo33 s^s1 l^133 w1^x331 w2^x332 w3=0  w4=0
soclin 01 02 03 04 w^w22 wo^wo22 s^s1 l^122 w1^x321 w2^x322 w3=0  w4=0
sbclin 04 03 05 06 w^w11         s^s1 l^111 w1^x311 w2^x312 w3^x311 w4^x312
soclin 06 05 07 08 w^w22 wo^wo22 s^s1 l^122 w1=0  w2=0  w3^x321 w4^x322
soclin 08 07 09 10 w^w33 wo^wo33 s^s1 l^133 w1=0  w2=0  w3^x331 w4^x332
soclin 10 09 37 38 w^w44 wo^wo44 s^s1 l^144 w1=0  w2=0  w3^x441 w4^x442
soclin 38 37 47 48 w^w55 wo^wo55 s^s1 l^155 w1=0  w2=0  w3=0    w4=0
       def4p  45 46 47 48  amp2
       amp2   01 02 03 04
       conc   11       01
       conc   02       12
       conc   03       13
       conc   14       04
       def4p  11 12 14 13  part2
       part2  01 02 03 04
       part2  03 05 06 02  flip
       def4p  01 05 06 04  coupl3

       slin   91       02  w^w50  l=5100       !six-port circuit
       smiter 02       03  w^w50
       slin   30       92  w^w50  l^lecon
       slin   31       30  w^w50  l^13031
       smiter 32       31  w^w50  l^13031
       coupl1 03 32 33 04
       slin   04       05  w^w50  l^10405
       pdv    05  08   06
       slin   06       93  w^w50  l=550
       smiter 08       09  w^w50
       slin   09       20  w^w50  l^10920
       smiter 20       21  w^w50
       slin   21       22  w^w50  l^12122
       smiter 23       22  w^w50
       slin   23       24  w^w50  l^12324
       smiter 25       24  w^w50
       slin   25       26  w^w50  l^12122
       smiter 26       27  w^w50
       slin   27       10  w^w50  l^10920
       smiter 10       11  w^w50
       slin   11       12  w^w50  l^11112
       smiter 28       12  w^w50
       smiter 13       29  w^w50
       slin   13       94  w^w50  l^11394
       smiter 33       34  w^w50
       slin   34       35  w^w50  l^13435
       pdv    35  46   36
       coupl2 28 39 29 36
       slin   39       40  w^w50  l^13940
       smiter 41       40  w^w50
       coupl3 19 41 18 45
       slin   45       55  w^w50  l=500
       smiter 55       56  w^w50
       slin   56       57  w^w50  l=500
```

```
        smiter 58       57  w^w50
        slin   58       95  w^w50  l=1440
        smiter 46       47  w^w50
        slin   47       48  w^w50  l^14748
        smiter 49       48  w^w50
        slin   49       50  w^w50  l^14950
        smiter 51       50  w^w50
        slin   51       52  w^w50  l^15152
        via    52       53  d1=10  d2=10   h=10.1  t=1  w^w50
        slin   18       53  w^w50  l^15152
        slin   19       96  w^w50  l=2000
        match  93
        match  94
        match  95
        def3p  91 92 96    spout
out
        spout  mag[s31] gr1
        spout  mag[s32] gr1
        spout  mag[s22] gr1
        spout  mag[s21] gr1
        spout  ang[s31] gr2
        spout  ang[s32] gr2
        spout  ang[s22] gr2
        spout  ang[s21] gr2
freq
        sweep   2   12   0.5
grid
        range   2   12   0.5
opt
        range   2   12   0.5
        spout   db[s22]<-18
```

PROGRAM No. 8

```
% Name: q_simu
% This program is to calculate the distribution of three qi points from
% simulation results.

./q_calc <$1 >q_p
./q_calc <$2 >>q_p
./q_calc <$3 >>q_p
./q_separe <q_p
rm q_p
DIR=$4
if test $# -lt 4
then
  DIR="t"
fi
if test $DIR = c
then
  ./tgraph /dev/crt hp300h <mag.cmd
  echo "Hit RETURN to continue"
  read ANS
  ./tgraph /dev/crt hp300h <ang.cmd
  echo "Hit RETURN to continue"
  read ANS
else
  if test $DIR = p
  then
    echo "Load paper in the plotter    and hit RETURN"
    read ANS
    ./tgraph /dev/rplotter hpgl <mag.cmd
    echo "Load paper in the plotter    and hit RETURN"
    read ANS
    ./tgraph /dev/rplotter hpgl <ang.cmd
  else
    ./tgraph <mag.cmd
    echo "Hit RETURN to continue"
    read ANS
    ./tgraph <ang.cmd
    echo "Hit RETURN to continue"
    read ANS
  fi
fi
clear
```

PROGRAM No. 9

```
1!NAME: "CIRCLE_SIN:,700,0"
2     GINIT
3     OPTION BASE 1
4     !
5     COM /Centre/ Qim(4),Qip(4),Aim(4),Aip(4),Rs(4),Bi(4)
6     COM /Gamma/ Gam(201),Pha(201)
7     COM /Wind/ Wxi,Wxa,Wyi,Wya,Facteur
8     COM /Quad/ Result(8,8),Racine(4,4,4),M
9     COM /Frequence/ Freq_debut,Freq_fin,Freq_step,Fact,Direct$[20]
10    Fl=0
11    Arret=1
12    Medium=CRT
13    ! PARAMETRES SIX-PORTS DE LI
14    Fadhel=1
15    SELECT Fadhel
16    CASE 0
17      ! SIX-PORTS DE LI PROPREMENT DIT
18      C1nom=3/8*SQR(3)/SQR(2)! .459   6.76 DB
19      C2nom=SQR(2)/SQR(3)    ! .816   1.76 DB= 2x6.76 dB
20      C3nom=1/SQR(2)*1.00    ! .707   3.00 DB
21    CASE 1
22      ! SIX-PORTS DE LI FACTEUR DE COUPLAGE MODIFIE
23      C1nom=.316!1/SQR(2)                ! 6.00 DB
24      C2nom=SQR(2)/SQR(3)!1/SQR(2)        ! 3.00 DB
25      C3nom=1/SQR(2)*1.00! 3.00 DB
26    END SELECT
27    C2=C2nom
28    C3=C3nom
29    T2=SQR(1-C2^2)
30    T3=SQR(1-C3^2)
31    C1nom_db=20*LGT(C1nom)
32    Er=2.17
33    FO=5
34    Theta=-3*PI/2
35    Freq_step=.02
36    Freq_debut=2
37    Freq_fin=3
38    Ff=Freq_fin+Freq_step/10
39    FOR Freq=Freq_debut TO Ff STEP Freq_step
40      L=Theta/(2*PI*FO*1.E+9/2.997925E+8*SQR(Er))
41      L=1.E-3*10.2
42      L1=L*5
43      L2=L*5*2+L*1
44      L3=L*5*2+L*1
45      Ld2=L*5
46      !  Ld1=0*Ld2+L          !   Ld1=l1+Ld2
47      Ld1=L*5
48      Fact=1.00
49      Ligne=(L*10+L)*Fact
50      ^=-2*PI*Freq*1.E+9/2.997925E+8*SQR(Er)
51      Philigne=^*Ligne
52      Directivity=10.0
53      Direct$=VAL$(-Directivity)
54      Dir_deb=40
55      Dir_fin=10!C1nom_db
56      ! FOR Directivity=Dir_deb TO Dir_fin STEP -1
57      Dir1=10^(-Directivity/20)
58      Dir1=0
59      IF Dir1=0 THEN Direct$="~"
```

```
60      A=1.      ! 0<A< 1
61      E1=SQR(C1nom^2*Dir1^2/(1+(1-A)*Dir1^2))
62      C1=SQR(C1nom^2-(1-A)*E1^2)
63      T1=SQR((1-C1nom^2)-A*E1^2)
64      Y=PI/2
65      Phaset1=^*L1
66      Phasec1=^*L1
67      Phasee1=0
68      Jk=0
69      IF Dir1 THEN Phasee1=^*L1+^*L1*Jk+Y
70      !
71      ! LIGNE INETR COMPOSANTES
72      Co=.085
73      Pha1=^*(.0782+Co)
74      ^1=-2*PI*Freq*1.E+9/2.997925E+8*SQR(1.10)
75      Pha2=2*^*(.0660)+2*^1*(.060)
76      Pha3=^*0
77      Pha4=^*0
78      Pha5=^*(.1175+Co)
79      Pha6=^*(4*L)*1.0
80      Pha7=^*(1*L)
81      Pha8=^*(1*L)
82      Pha9=^*((4*L)+Co)
83      Pha10=^*(1*L)
84      Pha11=^*(1*L)
85      Pha12=^*((1.5*L)+Co)
86      Pha13=^*((1.5*L)+Co)
87       ! COMPENSATION
88      Pha6=(Pha2+Pha7+Phasec1)*1      ! 360 ->17/28   ! 120 ->25/28  ! 28-3.5
89      !POWER DIVIDERS 1,2
90      D1=1/SQR(2)
91      D2=1/SQR(2)
92      Aa1=.500
93      Aa2=.500
94      D11=SQR(1-Aa1)
95      D12=SQR(1-(1-Aa1))
96      D21=SQR(1-Aa2)
97      D22=SQR(1-(1-Aa2))
98      Pd1=^*Ld1
99      Pd2=^*Ld2
100     ! COUPLEURS 2,3
101     Phaset2=^*L2
102     Phasec2=^*L2
103     Phasee2=^*L2+^*L2*Jk*Y
104     Phaset3=^*L3*1.00
105     Phasec3=^*L3*1.00
106     Phasee3=^*L3+^*L3*Jk+Y
107     IF Freq=Fd THEN GOSUB Sortie
108     !=======================================
109     !  PRINT T1,C1,E1,T1^2+C1^2+E1^2
110     ! CALCUL DE Q3
111     Mx7=D11
112     Px7=Pd1
113     Mx8=0
114     Px8=0
115     IF Dir1 THEN CALL Cf1(Mx7,Px7,Mx8,Px8,E1,Phasee1,T1,Phaset1,C1,
        Phasec1,Qim(1),Qip(1),Pha2)
116     !   PRINT "Q3: ",Qim(1),Qip(1)*180/PI
117     !   PRINT USING "K,2X,4D.3D,2X,4D.2D";"Q3:",Qim(1),Qip(1)*180/PI
118     ! CALCUL DE Q4
119     Mx5=D12*T2
```

```
120     Px5=Pd1+Phaset2+Pha3+Pha6
121     Mx6=D21*C2
122     Px6=Pd2+Phasec2+(+1)*PI/2+Pha4+Pha7
123     Cf1(Mx5,Px5,Mx6,Px6,E1,Phasee1,T1,Phaset1,C1,Phasec1,Qim(2),Qip(2),Pha2)
124     OUTPUT Medium USING "X,2D.2D,#";Freq
125     OUTPUT Medium USING "X,K,2D.3D,X,4D.2D,#";"Q4:",Qim(2),Qip(2)*180/PI
126     !=======================================
127 Q5:  !
128     ! CALCUL DE Q5
129     Mx1=D12*C2*T3
130     Px1=Pd1+Phasec2+Phaset3+(+1)*PI/2+Pha3+Pha6+Pha10
131     Mx222=D21*T2*T3
132     Px222=Pd2+Phaset2+Phaset3+Pha4+Pha7+Pha10
133     Mx233=D22*C3
134     Px233=Pd2+Phasec3+Philigne+(+1)*PI/2+Pha4+Pha8+Pha11
135     Rmx2=Mx222*COS(Px222)+Mx233*COS(Px233)
136     Imx2=Mx222*SIN(Px222)+Mx233*SIN(Px233)
137     Rmx2=PROUND(Rmx2,-10)
138     Imx2=PROUND(Imx2,-10)
139     Mx2=SQR(Rmx2^2+Imx2^2)
140     Ppp=PI/2*(1-SGN(Rmx2))
141     Pp=SGN(Imx2)*Ppp
142     Px2=Pp
143     IF Rmx2 THEN Px2=ATN(Imx2/Rmx2)+Pp+Ppp-SGN(Rmx2)*Pp
144     Cf1(Mx1,Px1,Mx2,Px2,E1,Phasee1,T1,Phaset1,C1,Phasec1,Qim(3),Qip(3),Pha2)
145     OUTPUT Medium USING "X,K,2D.3D,X,4D.2D,#";"Q5:",Qim(3),Qip(3)*180/PI
146 Q6:  !
147      ! CALCUL DE Q6
148     Mx3=Mx1*C3/T3
149     Px3=Px1+Phasec3-Phaset3+(+1)*PI/2
150     Mx322=Mx222*C3/T3
151     Px322=Px222+Phasec3-Phaset3+(+1)*PI/2
152     Mx333=Mx233*T3/C3
153     Px333=Px233+Phaset3-Phasec3-(+1)*PI/2
154     Rmx3=Mx322*COS(Px322)+Mx333*COS(Px333)
155     Imx3=Mx322*SIN(Px322)+Mx333*SIN(Px333)
156     Rmx3=PROUND(Rmx3,-10)
157     Imx3=PROUND(Imx3,-10)
158     Mx4=SQR(Rmx3^2+Imx3^2)
159     Ppp=PI/2*(1-SGN(Rmx3))
160     Pp=SGN(Imx3)*Ppp
161     Px4=Pp
162     IF Rmx3 THEN Px4=ATN(Imx3/Rmx3)+Pp+Ppp-SGN(Rmx3)*Pp
163     Cf1(Mx3,Px3,Mx4,Px4,E1,Phasee1,T1,Phaset1,C1,Phasec1,Qim(4),Qip(4),Pha2)
164     OUTPUT Medium USING "X,K,2D.3D,X,4D.2D,#";"Q6:",Qim(4),Qip(4)*180/PI
165     Center=1
166     FOR I=2 TO 4
167       ! Resultats(Qim(*),Qip(*),Fl,I,Center)
168     NEXT I
169     PRINT
170     IF Dir1 THEN CALL Cf1_modifie(Mx7,Px7,Mx8,Px8,E1,Phasee1,T1,
        Phaset1,C1,Phasec1,Aim(1),Aip(1))
171     Cf1_modifie(Mx5,Px5,Mx6,Px6,E1,Phasee1,T1,Phaset1,C1,Phasec1,Aim(2),
        Aip(2))
172     Cf1_modifie(Mx1,Px1,Mx2,Px2,E1,Phasee1,T1,Phaset1,C1,Phasec1,Aim(3),
        Aip(3))
173     Cf1_modifie(Mx3,Px3,Mx4,Px4,E1,Phasee1,T1,Phaset1,C1,Phasec1,Aim(4),
        Aip(4))
174     !============================================================
175     !CALCUL DES PUISSANCES
176     GOTO Frequence
```

```
177     Fr=1
178     Ga=Gam(Fr)
179     Ph=Pha(Fr)
180     IF NOT Center THEN
181       OUTPUT KBD USING "2D.3D,K,4D.2D,#";Gam(Fr),",",Pha(Fr)*180/PI
182       INPUT "GAMMA",Gam(Fr),Pha(Fr)
183     END IF
184     Pha(Fr)=Pha(Fr)*PI/180
185     IF Ga<>Gam(Fr) OR Ph<>Pha(Fr) THEN Fl=0
186     I1=2
187     IF Dir1 THEN I1=1 ! DIRECTIVITE NON NULLE
188     FOR I=I1 TO 4
189       Reel=Gam(Fr)*COS(Pha(Fr))-Qim(I)*COS(Qip(I))
190       Imag=Gam(Fr)*SIN(Pha(Fr))-Qim(I)*SIN(Qip(I))
191       Fx=SQR(Reel^2+Imag^2)
192       IF I=1 THEN Fx3=Fx
193       Bi(I)=Fx*Aim(I)*C1
194     NEXT I
195     IF NOT Dir1 THEN
196       Bi(1)=D1*T1/SQR(2)
197       Aim(1)=1
198       Fx3=1
199     END IF
200     Random=1
201     FOR I=2 TO 4
202       Rs(I)=Bi(I)/Bi(1)*Aim(1)/Aim(I)*Fx3*(1.00+.03*(2*RND-1))
203     NEXT I
204     ! PRINT Bi(*)
205     ! PRINT Rs(*)
206     Center=1  !0> CENTRE ET CERCLE  1> CENTRE
207 Frequence:    !
208     Resultats(Qim(*),Qip(*),Fl,I,Center,Rs(*),Arret)
209   NEXT Freq
210   GOTO Fgh
211   OUTPUT KBD USING "K,#";"N"
212   Direct$=VAL$(Directivity)
213   IF Dir1=0 THEN Direct$="-"
214   OUTPUT PRT USING "K,#";"Directivity: ",Direct$," dB  Phase shift: ",Fact
215 ! NEXT Directivity
216 Fgh:!
217   OUTPUT Medium
218   BEEP
219   STOP
220 Sortie:  !
221   ^=-^/1000
222   OUTPUT Medium;"Directivity: "&VAL$(Directivity)
223   OUTPUT Medium USING "2X,K,4D,#";"L1= ",-Pha1/^,"L2= ",-Pha2/^,"L3= ",
      -Pha3/^,"L4= ",-Pha4/^,"L4= ",-Pha4/^
224   OUTPUT Medium
225   OUTPUT Medium USING "2X,K,4D,#";"L5= ",-Pha5/^,"L5= ",-Pha5/^,"L6= ",
      -Pha6/^,"L7= ",-Pha7/^,"L8= ",-Pha8/^
226   OUTPUT Medium
227   OUTPUT Medium USING "2X,K,4D,#";"L9= ",-Pha9/^,"L10= ",-Pha10/^,"L11= ",
      -Pha11/^,"L12= ",-Pha12/^,"L13= ",-Pha13/^
228   OUTPUT Medium
229   OUTPUT Medium USING "2X,K,4D,#";"L1 Coupleur #1= ",L1*1000,"L2 Coupleur
      #2= ",L2*1000,"L3 Coupleur #3= ",L3*1000
230   OUTPUT Medium
231   OUTPUT Medium USING "2X,K,4D,#";"L1 Diviseur #1= ",Ld1*1000,"L2 Diviseur
      #2= ",Ld2*1000,"L DEphaseur= ",Ligne*1000
232   OUTPUT Medium
```

```
233   OUTPUT Medium USING "2X,K,2D.2D,#";"BALANCEMENT DE PHASE: ",Fact,"
      % Energie au port IsolE";A
234   OUTPUT Medium
235   OUTPUT Medium
236   ^=-^*1000
237   RETURN
238   END
239   SUB Cf1(Mx1,Px1,Mx2,Px2,Me1,Pe1,Mt1,Pt1,Cm,Cp,Qim,Qip,Pha2)
240     !    t1x1 + e1x2
241     !    ------------
242     !    t1x2 + e1x1
243     ! DENOMINATEUR
244     Ma1=Me1*Mx1
245     Pa1=Pe1+Px1
246     Ma2=Mt1*Mx2
247     Pa2=Pt1+Px2
248     Ma3=Me1*Mx2
249     Pa3=Pe1+Px2
250     Ma4=Mt1*Mx1
251     Pa4=Pt1+Px1
252     Prn=Ma1*COS(Pa1)+Ma2*COS(Pa2)
253     Pin=Ma1*SIN(Pa1)+Ma2*SIN(Pa2)
254     Prn=PROUND(Prn,-10)
255     Pin=PROUND(Pin,-10)
256     Md=SQR(Prn^2+Pin^2)
257     Ppp=PI/2*(1-SGN(Prn))
258     Pp=SGN(Pin)*Ppp
259     Pd=Pp
260     IF Prn THEN Pd=ATN(Pin/Prn)+Pp+Ppp-SGN(Pin)*Pp
261     !  PRINT Prn,Pin,Md,Pd
262     ! NUMERATEUR
263     Prn=Ma3*COS(Pa3)+Ma4*COS(Pa4)
264     Pin=Ma3*SIN(Pa3)+Ma4*SIN(Pa4)
265     Prn=PROUND(Prn,-10)
266     Pin=PROUND(Pin,-10)
267     Mn=SQR(Prn^2+Pin^2)
268     Ppp=PI/2*(1-SGN(Prn))
269     Pp=SGN(Pin)*Ppp
270     Pn=Pp
271     IF Prn THEN Pn=ATN(Pin/Prn)+Pp+Ppp-SGN(Pin)*Pp
272     ! PRINT Prn,Pin,Md,Pd
273     Qim=Mn/Md/Cm
274     Qip=Pn-Pd-Cp+(+1)*PI/2-Pha2    !-PI/3
275     GOTO Sd
276 Boucle:Qip=Qip-SGN(Qip)*2*PI
277 Sd: IF ABS(Qip)>PI THEN Boucle
278   SUBEND
279   !
280   SUB Cf1_modifie(Mx1,Px1,Mx2,Px2,Me1,Pe1,Mt1,Pt1,Cm,Cp,Qim,Qip)
281     !    t1x1 + e1x2
282     Ma1=Me1*Mx1
283     Pa1=Pe1+Px1
284     Ma2=Mt1*Mx2
285     Pa2=Pt1+Px2
286     Prn=Ma1*COS(Pa1)+Ma2*COS(Pa2)
287     Pin=Ma1*SIN(Pa1)+Ma2*SIN(Pa2)
288     Prn=PROUND(Prn,-10)
289     Pin=PROUND(Pin,-10)
290     Qim=SQR(Prn^2+Pin^2)
291     Ppp=PI/2*(1-SGN(Prn))
292     Pp=SGN(Pin)*Ppp
```

```
293     Qip=Pp
294     IF Prn THEN Qip=ATN(Pin/Prn)+Pp+Ppp-SGN(Pin)*Pp
295     GOTO Sd
296 Boucle:Qip=Qip-SGN(Qip)*2*PI
297 Sd: IF ABS(Qip)>PI THEN Boucle
298   ! PRINT Prn,Pin,Qim,Qip
299   SUBEND
300   !****************************************!
301   SUB Resultats(Ampl(*),Qip(*),Fl,I,Center,OPTIONAL Rs(*),Arret)
302     COM /Wind/ Wxi,Wxa,Wyi,Wya,Facteur
303     COM /Gamma/ Gam(*),Pha(*)
304     COM /Quad/ Result(*),Racine(*),M
305     COM /Frequence/ Freq_debut,Freq_fin,Freq_step,Fact,Direct$
306     GRAPHICS ON
307     Theta_debut=0
308     Theta_fin=2*PI
309     Theta_step=(Theta_fin-Theta_debut)/36
310     No_change=1
311     Passe=0
312     VIEWPORT 25,95,15,85
313     IF Arret THEN
314       IF Fl THEN Saut
315       OUTPUT KBD USING "K,#";0,"<"
316       INPUT " 0>CRT 1> PLOTTER",Unit
317       IF Unit THEN
318         PLOTTER IS 705,"HPGL"
319         OUTPUT 705;"IN;DF;"
320       ELSE
321         PLOTTER IS CRT,"INTERNAL"
322         GINIT
323       END IF
324 Saut: VIEWPORT 25,95,15,85
325       Wxi=-3
326       Wxa=3
327       Wyi=-3
328       Wya=3
329       Passe=1
330       IF NOT Fl THEN Suite
331       IF Fl THEN Point
332     END IF
333    !IF Fl THEN Point
334     ON KEY 1 LABEL "ZOOM",2 CALL Curseur
335     ON KEY 2 LABEL "CONT",2 GOSUB Suite
336     ON KEY 3 LABEL "NO_CHANGE",2 GOSUB Av_suite
337     ON KEY 4 LABEL "PASSE",2 GOTO Passe
338     ON KEY 5 LABEL "FINI",2 GOTO Final
339     LOOP
340     END LOOP
341 Passe:   !
342     Passe=1
343     GOTO Suite
344 Av_suite:No_change=0
345 Suite:    !
346     GCLEAR
347     Py1=.8
348     ALPHA OFF
349  !  OUTPUT KBD USING "K,#";Wxi,",",Wxa,",",Wyi,",",Wya
350   ! INPUT "Window",Wxi,Wxa,Wyi,Wya
351     CLIP ON
352     SHOW Wxi,Wxa,Wyi,Wya
353     CLIP Wxi,Wxa,Wyi,Wya
```

```
354     Wx_moy=(Wxi+Wxa)/2
355     Wy_moy=(Wyi+Wya)/2
356     Px=(Wxa-Wxi)/10
357     Py=(Wya-Wyi)/10
358     Facteur=Px1/Px
359    !PEN 2
360     AXES Px,Py,Wxi,Wyi,2,2
361     AXES Px,Py,Wxa,Wya,2,2
362     IF SGN(Wyi)<>SGN(Wya) THEN
363       MOVE 0,Wyi
364       DRAW 0,Wya
365     END IF
366     IF SGN(Wxi)<>SGN(Wxa) THEN
367       MOVE Wxi,0
368       DRAW Wxa,0
369     END IF
370     CLIP OFF
371     CSIZE 2.50
372     LORG 6
373     FOR G=Wxi TO Wxa+Px/10 STEP Px
374       MOVE G,Wyi
375       LABEL PROUND(G,-2)
376     NEXT G
377     LORG 8
378     FOR G=Wyi TO Wya+Py/10 STEP Py
379       MOVE Wxi,G
380       LABEL PROUND(G,-2)
381     NEXT G
382     LORG 4
383     CSIZE 2.5
384     MOVE (Wxi+Wxa)/2,Wya+2/2*Py
385     LABEL "Directivity: "&Direct$&" dB"
386     MOVE (Wxi+Wxa)/2,Wya+Py*2/4
387     LABEL "Phase balance: "&VAL$(ABS(Fact-1)*100)&" %"
388     MOVE (Wxi+Wxa)/2,Wya
389     LABEL "Frequency band: "&VAL$(Freq_debut)&" - "&VAL$(Freq_fin)&" GHz
        steps: "&VAL$(Freq_step*1000)&" MHz"
390     CSIZE 2
391     LORG 2
392     MOVE Wxi+Px/2,Wyi+3/2*Py
393     LABEL "q4 *****"
394     MOVE Wxi+Px/2,Wyi+Py*2/2
395     LABEL "q5 00000"
396     MOVE Wxi+Px/2,Wyi+Py/2
397     LABEL "q6 +++++"
398   ! LABEL "q6 ....."
399     LORG 5
400     CSIZE 5.0
401     PEN 1
402 Point:    !
403     IF F1 THEN CSIZE 2.0
404     IF Center THEN
405       FOR I=2 TO 4
406         MOVE Ampl(I)*COS(Qip(I)),Ampl(I)*SIN(Qip(I))
407         DRAW Ampl(I)*COS(Qip(I)),Ampl(I)*SIN(Qip(I))
408        !IF I=4 AND F1=0 THEN LABEL "|"
409         IF I=4 THEN LABEL "+"
410         IF I=2 THEN LABEL "*"
411         IF I=3 THEN LABEL 0
412       NEXT I
413     ELSE
```

```
414       FOR I=2 TO 4
415         IF No_change THEN Dessin
416         Quadratique(Ampl(*),Qip(*),I,Rs(*))
417         Xc=Ampl(I)*COS(Qip(I))
418         Yc=Ampl(I)*SIN(Qip(I))
419         Xi=Racine(I,1,1)
420         Xa=Racine(I,2,1)
421         Yi=Racine(I,1,2)
422         Ya=Racine(I,2,2)
423         IF Xi=0 AND Yi=0 AND Xa=0 AND Ya=0 AND M>2 THEN
424           Theta_debut=0
425           Theta_fin=2*PI
426           GOTO Bn
427         END IF
428         Rei=PROUND((Xc-Xi)*(-1),-4)
429         Imi=PROUND((Yc-Yi)*(-1),-4)
430         Rea=PROUND((Xc-Xa)*(-1),-4)
431         Ima=PROUND((Yc-Ya)*(-1),-4)
432         Ppp=PI/2*(1-SGN(Rei))
433         Pp=SGN(Imi)*Ppp
434         Theta_debut=Pp
435         IF Rei THEN Theta_debut=ATN(Imi/Rei)+Pp+Ppp-SGN(Imi)*Pp
436         GOTO Sdi
437 Bouclei:Theta_debut=Theta_debut-SGN(Theta_debut)*2*PI
438 Sdi:    IF ABS(Theta_debut)>PI THEN Bouclei
439         Ppp=PI/2*(1-SGN(Rea))
440         Pp=SGN(Ima)*Ppp
441         Theta_fin=Pp
442         IF Rea THEN Theta_fin=ATN(Ima/Rea)+Pp+Ppp-SGN(Ima)*Pp
443         GOTO Sda
444 Bouclea:Theta_fin=Theta_fin-SGN(Theta_fin)*2*PI
445 Sda:    IF ABS(Theta_fin)>PI THEN Bouclea
446         IF Theta_debut=Theta_fin THEN Theta_debut=Theta_debut+2*PI
447      ! IF Xc>0 THEN Theta_debut=Theta_debut+2*PI
448 Bn:        !
449      !     IF ABS(Theta_debut)>PI/2 THEN Theta_debut=Theta_debut+2*PI
      *SGN(Theta_debut)
450      !     IF ABS(Theta_fin)>PI/2 THEN Theta_fin=Theta_fin+2*PI
      *SGN(Theta_fin)
451         A1=SQR((Racine(I,1,1)-Wx_moy)^2+(Racine(I,1,2)-Wy_moy)^2)
452         Ac=SQR((Xc-Wx_moy)^2+(Yc-Wy_moy)^2)
453         IF Ac<A1 THEN
454           Theta_debut=Theta_debut-2*PI*SGN(Theta_debut)
455         END IF
456         IF Xc>Wxa AND (Racine(I,1,1)<=Wxa OR Racine(I,2,1)<=Wxa) THEN
457           Theta_debut=Theta_debut-2*PI*SGN(Theta_debut)
458           IF Theta_debut=-PI THEN Theta_debut=PI
459         END IF
460         Theta_step=(Theta_fin-Theta_debut)/50
461 Dessin:     !
462         MOVE Xc,Yc
463         LABEL "O"
464      !  CLIP ON
465         ALPHA OFF
466         FOR Angle=Theta_debut TO Theta_fin STEP Theta_step
467           MOVE Xc+Rs(I)*COS(Angle),Yc+Rs(I)*SIN(Angle)
468           DRAW Xc+Rs(I)*COS(Angle),Yc+Rs(I)*SIN(Angle)
469         NEXT Angle
470       NEXT I
471     END IF
472     IF NOT Passe THEN RETURN
```

```
473 Final:    !
474     ALPHA ON
475     Fl=1
476     OFF KEY
477   SUBEND
478   SUB Curseur
479     VIEWPORT 25,95,20,90
480     COM /Wind/ Wxi,Wxa,Wyi,Wya,Facteur
481     GRAPHICS INPUT IS KBD,"ARROW KEYS"
482     PLOTTER IS CRT,"INTERNAL"
483     SET LOCATOR X,Y
484     TRACK 3 IS ON
485     DIGITIZE X,Y
486     TRACK 3 IS OFF
487     Xi=Wxi
488     Xa=Wxa
489     Yi=Wyi
490     Ya=Wya
491     Q=1
492     LOOP
493       ON KEY 1 LABEL "POIDS: "&VAL$(Q),3 GOSUB Poids_aug
494       ON KEY 11,3 GOSUB Poids_dim
495       ON KEY 6 LABEL "FRAME",3 GOSUB Clipping
496       ON KEY 5 LABEL "CORRECT",3 GOTO Fsd
497       ON KEY 7 LABEL "INCXI: "&VAL$(Incxi),3 GOSUB Increment_xi
498       ON KEY 17,3 GOSUB Decrement_xi
499       ON KEY 8 LABEL "INCYI: "&VAL$(Incyi),3 GOSUB Increment_yi
500       ON KEY 18,3 GOSUB Decrement_yi
501       ON KEY 9 LABEL "INCXA: "&VAL$(Incxa),3 GOSUB Increment_xa
502       ON KEY 19,3 GOSUB Decrement_xa
503       ON KEY 4 LABEL "INCYA: "&VAL$(Incya),3 GOSUB Increment_ya
504       ON KEY 14,3 GOSUB Decrement_ya
505     END LOOP
506 Fsd:    !
507     OFF KNOB
508     Facteur=MAX((Wxa-Wxi)/(Xa-Xi),(Wya-Wyi)/(Yi-Ya))
509     OUTPUT KBD USING "K,#";Facteur
510     INPUT "FACTEUR",Facteur
511     Wxi=Xi
512     Wxa=Xa
513     Wyi=Yi
514     Wya=Ya
515     SUBEXIT
516 Clipping:    !
517     WAIT 1
518     PEN -1
519     FRAME
520     PEN 1
521     Prox=Wxa-Wxi
522     Proy=Wya-Wyi
523     Xi=(X-Wxi)/Prox*Incxi/Q+Wxi
524     Xa=(Wxa-X)/Prox*Incxa/Q+Wxa
525     Yi=(Y-Wyi)/Proy*Incyi/Q+Wyi
526     Ya=(Wya-Y)/Proy*Incya/Q+Wya
527     CLIP Xi,Xa,Yi,Ya
528     FRAME
529     RETURN
530 Poids_aug:    !
531     Q=Q*10
532     RETURN
533 Poids_dim:    !
```

```
534     Q=Q/10
535     RETURN
536 Increment_xi:    !
537     Incxi=Incxi+1
538     RETURN
539 Decrement_xi:    !
540     Incxi=Incxi-1
541     RETURN
542 Increment_yi:    !
543     Incyi=Incyi+1
544     RETURN
545 Decrement_yi:    !
546     Incyi=Incyi-1
547     RETURN
548 Increment_xa:    !
549     Incxa=Incxa+1
550     RETURN
551 Decrement_xa:    !
552     Incxa=Incxa-1
553     RETURN
554 Increment_ya:    !
555     Incya=Incya+1
556     RETURN
557 Decrement_ya:    !
558     Incya=Incya-1
559     RETURN
560   SUBEND
561     !###################################################################
562   SUB Quadratique(Ampl(*),Qip(*),K,Rs(*))
563     OPTION BASE 1
564     COM /Wind/ Wxi,Wxa,Wyi,Wya,Facteur
565     COM /Quad/ Result(*),Racine(*),M
566     MAT Result= (0)
567     MAT Racine= (0)
568     Reim(1)=Ampl(K)*COS(Qip(K))
569     Reim(2)=Ampl(K)*SIN(Qip(K))
570     Wind(1,1)=Wxi
571     Wind(1,2)=Wxa
572     Wind(2,1)=Wyi
573     Wind(2,2)=Wya
574     M=0
575     FOR I=1 TO 2
576       M1=I
577       M2=3-I
578       FOR J=1 TO 2
579         B=-2*Reim(I)
580         Ac=(-B/2)^2+(Wind(3-I,J)-Reim(3-I))^2-Rs(K)^2
581         Radical=B^2-4*Ac
582         IF Radical>=0 THEN
583           Ra=SQR(Radical)
584           Te=-(B+Ra)/2
585           Result(2*(I-1)+J,1)=Te
586           IF Wind(I,1)<=Te AND Te<=Wind(I,2) THEN
587             M=M+1
588             Racine(K,M,M1)=Te
589             Racine(K,M,M2)=Wind(3-I,J)
590           END IF
591           Tee=-(B-Ra)/2
592           Result(2*(I-1)+J,2)=Tee
593           IF Wind(I,1)<=Tee AND Tee<=Wind(I,2) THEN
594             M=M+1
```

```
595             Racine(K,M,M1)=Tee
596             Racine(K,M,M2)=Wind(3-I,J)
597           END IF
598         ELSE
599           Ra=SQR(-Radical)
600           Result(2*(I-1)+J,3)=-B/2
601           Result(2*(I-1)+J,4)=Ra/2
602         END IF
603         !       PRINT USING "4(3D.3D,X)";Result(2*(I-1)+J,1),
            Result(2*(I-1)+J,2),Result(2*(I-1)+J,3),Result(2*(I-1)+J,4)
604       NEXT J
605     NEXT I
606   ! PRINT USING "4(3D.3D,X)";Racine(*)
607     PRINT
608     PAUSE
609   SUBEND
```

```
        PROGRAM No. 10

      PROGRA CALIBRATION
C
C  NOMBER OF STANDARDS,  POINTS OF FREQUENCIES, THE STEP OF POINTS
C  OF FREQUENCIES,  NOMBER OF RESAUSES,
C  MAX DIMENSION OF MATRICES
C
C  RESOLUTION OF NON LINEAIRE SYSTEME BY OPTIMIZATION
C     IMPLICIT REAL (A-H)
C     IMPLICIT REAL (O-Z)
C
C     Modification for read format P
C
      PARAMETER(NSTD=13, NFREQ= 201, NPAS=1, NLIN=9)
      PARAMETER(NMAX=20, NNLIN=5)
      EXTERNAL FCN
      EXTERNAL LSJAC
C
C  VARIABLES GENERALES
      INTEGER I,J,K
      INTEGER FR,NFR
C  FICHIER DE PUISSANCE
      REAL PSTD(NSTD,NFREQ,4)
C  MATRICE LINEARISEE
      INTEGER STDVEC(NMAX)
      REAL ALIN(NMAX,NMAX), BLIN(NMAX), X(NMAX),X1(NMAX)
C  SOLUTION DU SYSTEME SURDETERMINE
      REAL TOL, RES(NMAX),FAC(NMAX,NMAX),RCOND
      INTEGER KBASIS,IPVT(NMAX)
C  COEFFICIENTS DE CALIBRATION
C  1=P, 2=Q, 3=R, 4=A2, 5=B2
      REAL SOL(NNLIN),SOL1(NNLIN)
C  PUISSANCES NORMALISEES POUR EQUATION NON-LINEAIRE
      REAL FCNQ
      COMMON /FCOEF/FCNQ(NSTD,3)
C  CHOIX DES EQUATION QUI FONT PARTIE DU SYS D'EQ NON-LIN
      INTEGER EQSYS(NSTD),NBSTD
C  SOLUTION DU SYSTEME NON-LINEAIRE
C    NORME DE L'ERREUR APRES SOLUTION
      REAL FNORM,XSCALE(NNLIN),FSCALE(NSTD),FVEC(NSTD),FJAC(NSTD,NNLIN)
      INTEGER ERRCOD,ERRSOL,INDEQ
C    PARAMETRES D'OPTIMISATION
      REAL RPARAM(7)
      INTEGER IPARAM(6),ELIM
      DATA XSCALE/NNLIN*1.0/,FSCALE/NSTD*1.0/
C
      OPEN(7,FILE='w.dat')
      ELIM=0
C     WRITE(7,*) NFR
C    PARAMETRES STANDARDS P.843 IMSL
      IPARAM(1)=0
C   LECTURE DE LA MATRICE DE PUISSANCE
      READ(5,*)  (((PSTD(I,K,J), J=1,4), K=1,NFREQ), I=1,NSTD)
      DO 100 FR=1,NFREQ,NPAS
        IF (PSTD(1,FR,1).NE.0.0) THEN
        WRITE(6,'(//,A,I4,2X,F5.2,/)') ' FREQUENCE: ',FR
C       CONSTRUCTION DU SYSTEME LINEAIRE .
C       CHOISIR LES EQUATION QUI FERONT PARTIE DU SYSTEME
C BOUCLE D'ESSAI DE 9 EQUATIONS PARMI 13
        DO 111 J1=1,NSTD-8
```

```
          DO 111 J2=J1+1,NSTD-7
           DO 111 J3=J2+1,NSTD-6
            DO 111 J4=J3+1,NSTD-5
             DO 111 J5=J4+1,NSTD-4
              DO 111 J6=J5+1,NSTD-3
               DO 111 J7=J6+1,NSTD-2
                DO 111 J8=J7+1,NSTD-1
                 DO 111 J9=J8+1,NSTD
                   STDVEC(1)=J1
                   STDVEC(2)=J2
                   STDVEC(3)=J3
                   STDVEC(4)=J4
                   STDVEC(5)=J5
                   STDVEC(6)=J6
                   STDVEC(7)=J7
                   STDVEC(8)=J8
                   STDVEC(9)=J9
        CALL SYSLIN(PSTD, NSTD , NFREQ, FR, STDVEC, ALIN,
     &               BLIN, NMAX)
C
C       SOLUTION DU SYSTEME LINEAIRE
C
        CALL LSQRR(9, NLIN, ALIN, NMAX, BLIN, TOL, X, RES, KBASIS)
C
C       CALCULS DES COEFFICIENTS.  PREMIERE APROXIMATION
C  1=P, 2=Q, 3=R, 4=A2, 5=B2
        ERRSOL=0
        IF ((X(2).LT.0.).OR.(X(3).LT.0.).OR.(X(1).EQ.0)) THEN
          WRITE(6,*) ' ------  PAS DE SOLUTION LINEAIRE'
C         WRITE(7,'(1X,F5.2,A,//)') FR,
C    &              k '------  PAS DE SOLUTION LINEAIRE'
C
C   UTILISATION D'UNE ANCIENNE SOLUTION SI POSSIBLE
C
          ERRSOL=1
        ELSE
          SOL(3)=(2*X(5)-X(7)*X(9))/(2*X(1)*X(9)-X(5)*X(7))
          SOL(2)=(2*X(4)-X(7)*X(8))/(2*X(1)*X(8)-X(4)*X(7))
          SOL(1)=SOL(2)+SOL(3)+(X(7)/X(1))
          IF((SOL(1).LT.0).OR.(SOL(2).LT.0).OR.(SOL(3).LT.0)) THEN
            WRITE(6,'(A,/)') '------  SOLUTION LINEAIRE NON VALIDE'
C
C   UTILISATION D'UNE ANCIENNE SOLUTION SI POSSIBLE
C
            ERRSOL=2
          ENDIF
        ENDIF
C
C   RECUPERATION D'UNE VIEILLE SOLUTION
C
        IF ( ERRSOL.NE.0) THEN
          DO 125 I=1,NNLIN
            SOL(I)=X1(I)
125       CONTINUE
        ELSE
          SOL(4)=SQRT(SOL(1)*SOL(3)*X(2))
          SOL(5)=SQRT(SOL(1)*SOL(2)*X(3))
C         DO 127 I=1,NNLIN
C           X1(I)=SOL(I)
C127       CONTINUE
        ENDIF
```

```
        WRITE(6,'(A,5(2X,F14.5),/)') ' PQRAB APROX:    ',(SOL(I),I=1,5)
        DO 170 I=1,NNLIN
          SOL1(I)=SOL(I)
 170    CONTINUE
C
C      EQUATIONS QUI CONSTITUENT LE SYSTEME NON-LINEAIRE
          DO 180 I=1,NSTD
             EQSYS(I)=I
 180      CONTINUE
C   COEFFICIENTS
          CALL CALCQ(PSTD, NSTD, NFREQ, FR, EQSYS)
C   VALEUR DE DEPART DE L'EQUATION
          CALL FCN(NSTD,NNLIN,SOL,X)
          FNORM=0.
          IF (ELIM.EQ.1) THEN
C   ELIMINATION D'UNE EQUATION
            DO 130 I=1,NSTD
              IF (FNORM.LT.ABS(X(I))) THEN
                FNORM=ABS(X(I))
                NEQU=I
              ENDIF
              WRITE(6,'(A,I3,2X,F10.7)') ' EQUATION NO.',I,X(I)
 130        CONTINUE
            WRITE(6,'(A,I4)') ' EQUATION ELIMINEE: ',NEQU
            NBSTD=NSTD-1
            DO 135 I=NEQU,NBSTD
              EQSYS(I)=EQSYS(I+1)
135         CONTINUE
          ELSE
            NBSTD=NSTD
          ENDIF
C   CALCUL DES NOUVELLES VALEURS DE DEPART
          CALL CALCQ(PSTD,NSTD,NFREQ,FR,EQSYS)
          CALL FCN(NBSTD,NNLIN,SOL,X)
C
C   PARAMETRES DE DEPART STANDARDS P.843
C         IPARAM(1)=0
          IPARAM(1)=0
C
          CALL U4LSF(IPARAM,RPARAM)
C
C   AUGMENTATION DES CRITERES D'OPTIMISATION
C
C
C         IPARAM(2)=8
C         RPARAM(1)=RPARAM(1)/1000.0
C         RPARAM(2)=RPARAM(2)/1000.0
C         RPARAM(4)=RPARAM(4)/1000.0
C
C
C
C   SOLUTION DE L'EQUATION NON-LINEAIRE
C
C    EMPECHER LES ERREURS D'INTERROMPRE LE PROG
          CALL ERSET(4,0,0)
          CALL UNLSJ(FCN,LSJAC,NBSTD,NNLIN,SOL,XSCALE,FSCALE,IPARAM,
     &               RPARAM,X,FVEC,FJAC,NBSTD)
          ERRCOD=IERCD()
          CALL ERSET(0,2,2)
C           WRITE(6,'(A,6(I6,2X))') ' IPARAM',(IPARAM(I),I=1,6)
C           WRITE(6,'(A,7(F10.6,2X))') ' RPARAM',(RPARAM(I),I=1,7)
```

```
          IF (ERRCOD .GT. 0) THEN
            WRITE(6,*) ' ***  ERREUR SUB UNLSJ, CODE: ',ERRCOD,' ***'
          END IF
          WRITE(6,'(/,A,5(2X,F14.5),/)') ' PQRAB ITERATIF:',
     &                                   (X(I),I=1,NNLIN)
          IF(X(1).LE.0.01 .OR. X(2).LE.0.01 .OR. X(3).LE.0.01 .OR.
     &       X(4).LE.0.01 .OR. X(5).LE.0.01) THEN
            GOTO 111
          ELSE
          WRITE(7,'(1X,I3,5(A,F12.7))') FR,',',X(1),',',X(2),',',X(3),
     &                ',',X(4),',',X(5)
          CALL FCN(NBSTD,NNLIN,X,SOL)
          FNORM=0.
          DO 161 I=1,NNLIN
            X1(I)=X(I)
161       CONTINUE
          DO 160 I=1,NBSTD
            WRITE(6,'(A,I3,2X,F10.7)') ' EQUATION NO.',I,SOL(I)
            FNORM=FNORM+SOL(I)*SOL(I)
 160      CONTINUE
          WRITE(6,'(A,E10.3)') ' ERREUR FIN FCN: ',SQRT(FNORM)
          GOTO 112
        ENDIF
111       CONTINUE
112       CONTINUE
      ENDIF
  100  CONTINUE
      CLOSE(7)
      STOP
      END

C
C   CONSTRUCTION DU SYSTEME LINEAIRE SELON L'EQUATION
C   3.11, P14.
C   NBSTD: NOMBRE DE STANDARDS UTILISES
C   STDVEC: CONTIENT LES NUMEROS DES STANDARDS A UTILISER

      SUBROUTINE SYSLIN(PSTD, NSTD, NFREQ, FR, STDVEC, ALIN,
     &                  BLIN, NMAX)
      REAL PSTD(NSTD, NFREQ, 4)
      REAL ALIN(NMAX, NMAX)
      REAL BLIN(NMAX)
      INTEGER FR, STDVEC(NMAX)
      INTEGER I
      REAL Q1, Q2, Q3


      DO 100 I=1,9
C       PUISSANCES NORMALISEES
C       DES STD DESIGNES PAR STDVEC
        Q1=PSTD(STDVEC(I),FR,2)/PSTD(STDVEC(I),FR,1)
        Q2=PSTD(STDVEC(I),FR,3)/PSTD(STDVEC(I),FR,1)
        Q3=PSTD(STDVEC(I),FR,4)/PSTD(STDVEC(I),FR,1)
C       MATRICE A
        ALIN(I,1)=Q1*Q1
        ALIN(I,2)=Q2*Q2
        ALIN(I,3)=Q3*Q3
        ALIN(I,4)=Q1*Q2
        ALIN(I,5)=Q1*Q3
        ALIN(I,6)=Q2*Q3
        ALIN(I,7)=Q1
```

```
        ALIN(I,8)=Q2
        ALIN(I,9)=Q3
C       MATRICE B
        BLIN(I)=-1.
100   CONTINUE
      RETURN
      END

C   CALCUL DES COEFICIENTS NORMALISES Q1,Q2,Q3 POUR LES EQ NON-LIN
      SUBROUTINE CALCQ(PSTD, NSTD, NFREQ, FR, EQSYS)
      INTEGER NSTD, NFREQ, EQSYS(NSTD), I, FR
      REAL PSTD(NSTD, NFREQ, 4), FCNQ
      COMMON /FCOEF/FCNQ(13,3)

      DO 100 I=1,NSTD
        FCNQ(I,1)=PSTD(EQSYS(I), FR, 2)/PSTD(EQSYS(I), FR, 1)
        FCNQ(I,2)=PSTD(EQSYS(I), FR, 3)/PSTD(EQSYS(I), FR, 1)
        FCNQ(I,3)=PSTD(EQSYS(I), FR, 4)/PSTD(EQSYS(I), FR, 1)
100   CONTINUE
      RETURN
      END

C   FONCTION NON-LINEAIRE A RESOUDRE
      SUBROUTINE FCN(M,N,X,F)
      INTEGER N,M,I
      REAL X(N), F(M)
      REAL FCNQ
      COMMON /FCOEF/FCNQ(13,3)

      DO 100 I=1,M
        F(I)=X(1)*FCNQ(I,1)*FCNQ(I,1)
     &       +X(2)*X(4)*X(4)*FCNQ(I,2)*FCNQ(I,2)
     &       +X(3)*X(5)*X(5)*FCNQ(I,3)*FCNQ(I,3)
     &       +(X(3)-X(1)-X(2))*X(4)*FCNQ(I,1)*FCNQ(I,2)
     &       +(X(2)-X(1)-X(3))*X(5)*FCNQ(I,1)*FCNQ(I,3)
     &       +(X(1)-X(2)-X(3))*X(4)*X(5)*FCNQ(I,2)*FCNQ(I,3)
     &       +X(1)*(X(1)-X(2)-X(3))*FCNQ(I,1)
     &       +X(2)*(X(2)-X(1)-X(3))*X(4)*FCNQ(I,2)
     &       +X(3)*(X(3)-X(1)-X(2))*X(5)*FCNQ(I,3)
     &       +X(1)*X(2)*X(3)
100     CONTINUE
        RETURN
        END

C     CALCUL DU JACOBIEN DE FCN
      SUBROUTINE LSJAC(M,N,X,FJAC,LDFJAC)
      INTEGER N,M,LDFJAC,I
      REAL X(N),FJAC(LDFJAC,N),Q
      COMMON /FCOEF/Q(13,3)

      DO 100 I=1,M
        FJAC(I,1)=Q(I,1)*Q(I,1) - X(4)*Q(I,1)*Q(I,2)
     &            -X(5)*Q(I,1)*Q(I,3)
     &            +X(4)*X(5)*Q(I,2)*Q(I,3) + (2*X(1)-X(2)-X(3))*Q(I,1)
     &            -X(2)*X(4)*Q(I,2) - X(3)*X(5)*Q(I,3) + X(2)*X(3)
        FJAC(I,2)=X(4)*X(4)*Q(I,2)*Q(I,2) - X(4)*Q(I,1)*Q(I,2)
     &            +X(5)*Q(I,1)*Q(I,3) - X(4)*X(5)*Q(I,2)*Q(I,3)
     &            -X(1)*Q(I,1) + (2*X(2)-X(1)-X(3))*X(4)*Q(I,2)
     &            -X(3)*X(5)*Q(I,3) + X(1)*X(3)
        FJAC(I,3)=X(5)*X(5)*Q(I,3)*Q(I,3) + X(4)*Q(I,1)*Q(I,2)
     &            -X(5)*Q(I,1)*Q(I,3) - X(4)*X(5)*Q(I,2)*Q(I,3)
```

```
     &            -X(1)*Q(I,1) -      X(2)*X(4)*Q(I,2)
     &            +(2*X(3)-X(1)-X(2))*X(5)*Q(I,3) + X(1)*X(2)
        FJAC(I,4)=X(2)*2*X(4)*Q(I,2)*Q(I,2)
     &            +(X(3)-X(1)-X(2))*Q(I,1)*Q(I,2)
     &            +(X(1)-X(2)-X(3))*X(5)*Q(I,2)*Q(I,3)
     &            +X(2)*(X(2)-X(1)-X(3))*Q(I,2)
        FJAC(I,5)=2*X(5)*X(3)*Q(I,3)*Q(I,3)
     &            +(X(2)-X(1)-X(3))*Q(I,1)*Q(I,3)
     &            +(X(1)-X(2)-X(3))*X(4)*Q(I,2)*Q(I,3)
     &            +X(3)*(X(3)-X(1)-X(2))*Q(I,3)
100   CONTINUE
      RETURN
      END
```

PROGRAM No. 11

```
1!    NOM:  "QPNTS_W"
2     !
4     !
5     !   Program to calculate  Qi points from parameters of calibration
6     !   C, D, E and P, Q, R, A2, B2
7     !
8     !   Ajout des rapports dans le calcul des points (standard #1)
9 !    FIND " SUB Home"
10    !
11    OPTION BASE 1
12    DEG
13    COM /Boite/ COMPLEX C(201),D(201),E(201),INTEGER Sgn(201),Max_points,
      REAL P(201),Q(201),R(201),A2(201),B2(201),Pmes(13,201,4)
14    COM /Point/ COMPLEX Q4(201),Q5(201),Q6(201)
15    COM /File/ REAL Npas,F_q$[20],F_puiss$[20],F_bte_b$[20],F_cal$[20]
16    !
17    REAL M,N,Alp,Alp1,X1,X2,X3,X4,E5,E6,F4,G4,F5,G5,F6,G6
18    REAL Dr,Di,Cr,Ci,Er,Ei
19    INTEGER F,I,J,K,Rapp,L
20    DIM Fichier$[20],A$[80]
21    REDIM C(28),D(28),E(28),Sgn(28),P(28),Q(28),R(28),A2(28),B2(28),
      Pmes(13,28,4)
23    !
24    Med=CRT
25    Rapp=1
26    Max_points=28   ! Grosseur des matrices de donnees
27    Npas=1          ! Pas dans la boucle de frequences
28    IF Sgn(1)=0 THEN
29      F_bte_b$="B3HP24:,700,1"
30      F_cal$="W3HP24:,700,1"
31      F_puis$="P3HP24:,700,1"
32      F_q$="Q4HP:,700,1"
33      MAT Sgn= (1)
34    END IF
35    ON KEY 5 GOSUB Lis_bte_b
36    ON KEY 6 GOSUB Lis_cal
37    ON KEY 16 GOSUB Lis_puiss
38    ON KEY 7 GOSUB Calcul_q
39    ON KEY 8 GOSUB Print_q
40    ON KEY 18 GOSUB Sauve_q
41 Menu:   !
42    Home
43    LOOP
44      PRINT TABXY(1,2);"Programme de calcul des points Qi"
45      PRINT TABXY(1,9);"Cle 5:     Lire Boite d'erreur format B"
46      PRINT TABXY(1,10);"Cle 6/16:  Lire Calibration (w)/ Lire puissance
        (format P)"
47      PRINT TABXY(1,11);"Cle 7:     Calcul des points Qi"
48      PRINT TABXY(1,12);"Cle 8/18:  Impression des points Qi/Sauve points q"
49    END LOOP
50    !
51 Lis_bte_b: !
52    Home
53 Aab:OUTPUT KBD USING "K,#";F_bte_b$
54    LINPUT "Fichier de boite d'erreur a lire: ",Fichier$
55    IF Fichier$="" THEN
56      GOTO Menu
57    ELSE
58      F_bte$=Fichier$
```

```
59    END IF
60    ON ERROR GOTO Lbtebug_b
61    ASSIGN @Ff TO F_bte$
62    ENTER @Ff;Fd,Ff,Fp,Max_point
63    ENTER @Ff;C(*),D(*),E(*),Sgn(*)
64    ASSIGN @Ff TO *
65    OFF ERROR
66    RETURN
67 Lbtebug_b:   !
68    SELECT ERRN
69    CASE 56  ! File name is undefined
70      BEEP
71      PRINT TABXY(1,18);ERRM$
72      GOTO Aab
73    CASE ELSE
74      DISP ERRM$
75      BEEP
76      PAUSE
77    END SELECT
78    OFF ERROR
79    RETURN
80    !
81    !
82 Lis_cal: !
83    Home
84 Aag:OUTPUT KBD USING "K,#";F_cal$
85    LINPUT "Fichier de calibration a lire: ",Fichier$
86    IF Fichier$="" THEN
87      GOTO Menu
88    ELSE
89      F_bte$=Fichier$
90    END IF
91    ON ERROR GOTO Lcalbug
92    ASSIGN @Ff TO F_bte$
93    ENTER @Ff;Fd,Ff,Fp,Sp,Puissance_cal
95    ENTER @Ff;P(*),Q(*),R(*),A2(*),B2(*)
96    ASSIGN @Ff TO *
97    OFF ERROR
98    RETURN
99 Lcalbug:   !
100   SELECT ERRN
101   CASE 56  ! File name is undefined
102     BEEP
103     PRINT TABXY(1,18);ERRM$
104     GOTO Aag
105   CASE ELSE
106     DISP ERRM$
107     BEEP
108     PAUSE
109   END SELECT
110   OFF ERROR
111   RETURN
112   !
113 Lis_puiss:   !
114   Home
115 Aah:OUTPUT KBD USING "K,#";F_puis$
116   LINPUT "Fichier de puissance a lire: ",Fichier$
117   IF Fichier$="" THEN
118     GOTO Menu
119   ELSE
120     F_puis$=Fichier$
```

```
121   END IF
122   ON ERROR GOTO Lpuibug
123   ASSIGN @Ff TO F_puis$
124   ENTER @Ff;Fd,Ff,Fp,Max_point
126   ENTER @Ff;Pmes(*)
127   ASSIGN @Ff TO *
128   OFF ERROR
129   RETURN
130 Lpuibug:  !
131   SELECT ERRN
132   CASE 56  ! File name is undefined
133     BEEP
134     PRINT TABXY(1,18);ERRM$
135     GOTO Aah
136   CASE ELSE
137     DISP ERRM$
138     BEEP
139     PAUSE
140   END SELECT
141   OFF ERROR
142   RETURN
143   !
144 Sauve_q:   !
145   Home
146 Aaq:OUTPUT KBD USING "K,#";F_q$
147   LINPUT "Fichier de points Qi a sauver: ",Fichier$
148   IF Fichier$="" THEN
149     GOTO Menu
150   ELSE
151     F_q$=Fichier$
152   END IF
153   ON ERROR GOTO Lqbug
154 Aaq1:  !
155   CREATE ASCII F_q$,Max_points/Npas+1
156   ASSIGN @Ff TO F_q$
157   FOR I=1 TO Max_points STEP Npas
158     A$=VAL$(PROUND(I,0))&" "&VAL$(PROUND(ABS(Q4(I)),-4))&" "&VAL
      $(PROUND(ARG(Q4(I)),-2))&" "&VAL$(PROUND(ABS(Q5(I)),-4))&" "&
      VAL$(PROUND(ARG(Q5(I)),-2))
159     A$=A$&" "&VAL$(PROUND(ABS(Q6(I)),-4))&" "&VAL$(PROUND(ARG(Q6(I)),-2))
160     OUTPUT @Ff;A$
161   NEXT I
162   ASSIGN @Ff TO *
163   OFF ERROR
164   RETURN
165 Lqbug:  !
166   SELECT ERRN
167   CASE 56  ! File name is undefined
168     BEEP
169     PRINT TABXY(1,18);ERRM$
170     GOTO Aaq
171   CASE 54   ! Duplicate file name
172     PURGE F_q$
173     GOTO Aaq1
174   CASE ELSE
175     DISP ERRM$
176     BEEP
177     PAUSE
178   END SELECT
179   OFF ERROR
180   RETURN
```

```
181           !
182 Calcul_q:   !
183            L=13
185   FOR I=1 TO Max_points STEP Npas
186     IF P(I)<>0 THEN !AND I<>151 THEN
187       IF Rapp=1 THEN
188         W4=Pmes(L,I,2)/Pmes(L,I,1)
189         W5=Pmes(L,I,3)/Pmes(L,I,1)
190         W6=Pmes(L,I,4)/Pmes(L,I,1)
191       ELSE
192         W4=0
193         W5=0
194         W6=0
195       END IF
196       !
197       M=SQR(R(I))
198       N=SQR(Q(I))
199       Alp=(P(I)-Q(I)-R(I))/(2*SQR(Q(I)*R(I)))
200       Alp1=SQR(1-PROUND(Alp,-3)^2)*Sgn(I)
201   !
202   ! POINT Q4
203       Q4(I)=-E(I)/D(I)
204   !
205   ! POINT Q5
206       Q5(I)=(E(I)-M)/(C(I)*M-D(I))
207   !
208   ! POINT Q6
209       Q6(I)=(E(I)-N*CMPLX(-Alp,Alp1))/(C(I)*N*CMPLX(-Alp,Alp1)-D(I))
210   !
211     END IF
212   NEXT I
213   !
214   BEEP 3000,1
215   RETURN
216   !
217 Print_q:  !
218   Home
219   FOR I=1 TO Max_points STEP Npas
220     IF (P(I)<>0) THEN
221       OUTPUT Med USING "X,3D,4X,3(4D.4D,X,4D.2D,2X)";I,ABS(Q4(I)),
          ARG(Q4(I)),ABS(Q5(I)),ARG(Q5(I)),ABS(Q6(I)),ARG(Q6(I))
222     END IF
223   NEXT I
224   PAUSE
225   Home
226   RETURN
227           !
228   END
229   !
230   SUB Home
231     GCLEAR
232     OUTPUT 2 USING "K,#";"K"
233   SUBEND
234   !
```